Fall 2013

Transmit Signal Design for MIMO Radar and Massive MIMO Channel Estimation

Andrew Jason Duly
Purdue University

Graduate School ETD Form 9
(Revised 12/07)

PURDUE UNIVERSITY
GRADUATE SCHOOL
Thesis/Dissertation Acceptance

This is to certify that the thesis/dissertation prepared

By Andrew Duly

Entitled
Transmit Signal Design for MIMO Radar and Massive MIMO Channel Estimation

For the degree of Doctor of Philosophy

Is approved by the final examining committee:

JAMES V. KROGMEIER, Co-Chair
Chair

DAVID J. LOVE, Co-Chair

MARK R. BELL

MICHAEL D. ZOLTOWSKI

To the best of my knowledge and as understood by the student in the *Research Integrity and Copyright Disclaimer (Graduate School Form 20)*, this thesis/dissertation adheres to the provisions of Purdue University's "Policy on Integrity in Research" and the use of copyrighted material.

Approved by Major Professor(s): JAMES V. KROGMEIER, Co-Chair

Approved by: V. Balakrishnan 12/2/2013
Head of the Graduate Program Date

TRANSMIT SIGNAL DESIGN FOR MIMO RADAR AND MASSIVE MIMO CHANNEL ESTIMATION

A Dissertation

Submitted to the Faculty

of

Purdue University

by

Andrew Jason Duly

In Partial Fulfillment of the

Requirements for the Degree

of

Doctor of Philosophy

December 2013

Purdue University

West Lafayette, Indiana

To my family

ACKNOWLEDGMENTS

I would like to thank my family for their continued support through my academic career. My parents, David and Petra, have been there from the beginning. I have treasured their continuous encouragement over the years. My brothers, Jeff and Tim, with whom I share a bond not only as siblings but also as electrical engineers. My wife, Jen, has had a front row seat to the daily challenges I encountered. Her support has been unfailing.

A special thanks to my advisors, David Love and James Krogmeier. Their knowledge and expertise has guided my work and way of thinking over the years. As mentors, they have helped sharpen my thinking to not only produce high quality work but also to present it in the most impactful way. I would also like to thank my committee members, Mark Bell and Michael Zoltowski. Their comments and suggestions have significantly improved the caliber of my work.

I was fortunate to develop a relationship with the Air Force Research Laboratory at Wright-Patterson Air Force Base in Ohio. A glimpse of the challenges associated with implementing antenna arrays in practice has greatly improved my perspective. Finally, the many conversations (both technical and otherwise) I have had with members of the TASC Lab have impacted my time at Purdue in a way I couldn't imagine otherwise. Thank you for the years I can reflect back upon with fondness and laughter.

TABLE OF CONTENTS

Page

LIST OF FIGURES

Figure Page

ABBREVIATIONS

CSI	channel state information
CSIR	channel state information at receiver
CSIT	channel state information at transmitter
FDD	frequency division duplex
LOS	line-of-sight
LP	linear precoding
LS	least squares
MAP	maximum a posteriori
MF	matched filter
MIMO	multiple-input multiple-output
MISO	multiple-input single-output
ML	maximum likelihood
MMSE	minimimum mean square error
MSE	mean square error
NLOS	non-line-of-sight
PA	phased array
PEP	pairwise error probability
RCS	radar cross section
SISO	single-input single-output
SAR	synthetic aperture radar
SINR	signal-to-interference-plus-noise ratio
SNR	signal-to-noise ratio
TDBF	time-division beamforming
TDD	time division duplex

ABSTRACT

Duly, Andrew Jason Ph.D., Purdue University, December 2013. Transmit Signal Design for MIMO Radar and Massive MIMO Channel Estimation. Major Professors: David J. Love and James V. Krogmeier.

The widespread availability of antenna arrays and the capability to independently control signal emissions from each antenna make transmit signal design increasingly important for radar and wireless communication systems. In the first part of this work, we develop the framework for a MIMO radar transmit scheme which trades off waveform diversity for beampattern directivity. Time-division beamforming consists of a linear precoder that provides direct control of the transmit beampattern and is able to form multiple transmit beams in a single pulse. The MIMO receive ambiguity function, which incorporates the receiver structure, reveals a space and delay-Doppler separability that emphasizes the importance of the transmit-receive beampattern and single-input single-output (SISO) ambiguity function. The second part of this work focuses on channel estimation for massive MIMO systems. As the size of arrays increase, conventional channel estimation techniques no longer remain practical. In current systems, training sequences probe wireless channels in orthogonal directions to obtain channel state information for block fading channels. The training overhead becomes significant as the number of transmit antennas increases, thereby creating a need for alternative channel estimation techniques. In this work, we relax the orthogonal restriction on the sounding vectors and introduce a feedback channel to enable closed-loop sounding vector design. A probability of misalignment framework is introduced, which provides a measure to sequentially design sounding vectors.

1. INTRODUCTION

Phased array radar took advantage of multiple antennas by forming spatial beams to cohere power in space. This added another dimension to design the transmit signal in: the spatial dimension. Phased array radars operated on the array manifold, transmitting power in a subset of the spatial domain that characterizes line-of-sight channels. In a similar manner, wireless communications were quick to adopt multiple antenna signaling schemes, a technology that has been called multiple-input multiple-output (MIMO) wireless communications. Unlike phased array, MIMO communications has the capability to transmit linearly independent waveforms out of each antenna. The radar community is recently starting to adopt this phenomenom and harness the advantages of waveform diversity in what is now considered MIMO radar.

Although two very similar technologies, current literature does not draw strong ties between MIMO radar and MIMO wireless communication. It is easy to see a close relationship exists, but the scarcity of papers on the subject could be attributed to the vastly different objectives used for each technology. Simply put, wireless communications estimates the transmit signal given the channel, whereas radar estimates the channel given the transmit signal. For wireless communications, the transmit signal includes symbols (and therefore bits) of information to be conveyed to the receiver. For radar, an estimate of the channel includes information on the target's range, velocity, and angle, among other parameters. The noncoherent MIMO radar literature [1, 2] seems to recognize a portion of this similarity, equating different look angles of a target to channel fading. Coherent MIMO radar literature does not explicitly make these connections, although the implicit similarities are everywhere. Furthermore, the hardware for coherent MIMO radar relates more to wireless communications than noncoherent MIMO radar does. The close proximity of the transmit

and receive antennas, grouped into arrays, more closely resembles the arrays used in point-to-point MIMO wireless communication.

For wireless systems with multiple antennas, MIMO adds the spatial dimension to the already well known time, frequency, and code dimensions. Independent fading across multiple spatial dimensions creates an opportunity to increase spectral efficiency [3] by increasing channel capacity while keeping the frequency band fixed. Knowlege of the channel's spatial structure can be exploited through beamforming and linear precoding to improve data throughput. In a similar fashion, phased array radars control the spatial properties of its emissions through the beamforming weights independently applied at each element. These beamforming weights were generally very specific to the physical geometry of the radar scene. For example, beamforming vectors were designed on the array manifold, a manifold in the M_t-dimensional space which maximized power in the direction θ from array boresight. Adaptive beamforming vectors exist, which perturb beamforming vectors from the array manifold to consider other phenomenom such as imperfect calibration of the array and interference in the channel. MIMO communications, on the other hand, is not necessarily tied to the array manifold. Environments that contain a large amount of multipath, known as highly scattering channels, are non-line-of-sight (NLOS) and off the array manifold. A linear algebra interpretation of the channel is assumed, and beamforming vectors are optimized in the M_t-dimensional vector space. In fact, channel capacity gains are most readily had for highly scattering, non-line-of-sight channels, where the SNR-maximizing beamforming vector is not on the array manifold.

Much like MIMO wireless communications, MIMO radar transmit schemes are not strictly tied to the array manifold. In light of this, a lot of intuition is lost when designing the transmit signals. Transmit waveforms are optimized according to some criteria, such as power on target, interference minimization, target location estimation, or target velocity estimation [2, 4–6]. Generally these optimizations must be performed numerically, and transmit waveforms are derived with very little intuition to the user except that they satisfy given spatial, delay, and Doppler constraints. To

counteract this, hybrid transmit schemes based on the phased array yet utilizing the waveform diversity of MIMO radar were explored in [7–9]. These techniques logically divided the array into subarrays, where each subarray behaved as a phased array and beamformed in a single direction. This created a transmit framework that was highly intuitive to the designer and included multiple orthogonal transmit waveforms. These papers traded off waveform diversity for simplicity of the hardware configuration and increased power on target. The spatial domain (the individual antennas of the array) was divided up to handle multiple orthogonal transmit signals. In order to logically assign transmit elements to subarrays, the array aperture size decreased to a set of smaller subarray apertures. A decreased aperture size decreases the array gain. This leaves the question: can multiple orthogonal signals be transmitted without decreasing the array aperture? The answer is yes, by dividing up the temporal domain of the transmit signal instead of the spatial domain. This scheme, termed time-division beamforming, is explored in this dissertation.

To accomplish this, we introduce the ideology of linear precoding. The transmit signal is viewed as the product of two signals, the linear precoder and the pulse matrix. Linear precoders are popular for coherent wireless communications [10], where knowledge of the wireless channel is exploited at the transmitter for improved SNR at the receiver. Linear precoders take advantage of the channel structure through either instantaneous channel knowledge or knowledge of the channel's second order statistics and are able to exploit the virtually independent directions of the channel to transmit multiple symbol streams. This enables improved data throughput for wireless communication. In fact, it was shown that with perfect channel knowledge, the MIMO channel capacity is achieved through linear precoding [11].

Linear precoding was applied to MIMO radar to maximize power across multple spatial angles [12]. Although not explicitly stated as a linear precoder, the mathematical framework of linear precoding was used over multiple pulses in [13]. When linear precoding is applied to the radar transmit signal, it gives a simple structure that trades off beamforming gain with waveform diversity. Once again, this beamform-

ing gain makes use of the entire array aperture, not just a portion of it as subarray methods do.

Many of the numerical solutions for MIMO radar transmit signals do not incorporate the decades of research available for coded waveforms with specific delay and Doppler properties. They mainly focus on designing waveforms with specific spatial properties [6,14,15]. This limits the utility of current schemes in practice, as they are only optimized in the spatial domain. Time-division beamforming, the MIMO radar transmit scheme presented in this work, is able to independently control the spatial and delay-Doppler properties through its unique pulse matrix structure. This provides a transmit scheme for MIMO radar that leverages existing waveforms designed with ample range and Doppler resolution.

Radar systems are not the only technology that require careful design of the transmit signal to estimate parameters of the channel. We already discussed the dichotomy between radar and wireless communications, where the former estimates the channel and the latter estimates the transmit signal. The performance of coherent wireless communications is dependent on the ability to accurately estimate the channel. In wireless channel estimation, the transmit signal (often called pilots or training sequences) is strategically designed to minimize channel estimation error. This premise is similar to radar, with the difference being which channel information is considered useful. Physical parameters such as the angle of dominant scattering paths are not as important for wireless communications, which mainly focuses on estimating the $M_t M_r$ complex channel gains. For the second half of this dissertation, we turn our attention from radar to wireless communication channel estimation and apply realistic constraints for emerging MIMO technologies with a large number of transmit antennas.

Accurate channel estimation for wireless communication is required to maximize link throughput. Beamforming vectors and linear precoders are designed according to the channel estimate. Beamforming gain is a term used in the receive SNR function to measure the spatial gain achieved by matching the transmit weights to the structure

of the channel. Inaccurate channel estimates reduce beamforming gain, lowering the effective SNR on receive and decreasing channel capacity [16].

Due to its importance, standard MIMO techniques are well documented for channel estimation. [17–19]. They include minimum mean square error channel estimation, least squares channel estimation, and maximum likelihood channel estimation. Furthermore, the training sequence is specifically designed according to any prior knowledge of the channel, such as the channel's second order statistics. If this is the case, optimal training sequences were considered in [19] for uncorrelated Rayleigh fading channels and in [20] for correlated channels.

Training for wireless communication transmits pilots known at both the transmitter and receiver with the sole purpose to estimate the channel. Resources are devoted to training in order to accurately estimate the channel. Beamformers or linear precoders are designed with knowledge of the estimated channel to maximize receive SNR for data transmission. Similar to MIMO radar, the pilots need to be designed in order to extract useful information from the channel. This useful information is application specific. An example would be to extract a channel estimate that minimizes the mean square error from the true channel. For line of sight channels, the example might be to estimate the angle of the dominant scattering path.

A well known result for channel estimation shows the length of the training phase to be proportional to the number of antennas for uncorrelated Rayleigh fading [19]. For systems with a large number of antennas, the overhead associated with training may become impractical. Massive MIMO communications, a subset of MIMO communications that deals with a large number of antennas, has been initially proposed for time-division duplexing (TDD) systems as a result [21]. It has been shown that given an infinite number of antennas, matched filtering and eigenbeamforming become optimal [22], specifically for the multiuser case. The problem then becomes obtaining accurate channel estimates in massive MIMO without burdening the system with training [23]. Suboptimal methods must be employed to accurately estimate the channel without over burdening the communication system with training.

One could interpret training as a mechanism to sound the channel and make conclusions on the channel based on the output. This is the interpretation we carry forth and denote the training sequence as a set of sounding vectors. In essence, the transmitter sounds the channel, and the receiver estimates the channel from received samples. Suppose now a feedback link could be utilized during the training phase. Instead of designing the entire training sequence up front, the sounding vectors could be sequentially designed as a function of the feedback. The transmitter could then sound the channel, the receiver observe the output, determine the next sounding vector, and the receiver feed back the designated sounding vector for the next channel use. This sequence of events could be repeated multiple times throughout the training phase. The addition of the feedback link to training has the potential to improve channel estimation for shorter duration training intervals.

We implement this feedback-enabled training scheme for a multiple-input single-output (MISO) wireless channel. Given the feedback link, many aspects of this system still need to be addressed. Conventional channel estimators jointly estimate the channel direction and channel magnitude. As we will show, designing beamforming vectors to maximize beamforming gain requires accurate estimation of the channel direction only. We derive a generalized channel direction estimator to serve this purpose. In addition, it is not apparent how to design the sounding vector for the following channel use. We would like to design the sounding vectors to probe the channel in the most useful directions, with a maximal reduction of uncertainty in the channel estimate. The sounding vectors would probe the channel space in directions that reveal the most information about the channel. To accomplish this, we calculate the posterior distribution of the channel. The difficulty comes in minimizing the variance of this distribution as a function of the sounding vectors. We simplify the problem by discretizing the channel space; restricting it to lie in some discrete space. We then draw inspiration from communication theory and choose sounding vectors from a codebook which minimize the derived probability of misalignment.

Although this feedback-enabled training scheme increases the system complexity required for training, the promise of shorter training intervals makes it a viable scheme for massive MIMO systems. The coherence time, the approximate time a channel remains static, is completely dictated by the environment. Given optimal training, if the number of transmit antennas increases, the time required to train will also increase while the coherence time remains fixed. For small arrays, the training interval for optimal pilots is not a burden and the increased signal processing necessary to implement a feedback-enabled training scheme may not be practical. However, for massive MIMO systems, the conventional training schemes must be modified in order for training to remain feasible.

2. RADAR BACKGROUND

Radars perform the duties of detecting, tracking, or imaging targets [24]. These tasks can be accomplished through a variety of radar systems, such as pulsed, continuous wave, or SAR. This dissertation concentrates on pulsed radar systems, and specifically looks at target detection and how recent advances in radar technology can improve detection performance. A pulsed radar can be summarized by emitting short bursts (or pulses) of energy and analyzing the echo. Echoes are returned from targets of interest, targets not of interest, and stationary matter in the environment (clutter). Noise and interference in the frequency band of interest also exist and must be considered on receive. The echoes from targets not of interest may degrade receiver performance much like the addition of interference and noise. Similar to clutter, these echoes are functions of the transmitted pulse. As simple as the aformentioned pulsed radar system sounds, the intricacies of each aspect has been extensively studied over the years. We now review the basics of transmit emission and receive processing to extract useful information about the target.

2.1 Radar Fundamentals

Our expressions here consider a single pulse on transmit. In practice, multiple pulses are used, and target detection can be performed jointly across multiple pulses. Transmit pulses are separated by a period of time known as the pulse repitition interval (PRI), whose inverse is more commonly known as the pulse repitition frequency (PRF). The PRF can be a static or time-changing parameter, and plays a critical role in the resolvable target Doppler [25].

Let us consider a single transmit pulse. The real transmit signal is defined as,

$$\widetilde{x}(t) = a(t)\cos\big(2\pi f_c t + \theta(t)\big)$$

for $0 \leq t \leq T$. We define $a(t)$ as the amplitude modulation, $\theta(t)$ as the phase modulation, and f_c as the given carrier frequency. Both $a(t)$ and $\theta(t)$ are baseband signals. In complex analytic form, the transmit signal can be notationally simplified to,

$$\begin{aligned} \widetilde{x}(t) &= \Re\left[a(t)e^{j(2\pi f_c t+\theta(t))}\right] \\ &= \Re\left[x(t)e^{j2\pi f_c t}\right] \end{aligned} \tag{2.1}$$

where $\Re[\cdot]$ denotes the taking the real part of its argument, $e^{j2\pi f_c t}$ is the complex carrier sinusoid and the complex analytic baseband signal is

$$x(t) = a(t)e^{j\theta(t)}.$$

Viewing the radar transmit pulse (and later receive structure) in the complex analytic form improves clarity of the signal processing ideas presented and simplifies notation.

For radar systems with a single antenna, a single-target radar channel can be modeled by an attenuation constant and a reflection coefficient. For algorithm development, sometimes the path attenuation is lumped into the target's reflection coefficient. In accordance with electromagnetic theory, the emitted radar pulse $\widetilde{x}(t)$ will reflect off of a target with a reflection coefficient commonly referred to as the target's radar cross section (RCS).

Targets are generally modeled as a collection of individual scatterers, which give a large variation in the radar cross section as a function of look angle [25]. A common set of models to statistically represent fluctuations in RCS are known as Swerling target models [26].

Assume τ to be the round trip delay from a target at range R such that $\tau = 2R/c$. The baseband receive signal, assuming the complex analytic transmit signal of (2.1)

$$y(t) = \alpha x(t-\tau) + n(t)$$

where α is the complex scattering parameter and $n(t)$ is the stationary complex additive Gaussian noise.

The receive signal $y(t)$ represents the signal captured by the radar's receive antenna which is reflected from the target. The decision on whether a target is present or not can be made using the output of a matched filter as a sufficient statistic. Let us denote the matched filter as,

$$h(t) = x^*(-t).$$

The output of the matched filter is given as,

$$\begin{aligned}
(y * h)(t) &= \int_{-\infty}^{\infty} y(s)h(t-s)\,\mathrm{d}s \\
&= \int_{-\infty}^{\infty} y(s)x^*(-(t-s))\,\mathrm{d}s \\
&= \int_{-\infty}^{\infty} \left[\alpha x(s-\tau) + n(s)\right] x^*(s-t)\,\mathrm{d}s \\
&= \alpha \int_{-\infty}^{\infty} x(u)x^*(u-(t-\tau))\,\mathrm{d}u + \int_{-\infty}^{\infty} n(u+\tau)x^*(u-(t-\tau))\,\mathrm{d}u
\end{aligned}$$

where we use the substitution $u = s - \tau$. Sampling the output of the matched filter at $t = \tau$ will maximize the signal's SNR.

The above result assumes the target is stationary. For many airborne and terrestrial applications, the effect of target velocity on the radar return must be considered. In addition to a target's scattering coefficient, a target in motion will also impart a Doppler shift on the reflected signal. The Doppler shift is a compressive effect, but for narrowband signals simplifies to a shift in frequency. A waveform is considered narrowband if,

$$\frac{2vTB}{c} \ll 1$$

where TB is the time-bandwidth product, c the speed of light, and v the radial velocity of the target towards a stationary radar. Given the radial velocity v, the Doppler frequency is defined as,

$$f_d = \frac{2v}{\lambda}$$

where λ is the carrier's wavelength. The effect of Doppler on narrowband signals is easiest seen in the frequency domain, where the signal is shifted by f_d.

An important tool to analyze characteristics of the transmit signal resides in the ambiguity function. Definitions of the ambiguity function differ throughout the current literature. We define the ambiguity function slightly different from [27], where it is defined as the envelope of the output of a matched filter when the input to the filter is a time-delayed and Doppler-shifted version of the original signal. According to Figure 2.1, we define the ambiguity function in a similar manner but as the complex output y^{mf} instead of its magnitude. To set up the problem, we look at the output of the matched filter,

$$h(t) = x^*(-t)e^{j2\pi\widehat{\gamma}t}$$

which is matched to the transmitted signal. The output of the matched filter with a noiseless receive signal $y(t) = x(t-\tau)e^{j2\pi\gamma t}$,

$$\begin{aligned}
(y * h)(t) &= \int_{-\infty}^{\infty} y(s)h(t-s)\,\mathrm{d}s \\
&= \int_{-\infty}^{\infty} x(s-\tau)e^{j2\pi\gamma s}x^*(-(t-s))e^{-j2\pi\widehat{\gamma}s}\,\mathrm{d}s \\
&= \int_{-\infty}^{\infty} x(s-\tau)x^*(s-t)e^{j2\pi s(\gamma-\widehat{\gamma})}\,\mathrm{d}s \\
&= \int_{-\infty}^{\infty} x(u)x^*(u+\tau-t)e^{j2\pi(u+\tau)(\gamma-\widehat{\gamma})}\,\mathrm{d}u \\
&= e^{j2\pi\tau(\gamma-\widehat{\gamma})}\int_{-\infty}^{\infty} x(u)x^*(u-(t-\tau))e^{j2\pi u(\gamma-\widehat{\gamma})}\,\mathrm{d}u
\end{aligned}$$

where we let $u = s - \tau$ and generalize the Doppler term of the matched filter. If we sample the output at $t = \widehat{\tau}$,

$$\begin{aligned}
(y * h)(\widehat{\tau}) &= e^{j2\pi\tau(\gamma-\widehat{\gamma})}\int_{-\infty}^{\infty} x(u)x^*(u-(\widehat{\tau}-\tau))e^{j2\pi u(\gamma-\widehat{\gamma})}\,\mathrm{d}u \\
&= e^{j2\pi\tau(\gamma-\widehat{\gamma})}\int_{-\infty}^{\infty} x(u)x^*(u-\Delta\tau)e^{j2\pi u\Delta\gamma}\,\mathrm{d}u
\end{aligned}$$

where $\Delta\tau = \widehat{\tau} - \tau$ and $\Delta\gamma = \gamma - \widehat{\gamma}$. In this fashion, we can describe the complex ambiguity function as,

$$\chi(\tau,\nu) = e^{j2\pi\tau(\gamma-\widehat{\gamma})}\int_{-\infty}^{\infty} x(t)x^*(t-\Delta\tau)e^{j2\pi\Delta\gamma t}\,\mathrm{d}t$$

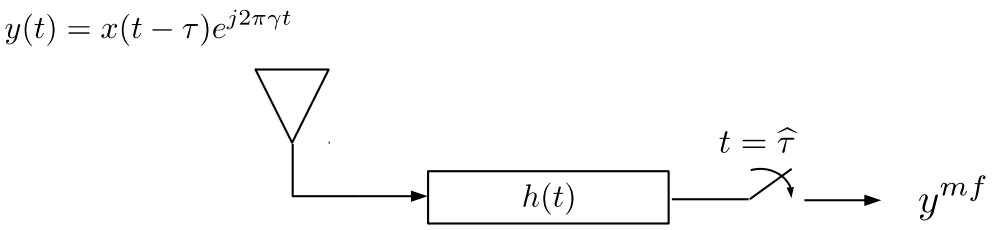

Fig. 2.1. A block diagram denoting the output to a matched filter with mismatched delay and Doppler parameters.

where $x(t)$ is the transmit signal, $\Delta\tau$ is the delay mismatch and $\Delta\gamma$ the Doppler mismatch of the matched filter to the incoming signal.

Another useful interpretation of the ambiguity function is explained as the correlation from the returns of two targets closely spaced in the delay and Doppler domain. The ambiguity function is a two-dimensional function useful in characterizing the resolution between two targets close in delay (range) and Doppler (velocity). As one will note, the conventional definition of the ambiguity function applies for a single waveform. Extensions to multiple transmit waveforms and receive matched filters exist, and the interpretation of the ambiguity function as the output of a matched filter for MIMO radar is addressed in this work. As a result, an understanding of the ambiguity function for a single waveform will remain essential for our later work, where we look at a generalization of the ambiguity function for MIMO radar.

2.2 Phased Array Radar

Phased array radar deals with the same objectives as traditional radar with the added capability of multiple antennas. Multiple antennas can aid in target detection through either an array of antennas on transmit, an array of antennas on receive, or both. For illustrative purposes, consider a linear array of M_r antennas on receive. If the target is assumed to be in the far field, the impinging wavefront on the receive array is assumed to be flat. Figure 2.2 illustrates an impinging wavefront from angle θ relative array boresight.

Due to the geometry of the problem, for a narrowband receive signal it can be approximated that each receive antenna observes the same signal with a specific phase shift given by the array geometry. Given the carrier wavelength λ, the angle of arrival θ, and the distance from array phase center as d_i, the phase shift for the i^{th} antenna is

$$\phi_i = \frac{2\pi}{\lambda} d_i \sin(\theta).$$

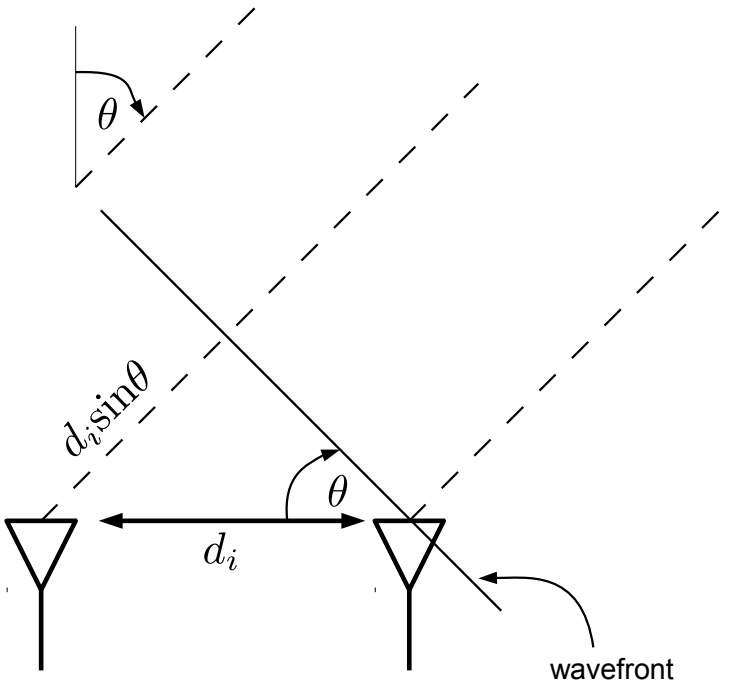

Fig. 2.2. Geometry of a linear array with an impinging wavefront. Details the additional distance traveled by the wavefront from one antenna to the next.

Putting this phase progression in vector form, we can define what is typically referred to as the *array manifold* or *steering vector*, where the first element is considered the array phase center,

$$\mathbf{a}_r(\theta) = \begin{bmatrix} 1 & e^{j\frac{2\pi}{\lambda}d_2\sin(\theta)} & \dots & e^{j\frac{2\pi}{\lambda}d_{M_r}\sin(\theta)} \end{bmatrix}$$

The array manifold is parameterized by the angle of arrival, θ, of the impinging wavefront from array boresight. Array boresight is the direction perpendicular to the dimension of the array. The array manifold interpretation simplifies for uniform linear arrays (ULA) as,

$$\mathbf{a}_r(\theta) = \begin{bmatrix} 1 & e^{j\frac{2\pi}{\lambda}d\sin(\theta)} & \dots & e^{j(M_r-1)\frac{2\pi}{\lambda}d\sin(\theta)} \end{bmatrix}$$

where d is the common spacing between each and every element. A general rule-of-thumb for array designers is to space antenna elements a distance of $\lambda/2$ apart from each other. The reason for this is two-fold; any greater spacing would alias the spatial sampling and result in grating lobes [25], and any closer spacing would increase the mutual coupling [28]. Hence, if we set $d = \lambda/2$, the array manifold expression simplifies even further as,

$$\mathbf{a}_r(\theta) = \begin{bmatrix} 1 & e^{j\pi\sin(\theta)} & \dots & e^{j(M_r-1)\pi\sin(\theta)} \end{bmatrix}$$

Conventional phased array systems phase shift and combine the output of each antenna in the array on receive. In the radar literature, this is referred to as *receive beamforming*. In the wireless communications literature, this is commonly referred to as *receive combining*. No matter the label used, the result is shown in Figure 2.3, where $w_i e^{j\phi_i}$ represent the complex weights applied to each antenna. Mathematically, this can be written in vector form as,

$$\mathbf{w} = \begin{bmatrix} w_1 e^{j\phi_1} & w_2 e^{j\phi_2} & \dots & w_{M_r} e^{j\phi_{M_r}} \end{bmatrix}^*.$$

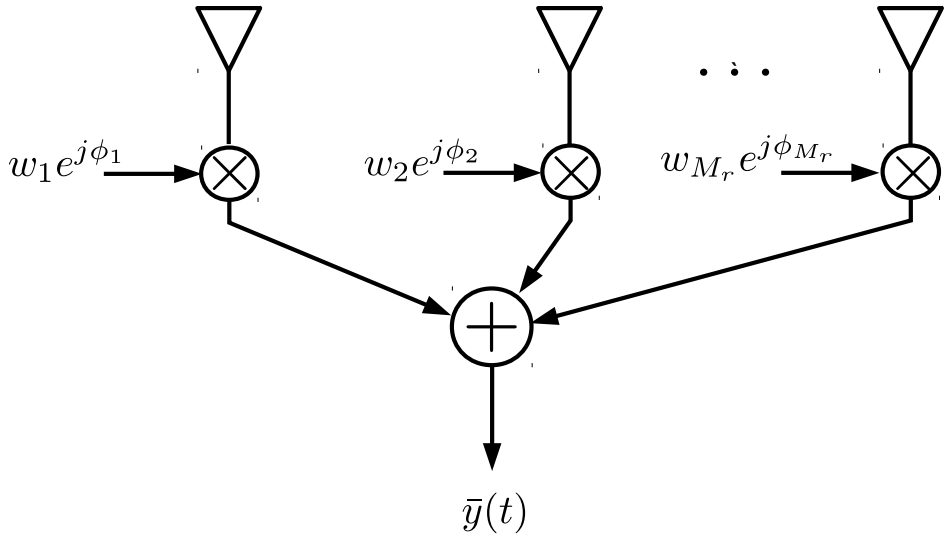

Fig. 2.3. The receive beamformer weights the output from each antenna and sums them to produce output $\bar{y}(t)$.

Let us define the receive signal at each element of the phased array as,

$$\mathbf{y}(t) = \begin{bmatrix} y_1(t) \\ y_2(t) \\ \vdots \\ y_{M_r}(t) \end{bmatrix}.$$

After receive beamforming, the scalar output is given by,

$$\bar{y}(t) = \mathbf{w}^* \mathbf{y}(t).$$

In general, these amplitude and phase weights are time-independent and remain fixed for the entire pulse duration. They can be adjusted on a pulse-by-pulse basis. However, as technology improves, this restriction may no longer be relevant and improved receive processing may result. The ability to generalize receive beamforming to replace the scalar weights by matched filters (or sets of matched filters) sets the foundation for the mathematics of MIMO radar.

2.3 MIMO Radar

Phased array radars have been known to provide increased target detection due to their ability to spatially distribute transmit power in the radar channel. From a hardware perspective, a single high power amplifier is no longer required, as was the case for a single antenna. The task of amplifying the transmit signal can now be distributed across the array aperture, with a power amplifier behind each transmit element. With the addition of phase shifters at each element, the array can electronically steer its transmit beam by controlling each element's phase shift; a huge benefit over mechanically steered antennas. These advantages have led to the widespread adoption of phased array radars.

Wireless communications saw capacity improvements with the capability to transmit and receive using multiple antennas. In addition to phased array techniques for communications, which increased receive SNR, the increase in available spatial dimensions for high scattering channels provided the structure to transmit multiple symbol streams. The wireless channel capacity has been shown to scale with the number of antennas (specifically the minimum number of antennas at either the transmitter or receiver [3]). The ability to increase the capacity of a link by fixing the bandwidth (hence increasing spectral efficiency) prompted a large interest in MIMO wireless communications.

The ability to transmit linearly independent waveforms out of each array element is improving radar in a manner similar to wireless communications. Waveform diversity allows increased performance of target detection, angle of arrival, localization, and target tracking [29]. There are two major classifications for MIMO radar; noncoherent MIMO radar [1, 2] and coherent MIMO radar [30]. The work of this dissertation focuses on the latter. Noncoherent MIMO radar expands traditional multistatic radar with geographically disparate transmitting and receiving sites. It is assumed the receivers are separated far enough from each other that the returns from the target to each receiver are subject to different scattering, as shown in Figure 2.4. This

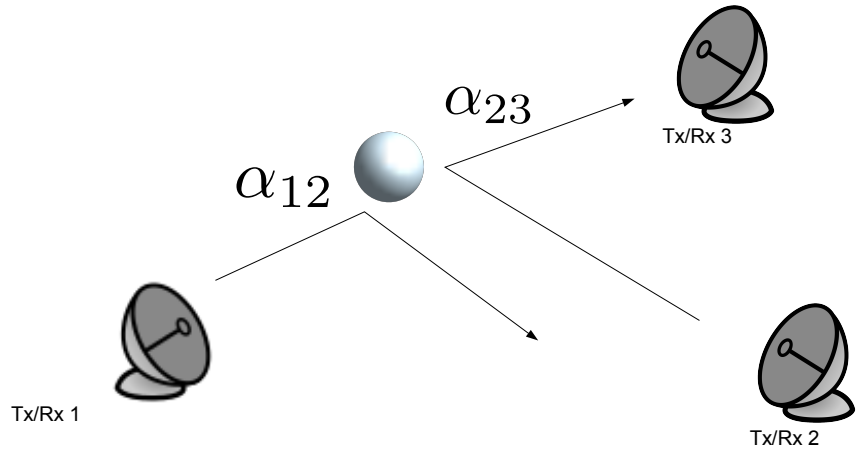

Fig. 2.4. Noncoherent MIMO radar with geographically separated transmit and receive antennas.

reduces the chance that each and every return from the target experiences a large attenuation due to poor scattering from the target. The terminology and methods in the noncoherent MIMO radar literature are closely related to rich scattering channels in communications, and performance can be written in a similar language. However, noncoherent MIMO radar suffers from the challenges of synchronizing the widely spaced transmit and receive sites to achieve such gains.

Coherent MIMO radar is the framework used in this work to define time-division beamforming. It assumes the transmit elements (and the receive elements) are closely spaced to each other. The size of the aperture for the transmit or receive array is on the order of wavelengths. Hence, all emitted waveforms experience the same scattering for a target in the far field. Although coherent MIMO suffers from low backscatter due to the coherent scattering assumption, its principles are directly applicable to implement on antenna arrays. Arrays have already proven themselves useful in radar applications (i.e., phased arrays) and coherent MIMO radar promises to be the next step.

The current state of the art for coherent MIMO systems is summarized in the tutorial paper of [30]. We now present the mathematical framework for classical MIMO radar and show its properties.

MIMO radar provides the capability to transmit linearly independent waveforms from each antenna. This is an improvement over phased array radar, which transmits the same waveform which is phase shifted and/or amplitude weighted at every element. For a MIMO radar with M_t transmit antennas, we define the continuous time transmit signal

$$\mathbf{X}(t) = \begin{bmatrix} x_1(t) \\ x_2(t) \\ \vdots \\ x_{M_t}(t) \end{bmatrix}.$$

The transmit signal is restricted by a total power constraint, defined as

$$\int_{-\infty}^{\infty} \mathbf{X}^*(t)\mathbf{X}(t)\, \mathrm{d}t \leq \rho$$

where it is assumed $x_i(t)$ has support on the interval $[0, T]$. The time-covariance matrix for a length T transmit signal is defined as,

$$\mathbf{R} = \int \mathbf{X}(t)\mathbf{X}^*(t)\, \mathrm{d}t.$$

The transmit time-covariance matrix is used to calculated the transmit beampattern, which is a measure of the transmit energy distributed in space,

$$S(\theta) = \mathbf{a}_t^*(\theta)\mathbf{R}\mathbf{a}_t(\theta) \tag{2.2}$$

where $\mathbf{a}_t(\theta)$ is the transmit steering vector towards angle θ.

In its most general case, MIMO radar considers a set of M_t orthogonal waveforms to be transmitted from the M_t antennas. This orthogonality constraint simplifies the transmit time-covariance matrix to $\mathbf{R} = \frac{\rho}{M_t}\mathbf{I}$. Consequently, plugging $\mathbf{R} = \frac{\rho}{M_t}\mathbf{I}$ into (2.2) gives a beampattern that is independent of angle. Herein reveals one of the largest benefits of MIMO radar: an omnidirectional beampattern. Spatial knowledge

of the radar scene does not need to be known in advance. MIMO radar's biggest advantage can also be its largest drawback: an omnidirectional beampattern lacks an increase in power on target and cannot take advantage of the array gain. To illustrate this, we show a simple example of power on a target located at angle θ from transmit array boresight. For a MIMO radar with orthogonal signaling and $\|\mathbf{X}\|_F^2 = \rho$, the power on target is denoted as,

$$\begin{aligned} P_{\text{MIMO}} &= |\mathbf{a}_t^*(\theta)\mathbf{X}|^2 \\ &= \mathbf{a}_t^*(\theta)\mathbf{X}\mathbf{X}^*\mathbf{a}_t(\theta) \\ &= \mathbf{a}_t^*(\theta)\left(\frac{\rho}{M_t}\mathbf{I}\right)\mathbf{a}_t(\theta) \\ &= \frac{\rho}{M_t}\|\mathbf{a}_t(\theta)\|^2 \\ &= \rho \end{aligned}$$

where the array manifold has norm $\|\mathbf{a}_t(\theta)\|^2 = M_t$. Now consider the phased array transmit signal, with a single transmit waveform $\mathbf{X} = \mathbf{f}\mathbf{p}^*$. We let the beamforming vector steer towards θ, $\mathbf{f} = \frac{\mathbf{a}_t(\theta)}{\sqrt{M_t}}$ with $\|\mathbf{f}\|^2 = 1$ and $\|\mathbf{p}\|^2 = \rho$. This gives the same total power constraint as for the MIMO transmit signal, namely $\|\mathbf{X}\|_F^2 = \rho$. The power on target is,

$$\begin{aligned} P_{\text{PA}} &= |\mathbf{a}_t^*(\theta)\mathbf{X}|^2 \\ &= \mathbf{a}_t^*(\theta)\mathbf{f}\mathbf{p}^*\mathbf{p}\mathbf{f}^*\mathbf{a}_t(\theta) \\ &= \rho\mathbf{a}_t(\theta)\mathbf{f}\mathbf{f}^*\mathbf{a}_t(\theta) \\ &= \rho M_t. \end{aligned}$$

From this canonical example, the phased array is able to increase the power on target by a factor of M_t, which is equal to the number of transmit elements. This is commonly referred to as the array gain for phased array, which explains the ability of the signal emissions from each antenna to constructively interfere at a specific angle. This is in contrast to the given orthogonal MIMO radar transmit signal example, where the orthogonal waveforms cannot coherently combine for any specific angle.

In general, the MIMO radar literature is not restricted to orthogonal signal sets. Hybrid schemes, where the number of orthogonal waveforms is less than the number of transmit antennas, are also considered as a colocated MIMO radar technology. The number of orthogonal waveforms can be observed by the rank of the transmit time-covariance matrix, where a set of M_t orthogonal waveforms will give a full-rank covariance matrix and a phased array radar transmit signal will give a rank-1 covariance matrix. This leaves an open area to design signal sets whose time-covariance matrix is of arbitrary rank. Time-division beamforming presents a simple and intuitively pleasing solution to this problem.

3. TIME-DIVISION BEAMFORMING FOR MIMO RADAR

3.1 Introduction to Time-Division Beamforming

The ability of MIMO radars to transmit linear independent waveforms gives flexibility to improve multiple target detection and estimation over legacy phased array systems. The returns from multiple targets were shown to be linearly independent in [31], where adaptive receive beamforming was shown to improve multiple target detection performance. Signal design becomes a challenge as it has been shown the transmit beampattern is a function of the auto- and cross-correlations of the transmit signals [32]. Commonly, MIMO radars transmit orthogonal waveforms out of each transmit antenna [33]. This waveform orthogonality is achieved through waveform coding (amplitude, phase, or both), and, with the use of isotropic array elements, the MIMO radar produces an omnidirectional beampattern. However, an omnidirectional beampattern is not always desirable. In some applications, it may be required to cohere power in certain spatial directions, accomplished through careful design of the transmit signal cross-correlations [32]. To further complicate matters, clutter in the radar scene may reduce the benefits of orthogonal waveforms on transmit. In [34], a set of waveforms with low auto- and cross-correlations performed poorly due to an inability to cancel out interference from clutter. To characterize this, a MIMO cancellation ratio is introduced to serve as an alternative metric to design adaptive MIMO radar waveforms.

In the co-located MIMO radar literature, transmit signal design can be divided into two stages. First, a transmit signal covariance matrix $\mathbf{R}$ is obtained for a direc-

tional beampattern $S(\theta)$ according to some continuous or discrete measure. Second, the transmit signal $\mathbf{X}$ is designed to match the given covariance matrix $\mathbf{R}$. In [6], a sequential quadratic programming is presented which designs a covariance matrix $\mathbf{R}$ to match a particular beampattern. Given a desired full rank $\mathbf{R}$, a suitable transmit signal can be derived by a number of matrix decomposition methods, such as eigenvalue or Cholesky decomposition. In general, transmit signals designed using these methods are amenable to a total power constraint. To solve for a transmit signal under a constant modulus constraint, an iterative approach [35] and a random approach [32] have been developed. No guarantees, however, can be made as to how closely the transmit signal covariance matrix matches a desired $\mathbf{R}$.

Low rank covariance matrices may be of interest, especially if hardware limitations restrict the number of linear independent waveforms emitted from the array. Optimization techniques for MIMO radar waveform design with low-rank covariance matrices were considered in [36, 37]. Subarray techniques, presented in [7–9], are alternative ways of designing low rank covariance matrices. Subarray MIMO radars are designed with $M < M_t$ orthogonal waveforms and form a covariance matrix with rank M.

If a priori information on targets, clutter, or noise is present, one may wish to maximize target detection or parameter estimation performance. This relaxes the objective of designing the transmit signal to match a given beampattern and places more focus on the target, clutter, and noise information. Maximizing power in the direction of known or estimated targets is discussed in [6], where sequential quadratic programming methods design signals to approximate given beampatterns. Optimization of the signal to interference plus noise ratio (SINR) for multiple targets was investigated in [38] due to its widespread use for the single target case. Similar to this paper, it was noted that a max-min opimization was required to accurately estimate the scattering coefficients of multiple targets. An information theoretic objective was introduced in [38], which combines metrics such as power on target, SINR, and separation of the target and clutter subspaces. In this work, we use a similar max-

min approach to optimize the time-division beamforming signal for receive SINR. Extending the ideas and advantages of the phased array to the MIMO radar, [7] introduces the notion of disjoint subarrays and [8, 9] design the transmit signal using overlapping subarrays. The idea of dividing the total transmit array into subarrays, where the transmit signal is designed according to subarray steering vectors, trades off advantages of the phased array and omnidirectional MIMO radar.

Time division multiple access (TDMA) and beamspace MIMO motivate the time-division beamforming transmit scheme presented in this work. TDMA in wireless communications schedules users in non-overlapping time slots. In radar, TDMA commonly refers to transmitting from a single element at a time [39]. For beamspace MIMO [40], the transmit signal is represented by its singular value decomposition, $\mathbf{X} = \mathbf{USV}^*$, where the columns of $\mathbf{U}$ represent the set of transmit beamforming vectors transmitted simultaneously inside a given pulse $\mathbf{X}$. Hence, for a given pulse, the transmit signal is a weighted sum of the beamforming vectors. Slow-time beamspace MIMO [13, 41] designs the transmit signal across multiple pulses (in slow-time), while making note of its use in fast-time. Time-division beamforming leverages these ideas to create a signal that temporally multiplexes beamforming vectors.

3.2 System Setup

A target is considered to lie in the same plane as the antenna array such that the its position can be described using two-dimensional spherical coordinates (r_0, θ_0), where r_0 represents the distance from a set of co-located[1] transmit and receive arrays and θ_0 is the target's angle from array boresight. The target is assumed to be in the array's far field, such that the impinging signal on the receive array is viewed as a plane wave. The receiver samples the output of the matched filters for range ($\widehat{r}_0$ and the receive beamformer samples the angle bin centered at $\widehat{\theta}_0$). The array structure

[1]For the transmit and receive array to be co-located, the target range r_0 must be much larger than the separation between transmit and receive array such that both arrays view the target at the same angle.

can be general in nature (this work is not restricted to uniform linear arrays), with only an array phase center and a reference angle (termed array boresight) required. A signal is transmitted from the m^{th} transmit element, reflected from a single target with delay $\tau_0 = 2r_0/c$, Doppler γ_0, and angle θ_0, and received at the j^{th} receive element is described by baseband signal

$$y_j(t) = \alpha_0 x_m(t-\tau_0) e^{j\psi_m} e^{j\psi_j} e^{j2\pi\gamma_0 t} + v(t)$$

where α_0 is the target's radar cross section (RCS), ψ_m (ψ_j) is the phase shift induced by the path between the m^{th} transmit element (j^{th} receive element) and the target, and $v(t)$ is the continuous time complex additive white Gaussian noise with $v(t) \sim \mathcal{CN}(0, \sigma_n^2)$. For narrowband signals, we can approximate the receive signal at a given element as a phase shifted version of the receive signal at the phase center of the array. In vector form, this is best represented by the array steering vectors. The signal received by all M_r elements in vector form

$$\mathbf{Y}(t) = \alpha_0 \mathbf{a}_r(\theta_0)\mathbf{a}_t^*(\theta_0)\mathbf{X}(t-\tau_0)e^{j2\pi\gamma_0 t} + \mathbf{V}(t) \tag{3.1}$$

where $(\cdot)^*$ denotes complex conjugate transpose, $\mathbf{V}(t) \sim \mathcal{CN}(\mathbf{0}, \sigma_n^2\mathbf{I})$ describes the independent and identically distributed additive white Gaussian noise vector at the M_r receive elements, $\mathbf{X}(t-\tau_0)$ is the set of M_t transmit signals with delay τ_0, and $\mathbf{a}_t(\theta_0)$, $\mathbf{a}_r(\theta_0)$ represent the transmit and receive steering vectors, respectively. Although the results of this paper hold for a general array structure, the simulations presume a uniform linear array with interelement spacing d and transmit and receive steering vectors of the form,

$$\begin{aligned}
\mathbf{a}_t^*(\theta) &= \begin{bmatrix} 1 & e^{j\frac{2\pi}{\lambda}d\sin(\theta)} & \dots & e^{j\frac{2\pi}{\lambda}(M_t-1)d\sin(\theta)} \end{bmatrix} \\
\mathbf{a}_r^T(\theta) &= \begin{bmatrix} 1 & e^{j\frac{2\pi}{\lambda}d\sin(\theta)} & \dots & e^{j\frac{2\pi}{\lambda}(M_r-1)d\sin(\theta)} \end{bmatrix}
\end{aligned}$$

where λ is the carrier wavelength.

A MIMO radar has the ability to transmit different waveforms from each of the M_t elements in the array, and in general can be described by

$$\mathbf{X}(t) = \begin{bmatrix} x_1(t) \\ x_2(t) \\ \vdots \\ x_{M_t}(t) \end{bmatrix}.$$

The m^{th} baseband transmit signal is composed of a shifted chip waveform modulated by complex amplitude scalars,

$$x_m(t) = \sum_{n=1}^{N} x_{m,n}\, u\left(t - (n-1)t_b\right) \tag{3.2}$$

where $u(t)$ is the unit-energy length t_b chip waveform, $x_{m,n} \in \mathbb{C}$ is the complex chip value, and the transmit signal is of length $T_0 = t_b N$. The discrete MIMO radar transmit signal is then defined by the $M_t \times N$ matrix $\mathbf{X}$, where $[\mathbf{X}]_{m,n} = x_{m,n}$.

The discrete transmit signal will be constrained under a total power constraint,

$$\operatorname{tr}\left(\mathbf{X}\mathbf{X}^*\right) \leq \rho N \tag{3.3}$$

where ρ is a power scale factor.

3.3 Time-Division Beamforming

For a single transmission in a pulsed co-located MIMO radar, the current MIMO radar literature (see [33] for an overview) emphasizes the use of orthogonal waveforms at the transmitter. Orthogonality of the M_t waveforms is commonly achieved via waveform coding, an idea similar to spatial multiplexing in MIMO wireless communications [17]. Implementation of waveform orthogonality in the spatial domain gives subarray MIMO radars [7–9], where an orthogonal waveform is transmitted from each spatially disparate subarray. Beamspace MIMO radars [40] transmit waveforms on orthogonal beams, where the beamforming vectors are orthogonal in the M_t-dimensional space. With these types of orthogonal MIMO radars in mind, we

propose an additional transmit scheme consisting of orthogonal waveforms in the time domain.

Time-division beamforming is defined through temporally multiplexing a set of pulses onto different beamforming vectors. Before we mathematically introduce the structure of time-division beamforming, we first define linear precoding as a design technique that resolves the transmit signal into a product of two matrices [10]

$$\mathbf{X}(t) = \mathbf{F}\mathbf{P}(t). \tag{3.4}$$

The M_t-element transmit signal matrix $\mathbf{X}(t)$ is the product of a linear precoder $\mathbf{F} \in \mathbb{C}^{M_t \times M}$ and an M-element continuous pulse matrix $\mathbf{P}(t)$, where $1 \leq M \leq M_t$. Time-division beamforming uses the linear precoding framework with a specific pulse matrix, namely

$$\begin{aligned} \mathbf{X}(t) &= \mathbf{F}\mathbf{P}(t) \\ &= \begin{bmatrix} \mathbf{f}_1 & \mathbf{f}_2 & \cdots & \mathbf{f}_M \end{bmatrix} \begin{bmatrix} p_1(t) \\ p_2\left(t - \frac{T_0}{M}\right) \\ \vdots \\ p_M\left(t - (M-1)\frac{T_0}{M}\right) \end{bmatrix} \end{aligned} \tag{3.5}$$

where $\mathbf{f}_m$ is an $M_t \times 1$ beamforming vector with $\sum_{m=1}^{M} \|\mathbf{f}_m\|^2 = \rho/M$, ρ is a power scaling factor, and the pulse matrix is comprised of time-shifted instances of subpulses, $p_m(t)$, each with with support $[0, \frac{T_0}{M}]$. The subpulse is defined in terms of chip waveforms,

$$p_m(t) = \sum_{n=1}^{N/M} p_{mn}\, u\left(t - (n-1)t_b\right)$$

where $u(t)$ is the unit-energy length t_b chip waveform and $p_{mn} \in \mathbb{C}$ is the complex chip value. The continuous time subpulse is similar to the continuous time transmit signal in (3.2) with reduced support. The M pulses in (3.5) are *temporally orthogonal* as they are time-shifted by T_0/M, equal to the support of $p_m(t)$. This is depicted graphically in Figure 3.1. Under similar assumptions to [33], we model the set of M

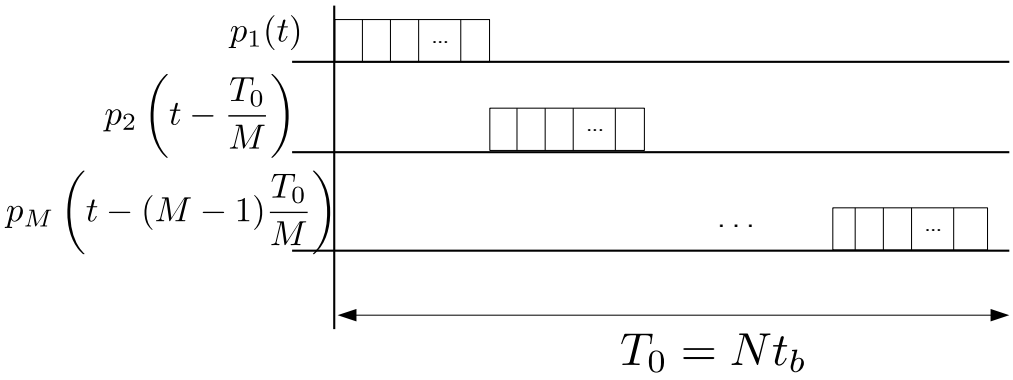

Fig. 3.1. A pictorial representation of the M pulses with temporal orthogonality.

subpulses as orthogonal,

$$\int p_m(t)p_n(t-\tau)\,\mathrm{d}t \approx 0 \tag{3.6}$$

for all m, n, τ excluding the self correlation case ($m = n$ at $\tau = 0$). The discrete subpulse $\mathbf{p}_m = \left[p_{m1}, p_{m2}, \ldots p_{m\frac{N}{M}}\right]$ is constrained such that $\|\mathbf{p}_m\|^2 = N$. Typically $N \gg M$, and hence we assume N/M is an integer. The transmit signal of (3.5) can also be interpreted as the set subpulses successively projected onto the M beamforming vectors,

$$\mathbf{X}(t) \;=\; \sum_{m=1}^{M} \mathbf{f}_m p_m\left(t-(m-1)\frac{T_0}{M}\right).$$

Inspecting the transmit signal with a finer temporal granularity, the time-division beamforming transmit signal is subdivided into M subintervals. For each subinterval, the m^{th} subpulse is projected onto the m^{th} beamforming vector. These subintervals are non-overlapping; a single beamforming vector is transmitted for each subinterval. This allows for easy implementation of multiple beamforming vectors with a per-element transmit power constraint or the requirement for constant modulus signals transmitted out of each element. A visual representation of time-division beamforming is shown in Figure 3.2. This normalized plot shows the transmit signal as a function of spatial angle and time (within T_0) for $M = 3$. The beamforming vectors are set to the array manifold of an $M_t = 9$ element array, with $\mathbf{f}_m = \sqrt{\frac{\rho}{M_t M}}\mathbf{a}_t(\theta_m)$. The sum beampattern, which is the instantaneous beampattern integrated over the entire pulse duration, is shown in Figure 3.3. Much like the interpretation in [42], the sum beampattern is the sum of each subinterval's beampattern. For the case presented, the sum beampattern is the sum of the three beams pointed in three different directions.

Note that time-division beamforming generalizes the concept of a phased array and always includes phased array transmission as a special case. Consider a phased array transmission $\mathbf{f}_{\text{phase}}p_{\text{phase}}(t)$ where $\mathbf{f}_{\text{phase}}$ denotes a ρ-norm beamforming vector and $p_{phase}(t)$ represents a pulse with energy N having support $[0, T_0]$. Typically $\mathbf{f}_{\text{phase}}$ is chosen using the transmit array respone vector as $\mathbf{f}_{\text{phase}} = \sqrt{\frac{\rho}{M_t}}\mathbf{a}_t(\widehat{\theta}_0)$.

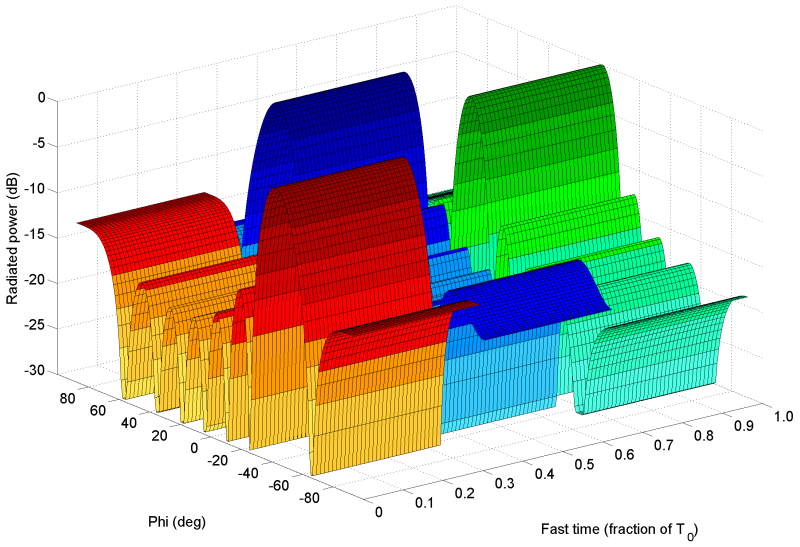

Fig. 3.2. Time-division beamforming transmit signal with $M = 3$ subintervals, designed for targeting spatial angles $\boldsymbol{\theta} = [-40°, 45°, 5°]$.

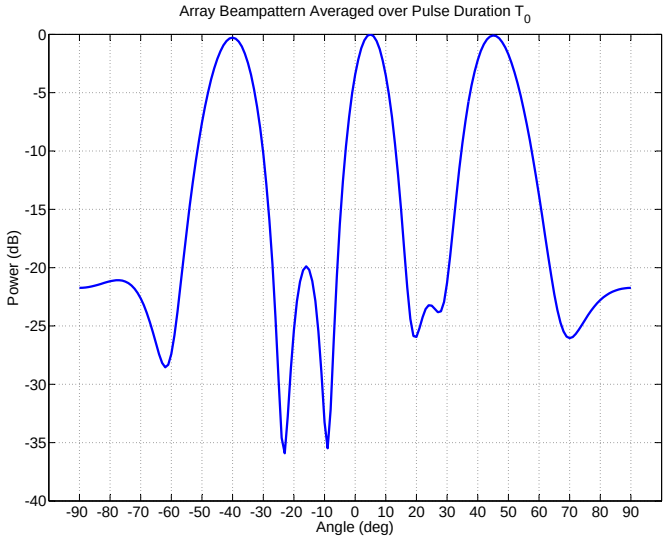

Fig. 3.3. Sum beampattern for the time-division beamforming signal of Figure 3.2.

This single phased array pulse can be written in time-division beamforming notation by letting $p_m(t) = \sqrt{\frac{N}{\mathcal{E}_m}} p_{phase}\left(t + (m-1)\frac{T_0}{M}\right)$ for $0 \leq t \leq \frac{T_0}{M}$ where $\mathcal{E}_m = \int_{(m-1)\frac{T_0}{M}}^{m\frac{T_0}{M}} |p_{\text{phase}}(t)|^2 \, \mathrm{d}t$. The beamforming vectors are defined as $\mathbf{f}_m = \sqrt{\frac{\rho \mathcal{E}_m}{M_t N}} \mathbf{a}_t(\widehat{\theta}_0)$. The pulse $p_{\text{phase}}(t)$ can then be written as,

$$p_{\text{phase}}(t) = \sum_{m=1}^{M} \sqrt{\frac{\mathcal{E}_m}{N}} p_m \left(t - (m-1)\frac{T_0}{M}\right)$$

Intrapulse steering and its effect on the transmit signal's beampattern were observed in [43, 44]. The transmit beampattern specifies the amount of power radiated as a function of angle from array boresight. For narrowband signals, it can be written as a function of the transmit matrix,

$$S_T(\theta) = |\mathbf{a}_t^*(\theta)\mathbf{X}|^2 \tag{3.7}$$

where θ is the angle from array boresight. To more accurately describe $S_T(\theta)$, we label it as the sum beampattern since it characterizes the amount of power directed towards a specific angle over the entire pulse duration, $T_0 = t_b N$. The sum beampattern can be expressed as the sum of instantaneous beampatterns,

$$S_T(\theta) = \sum_{n=1}^{N} |\mathbf{a}_t^*(\theta)\mathbf{x}_n|^2 .$$

We term the beampattern produced by each column of the transmit signal matrix, $S_n(\theta) = |\mathbf{a}_t^*(\theta)\mathbf{x}_n|^2$, as the instantaneous beampattern. Hence, the sum beampattern can be formed by beamspoiling or intrapulse beamsteering [43], and better control of the sum beampattern can be had by designing $\mathbf{x}_n$ [44]. It is interesting to point out that even if the sum beampattern is omnidirectional, the instantaneous beampattern may be very directive in nature. Time-division beamforming builds upon these observations, providing a clear example of a MIMO transmit signal with intrapulse steering according to the M beamforming vectors.

With the assumption that $M \leq M_t \leq N$, the rank$(\mathbf{R}) \leq M$ is completely determined by the beamforming vectors. We note that the transmit signal covariance matrix is,

$$\mathbf{R} = \frac{1}{N} \int \mathbf{X}(t)\mathbf{X}^*(t) \, \mathrm{d}t = \mathbf{F}\mathbf{F}^*.$$

This indicates time-division beamforming covariance matrices are intrinsically low-rank, and serve as an alternative design strategy towards the optimization in [36] to design transmit signals with low-rank covariance matrices. Observe that given the linear precoding framework with orthogonal pulses, the transmit beampattern reduces to,

$$\begin{aligned} S_T(\theta) &= N\mathbf{a}_t^*(\theta)\mathbf{R}\mathbf{a}_t(\theta) \\ &= N\mathbf{a}_t^*(\theta)\mathbf{F}\mathbf{F}^*\mathbf{a}_t(\theta). \end{aligned}$$

We can then conclude the transmit beampattern in (3.7) is only a function of the beamforming vectors in $\mathbf{F}$. The pulse matrix, which includes the set of orthogonal subpulses, has no impact on the transmit beampattern.

In many ways, time-division beamforming is similar to subarray MIMO radar transmit schemes. In general, subarray schemes divide the M_t element array into M subarrays. One of M orthogonal waveforms is transmitted from a subarray of M_t/M elements for a duration of T_0. In comparison, time-division beamforming transmits one of M orthogonal waveforms from M_t elements for a duration of T_0/M. The tradeoff lies in the fact that subarray schemes use fewer elements to transmit for a longer duration, where time-division beamforming uses more elements to transmit for a shorter duration. The advantage of time-division beamforming lies in it's beamforming gain; using the full array at any given time. This tradeoff will be analyzed with the receive SINR performance metric later in the paper.

3.3.1 Receiver Design

The linear MIMO radar receiver applies matched filtering and receive combining (also referred to as receive beamforming) to the target return received in the presence of interference and additive noise. The linear receive model will be developed for a single target case, and subsequently extended to the M target scenario. In [4], it was shown that a set of matched filter outputs form a sufficient statistic for angle estimation and target detection given orthogonal waveforms on transmit. If the

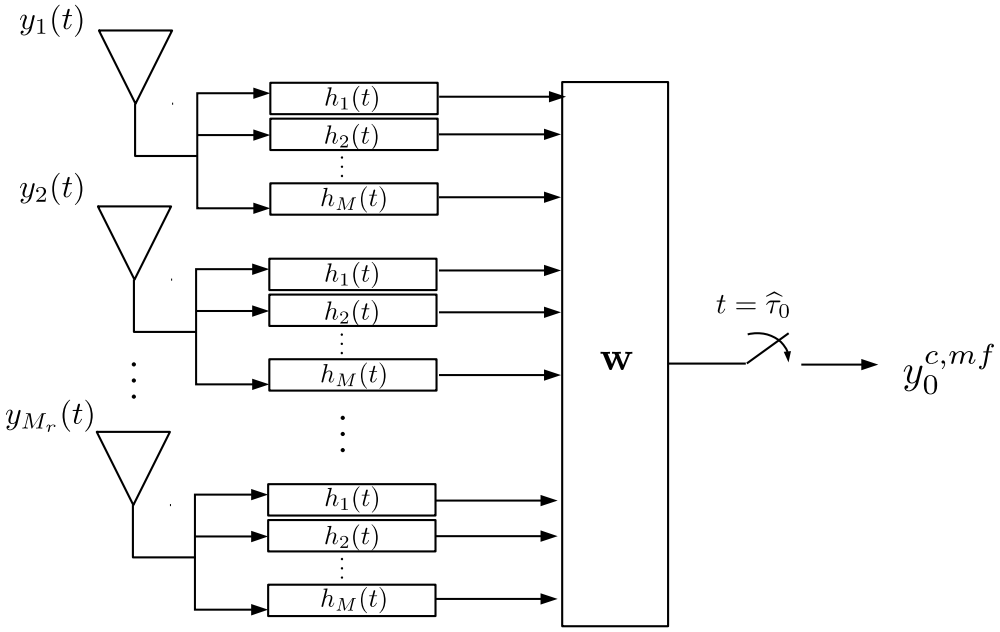

Fig. 3.4. A linear receiver with a bank of M matched filters behind each receive element and a linear receive combiner $\mathbf{w}$.

transmit signal is designed using the linear precoder in (3.4), the receiver need only contain a bank of M matched filters behind each receive element. The bank of M matched filters are denoted by an $M \times 1$ vector $\mathbf{H}(t) = \frac{1}{N}\mathbf{P}^*(-t)e^{j2\pi\widehat{\gamma}_0 t}$. As shown in Figure 3.4, this bank of matched filters is replicated behind each antenna element, where $h_m(t) = \frac{1}{N}p_m^*((m-1)\frac{T_0}{M} - t)e^{j2\pi\widehat{\gamma}_0 t}$ is the m^{th} element of $\mathbf{H}(t)$. After matched filtering, the received signal (up to a constant phase ambiguity due to Doppler) is described by an $M_r \times M$ matrix $\mathbf{Y}^{mf}(\Delta\tau_0, \Delta\gamma_0, \theta_0, \widehat{\theta}_0)$,

$$\mathbf{Y}^{mf}(\Delta\tau_0, \Delta\gamma_0, \theta_0, \widehat{\theta}_0) \;=\; \alpha_0 \mathbf{a}_r(\theta_0)\mathbf{a}_t^*(\theta_0)\mathbf{F}\boldsymbol{\mathcal{X}}_p(\Delta\tau_0, \Delta\gamma_0) + \bar{\mathbf{V}} \tag{3.8}$$

where $\Delta\tau_0 = \widehat{\tau}_0 - \tau_0$ and $\Delta\gamma_0 = \gamma_0 - \widehat{\gamma}_0$ are the delay and Doppler mismatch, respectively, and $\bar{\mathbf{V}}$ is the noise correlation matrix after matched filtering with $\text{vec}\left(\bar{\mathbf{V}}\right) \sim$

$\mathcal{CN}(0, \frac{\sigma_n^2}{N}\mathbf{I})$. The pulse correlation matrix $\boldsymbol{\mathcal{X}}_p(\Delta\tau_0, \Delta\gamma_0)$ is the output of the matched filter bank to the set of M pulses mismatched in delay by $\Delta\tau_0$ and Doppler by $\Delta\gamma_0$,

$$\boldsymbol{\mathcal{X}}_p(\Delta\tau_0, \Delta\gamma_0) = \frac{1}{N}\int_{-\infty}^{\infty} \mathbf{P}(t)\mathbf{P}^*(t-\Delta\tau_0)e^{j2\pi\Delta\gamma_0 t}\,\mathrm{d}t. \tag{3.9}$$

Note that $\boldsymbol{\mathcal{X}}_p(\Delta\tau_0, \Delta\gamma_0) \to \mathbf{I}_M$ as $\Delta\tau_0 \to 0$ and $\Delta\gamma_0 \to 0$, as the set of M pulses are designed to be orthogonal.

Adaptive or non-adaptive processing techniques combine the outputs of the matched filter banks to perform receive combining and produce a decision statistic

$$y_0^{c,mf}(\Delta\tau_0, \Delta\gamma_0, \theta_0, \widehat{\theta}_0) \;=\; \mathbf{w}^*\mathrm{vec}\left(\mathbf{Y}^{mf}(\Delta\tau_0, \Delta\gamma_0, \theta_0, \widehat{\theta}_0)\right), \tag{3.10}$$

where vec$(\cdot)$ vertically stacks the columns of its argument matrix into a single vector. The $M_rM \times 1$ receive combiner $\mathbf{w}$ operates on the received signal from all M_r elements processed over all M subintervals.

3.3.2 Multiple Target Scenario

Thus far, we have described the setup for a co-located MIMO radar with a single target. In the general case, M targets are located at different angles. Let $\boldsymbol{\theta} = [\theta_1, \ldots, \theta_M]$. The targets' ranges and Dopplers are all taken to be equal, as this represents the worst-case scenario[2],

$$\mathbf{Y}(t) = \sum_{m=1}^{M} \alpha_m \mathbf{a}_r(\theta_m)\mathbf{a}_t^*(\theta_m)\mathbf{X}(t-\tau_0)e^{j2\pi\gamma_0 t} + \mathbf{V}(t). \tag{3.11}$$

The receive signal after matched filtering is described by

$$\mathbf{Y}^{mf}(\Delta\tau_0, \Delta\gamma_0, \boldsymbol{\theta}, \widehat{\boldsymbol{\theta}}) \;=\; \sum_{m=1}^{M} \alpha_m \mathbf{a}_r(\theta_m)\mathbf{a}_t^*(\theta_m)\mathbf{F}\boldsymbol{\mathcal{X}}_p(\Delta\tau_0, \Delta\gamma_0) + \bar{\mathbf{V}}.$$

Since we analyze this multiple target scenario for a single multidimensional pulse (a single burst of energy), the same transmit signal must be used for all M targets. A

[2]Multiple targets at the same range and Doppler represent the worst case for detection performance as the targets' delay and Doppler cannot aid in detection by range or Doppler gating. This does not consider the fact that different Dopplers will diminish the orthogonality properties of the waveforms on receive.

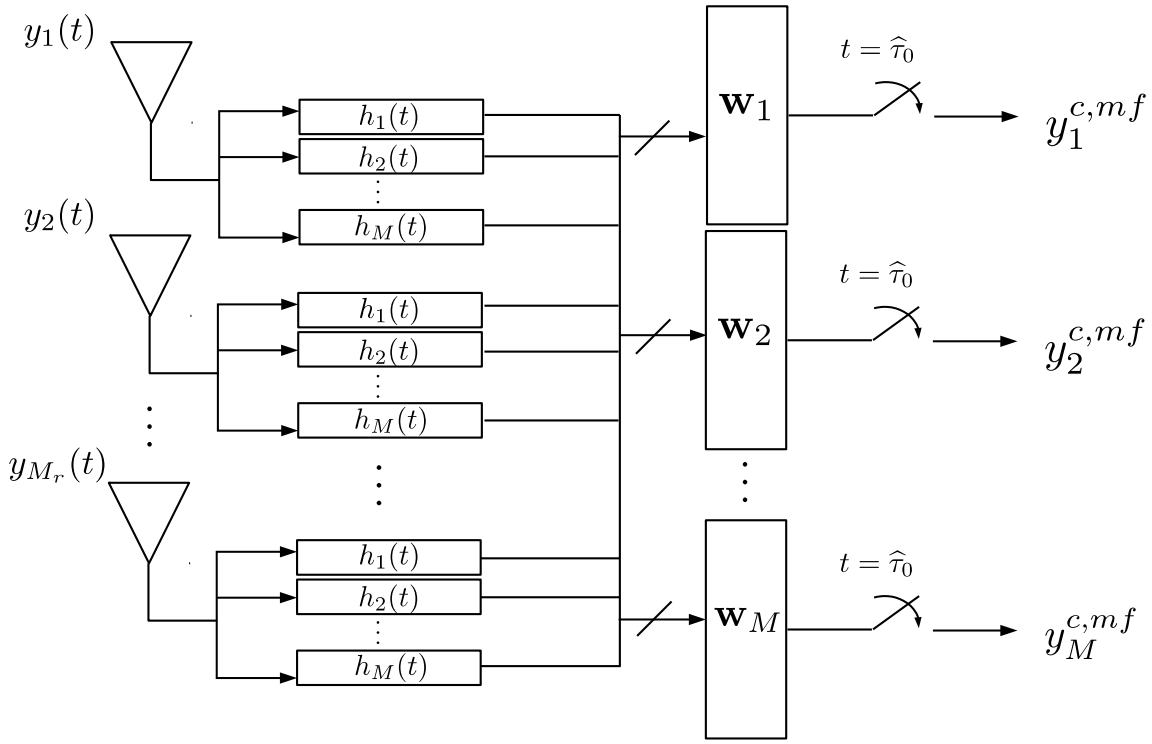

Fig. 3.5. A linear receiver with a bank of M matched filters behind each element, with a set of receive combiners designed for each of the M targets.

receive combiner can be used for each target to distinguish the return of interest from the other targets. The decision statistic for the m^{th} target is formed after projecting the vectorized matched filter output onto the m^{th} receive combiner

$$y_m^{c,mf}(\Delta\tau_0, \Delta\gamma_0, \boldsymbol{\theta}, \widehat{\boldsymbol{\theta}}) = \mathbf{w}_m^* \text{vec}\left(\mathbf{Y}^{mf}(\Delta\tau_0, \Delta\gamma_0, \boldsymbol{\theta}, \widehat{\boldsymbol{\theta}})\right).$$

Figure 3.5 details the linear receiver for M target detection. A matched filter bank exists behind each antenna element, with a separate linear combiner for all M targets. The output of the m^{th} combiner is the decision statistic $y_m^{c,mf}(\Delta\tau_0, \Delta\gamma_0, \boldsymbol{\theta}, \widehat{\boldsymbol{\theta}})$.

3.3.3 Beampattern

Given an ideal point scatterer in the far field for a specified transmit signal and receive combiner, the transmit-receive beampattern is the receive power as a function of the point scatterer's angle. For a linear precoded transmit signal, it can mathematically be described as the square of the decision statistic in (3.10) with zero delay and Doppler mismatch and unit-amplitude RCS,

$$\begin{aligned} S_{TR}(\theta_0, \widehat{\theta}_0) &= \left| y_0^{c,mf}(\Delta\tau_0 = 0, \Delta\gamma_0 = 0, \theta_0, \widehat{\theta}_0) \right|^2 \\ &= \left| \mathbf{w}^* \left(\mathbf{I}_M \otimes \mathbf{a}_r(\theta_0) \mathbf{a}_t^*(\theta_0) \right) \mathrm{vec}(\mathbf{F}) \right|^2 \\ &= \left| \mathbf{w}^* \left(\mathbf{I}_M \otimes \mathbf{a}_r(\theta_0) \right) \left(\mathbf{I}_M \otimes \mathbf{a}_t^*(\theta_0) \right) \mathrm{vec}(\mathbf{F}) \right|^2 \\ &= \left| \mathbf{a}_r^T(\theta_0) \mathbf{W}^c \mathbf{F}^T \mathbf{a}_t^c(\theta_0) \right|^2 \\ &= \left| \mathbf{a}_t^*(\theta_0) \mathbf{F} \mathbf{W}^* \mathbf{a}_r(\theta_0) \right|^2 \end{aligned} \tag{3.12}$$

where $\otimes$ denotes the Kronecker product, $\mathbf{w}$, $\mathbf{F}$ are the designed receive combiner and linear precoder, and $\mathbf{w} = \mathrm{vec}(\mathbf{W})$.

3.4 Ambiguity Function Analysis

A general form for the MIMO receive ambiguity function is derived using the transmit signal, matched filter, and receive combiner. For time-division beamforming, the MIMO receive ambiguity function is shown to display a space and delay-Doppler separability.

3.4.1 MIMO Receive Ambiguity Function

The single-intput single-output (SISO) ambiguity function is defined the output of a matched filter when the input is a Doppler-shifted and time-delayed version of the original signal $p(t)$ [27],

$$\mathcal{X}(\Delta\tau_0, \Delta\gamma_0) = \frac{1}{N} \int_{-\infty}^{\infty} p(t) p^*(t - \Delta\tau_0) e^{j2\pi\Delta\gamma_0 t} \, \mathrm{d}t \tag{3.13}$$

where $\Delta\tau_0$ is the delay mistmatch and $\Delta\gamma_0$ is the Doppler mismatch for the received signal $p(t)$. The $1/N$ factor is included in the definition to normalize the waveforms to unit-energy and also to stay consistent with the notation as the output of the matched filter. The ambiguity function is useful to study the characteristics of the receive signal when the estimate of target delay and Doppler is slightly inaccurate. The ambiguity function for a single waveform and single antenna can be interpreted in two different ways. One interpretation looks at the output of a matched filter, when the matched filter is set to the same transmitted waveform with delay $\Delta\tau_0$ and Doppler $\Delta\gamma_0$. The other interpretation is to consider two closely spaced targets. These targets are spaced close together in both the delay and Doppler domains. The ambiguity function then measures the correlation of the returns from these two closely spaced targets. The latter definition has been extended to MIMO radar in [42], and we extend the definition of a SISO ambiguity function using matched filters in this work. For co-located arrays and narrowband signal assumptions, four scalar target parameters are required to define the MIMO receive ambiguity function: delay mismatch, Doppler mismatch, and the true and estimated angles from array boresight. Unlike for delay and Doppler, the ambiguity function cannot be defined in terms of angle mismatch and must be defined in terms of θ_0 and $\widehat{\theta}_0$ as the ambiguity function is not angle invariant.

The MIMO ambiguity function of [42] looks at a similar noiseless receive signal. They include the case for M_t orthogonal waveforms. Under the far field, coherent scattering, and narrowband signal assumptions, we can write the receive signal for general MIMO radar as,

$$\bar{\mathbf{Z}}(t;\theta_0,\tau_0,\gamma_0) = \mathbf{a}_r(\theta_0)\mathbf{a}_t^*(\theta_0)\mathbf{P}(t-\tau_0)e^{j2\pi\gamma_0 t}$$

where $\mathbf{X}(t) = \rho\mathbf{P}(t)$ is the set of M_t transmit waveforms. Since ρ is a scalar power constraint, we will remove it from the ambiguity function expressions to simplify notation. The correlation of the returns from two closely spaced targets is,

$$\begin{aligned} \boldsymbol{\mathcal{X}}_{\text{MIMO}} &= \text{tr}\left[\int \bar{\mathbf{Z}}(t;\theta_0,\tau_0,\gamma_0)\bar{\mathbf{Z}}^*(t;\widehat{\theta}_0,\widehat{\tau}_0,\widehat{\gamma}_0)\,\mathrm{d}t\right] \\ &= \mathbf{a}_r^*(\theta_0)\mathbf{a}_r(\widehat{\theta}_0)\cdot\mathbf{a}_t^*(\theta_0)\boldsymbol{\mathcal{X}}_p(\Delta\tau_0,\Delta\gamma_0)\mathbf{a}_t(\widehat{\theta}_0) \end{aligned} \tag{3.14}$$

As was noted in [42], this MIMO ambiguity function displays a separability between space and time.

Previous work has shown in great detail the extension of the ambiguity function to multiple transmit antennas by analyzing the correlation between the receive signals from two closely spaced targets. The question remains whether there is a similar interpretation if we extend the concept that considers the ambiguity function as the output of a matched filter. In order to do this, we must consider a linear receive combiner in addition to the bank of matched filters behind each element in our definition. We now explore this idea further.

The matched filter banks, linear precoder, and receive combining vectors are designed for a single target with parameters $\widehat{\Omega}_0 = [\widehat{\tau}_0, \widehat{\gamma}_0, \widehat{\theta}_0]$. For a MIMO radar that employs the general linear precoding framework with M orthogonal waveforms at the transmitter and the receiver output of (3.8), the noiseless received signal from a single target with true parameters $\Omega_0 = [\tau_0, \gamma_0, \theta_0]$ is

$$\mathbf{Z}(t) = \mathbf{a}_r(\theta_0)\mathbf{a}_t^*(\theta_0)\mathbf{F}\mathbf{P}(t-\tau_0)e^{j2\pi\gamma_0 t}.$$

Matched filtering the noiseless receive signal gives an $M_r \times M$ matrix

$$\mathbf{Z}^{mf}(\Delta\tau_0,\Delta\gamma_0,\theta_0,\widehat{\theta}_0) = \mathbf{a}_r(\theta_0)\mathbf{a}_t^*(\theta_0)\mathbf{F}\boldsymbol{\mathcal{X}}_p(\Delta\tau_0,\Delta\gamma_0)$$

where $\Delta\tau_0 = \tau_0 - \widehat{\tau}_0$, $\Delta\gamma_0 = \gamma_0 - \widehat{\gamma}_0$, and $\boldsymbol{\mathcal{X}}_p(\Delta\tau_0,\Delta\gamma_0)$ is as defined in (3.9). $\mathbf{Z}^{mf}(\Delta\tau_0,\Delta\gamma_0,\theta_0,\widehat{\theta}_0)$ is similar to the matched filter output of the receive signal in (3.8) only without receiver noise, which is consistent with the SISO ambiguity func-

tion definition. It will be useful to describe the outputs of the bank of matched filters in Figure 3.5 in vector form,

$$\text{vec}\left(\mathbf{Z}^{mf}(\Delta\tau_0, \Delta\gamma_0, \theta_0, \widehat{\theta_0})\right) = \left(\boldsymbol{\mathcal{X}}_p(\Delta\tau_0, \Delta\gamma_0) \otimes \mathbf{a}_r(\theta_0)\mathbf{a}_t^*(\theta_0)\right)\text{vec}\left(\mathbf{F}\right)$$

where $\otimes$ is the Kronecker product and the identity $\text{vec}(\mathbf{AXB}) = \left(\mathbf{B}^T \otimes \mathbf{A}\right)\text{vec}(\mathbf{X})$ is used to transform a vectorized matrix product into a Kronecker product. We can now show the ambiguity function result for a general transmit signal $\mathbf{X}(t) = \rho\mathbf{P}(t)$ which includes the receive combiner.

Definition 3.4.1 *The MIMO receive ambiguity function for a general MIMO transmit signal* $\mathbf{X}(t)$

$$\begin{aligned}
\mathcal{X}_{MIMO\text{-}Rx}(\Delta\tau_0, \Delta\gamma_0, \theta_0, \widehat{\theta_0}) &= y_0^{c,mf} \\
&= \mathbf{w}^* vec\left(\mathbf{a}_r(\theta_0)\mathbf{a}_t^*(\theta_0)\boldsymbol{\mathcal{X}}_p(\Delta\tau_0, \Delta\gamma_0)\right) \\
&= \mathbf{a}_t^*(\theta_0)\boldsymbol{\mathcal{X}}_p(\Delta\tau_0, \Delta\gamma_0)\mathbf{W}^*\mathbf{a}_r(\theta_0) \qquad (3.15) \\
&= \mathbf{w}^*\left(\mathbf{I} \otimes \mathbf{a}_r(\theta_0)\right)\left(\mathbf{I} \otimes \mathbf{a}_t^*(\theta_0)\right) vec\left(\boldsymbol{\mathcal{X}}_p(\Delta\tau_0, \Delta\gamma_0)\right) \qquad (3.16) \\
&= vec(\mathbf{a}_r^*(\theta_0)\mathbf{W})^* vec\left(\mathbf{a}_t^*(\theta_0)\boldsymbol{\mathcal{X}}_p(\Delta\tau_0, \Delta\gamma_0)\right) \qquad (3.17) \\
&= \mathbf{a}_r^T(\theta_0)\mathbf{W}^c\boldsymbol{\mathcal{X}}_p^T(\Delta\tau_0, \Delta\gamma_0)\mathbf{a}_t^c(\theta_0) \qquad (3.18) \\
&= \mathbf{a}_t^*(\theta_0)\boldsymbol{\mathcal{X}}_p(\Delta\tau_0, \Delta\gamma_0)\mathbf{W}^*\mathbf{a}_r(\theta_0). \qquad (3.19)
\end{aligned}$$

where $\mathbf{w} = vec(\mathbf{W})$.

We note that for the specific case of receive combiner, $\mathbf{W} = \mathbf{a}_r(\widehat{\theta_0})\mathbf{a}_t^*(\widehat{\theta_0})$, the MIMO receive ambiguity function simplifies to the MIMO ambiguity function of [42], which was repeated in this work in (3.14).

If we consider a linear precoded MIMO transmit signal, we get a very similar form of MIMO receive ambiguity function as for the general transmit signal.

Corollary 1 *Consider a linear precoded MIMO transmit signal of the form* $\mathbf{X}(t) = \mathbf{FP}(t)$. *The MIMO receive ambiguity function reduces to,*

$$\mathcal{X}_{LP}(\Delta\tau_0, \Delta\gamma_0, \theta_0, \widehat{\theta_0}) = \mathbf{a}_t^*(\theta_0)\mathbf{F} \cdot \boldsymbol{\mathcal{X}}_p(\Delta\tau_0, \Delta\gamma_0) \cdot \mathbf{W}^*\mathbf{a}_r(\theta_0). \qquad (3.20)$$

A separability exists between $\boldsymbol{\mathcal{X}}_p(\Delta\tau_0, \Delta\gamma_0)$ *and the transmit weights,* $\mathbf{a}_t^*(\theta_0)\mathbf{F}$*, and receive weights,* $\mathbf{W}^*\mathbf{a}_r(\theta_0)$*.*

In [45], the separability property of phased array radar is shown for a four-dimensional ambiguity function of delay, Doppler, azimuth, and elevation. The azimuth and elevation properties of the ambiguity function are designed independently from the delay and Doppler properties for a single phase-shifted transmit signal. We show the result in [45] is similar to Definition 3.4.1.

Corollary 2 *Consider a phased array transmit signal. For any* M*, let* $\mathbf{f}_m = \sqrt{\frac{\rho\mathcal{E}_m}{M_t N}}\mathbf{a}_t(\widehat{\theta}_0)$ *and* $p_m(t) = \sqrt{\frac{N}{\mathcal{E}_m}}p_{phase}\left(t + (m-1)\frac{T_0}{M}\right)$*. Let* $\mathbf{E} = \text{diag}(\sqrt{\mathcal{E}_1}, \sqrt{\mathcal{E}_2}, \ldots, \sqrt{\mathcal{E}_M})$ *such that* $[\mathbf{E}]_{m,m} = \sqrt{\mathcal{E}_m}$*. By designing the receive combiner to be* $\mathbf{w} = \frac{1}{\sqrt{M_r N}}\left(\mathbf{E} \otimes \mathbf{a}_r(\widehat{\theta}_0)\right)$*, we can simplify the MIMO receive ambiguity function as*

$$\begin{aligned}\mathcal{X}_{PA}(\Delta\tau_0, \Delta\gamma_0, \theta_0, \widehat{\theta}_0) = &\left(\sqrt{\frac{\rho}{M_t M_r}}\mathbf{a}_r^*(\widehat{\theta}_0)\mathbf{a}_r(\theta_0)\mathbf{a}_t^*(\theta_0)\mathbf{a}_t(\widehat{\theta}_0)\right) \\ &\cdot \int p_{phase}(t)p_{phase}^*(t - \Delta\tau_0)e^{j2\pi\Delta\gamma_0 t}\,\mathrm{d}t\end{aligned}$$

where the MIMO receive ambiguity function is a scaled version of the ambiguity function for $p_{phase}(t)$*, with the scale factor dependent on the mismatch between* $\widehat{\theta}_0$ *and* θ_0*.*

Considering one last special case, assume the set of M subpulses are identical, $p_1(t) = \cdots = p_M(t) = p(t)$.

Corollary 3 *For large* N *and common subpulses, the ambiguity function simplifies to*

$$\mathcal{X}_{TDBF}\left(\Delta\tau_0, \Delta\gamma_0, \theta_0, \widehat{\theta}_0\right) = \mathbf{a}_t^*(\theta_0)\mathbf{F}\mathbf{W}^*\mathbf{a}_r(\theta_0) \cdot \mathcal{X}(\Delta\tau_0, \Delta\gamma_0). \tag{3.21}$$

The MIMO receive ambiguity function simplifies to the product of the SISO ambiguity function in (3.13) *and the complex argument of the transmit-receive beampattern,* $S_{TR}(\theta_0, \widehat{\theta}_0)$*, in* (3.12)*.*

Proof: For large N and small delay mismatch $\Delta\tau_0$, we assume the pulse correlation matrix in (3.9) behaves like a scaled identity,

$$\boldsymbol{\mathcal{X}}_p(\Delta\tau_0, \Delta\gamma_0) = \mathbf{I}_M \frac{1}{N} \int p(t)p^*(t - \Delta\tau_0)e^{j2\pi\Delta\gamma_0 t}\, \mathrm{d}t.$$

The expression is then simplified by $|ab|^2 = |a|^2|b|^2$ for $a, b \in \mathbb{C}$. ■

The effect of delay and Doppler rest solely in the $\mathcal{X}(\Delta\tau_0, \Delta\gamma_0)$ term. As a result, $p(t)$ can be designed using signals with favorable delay-Doppler properties, many of which are detailed in [46]. The spatial properties rest soley in the transmit-receive beampattern evaluated at θ_0. Hence, Corollary 3 states, under time-division beamforming, the temporal and spatial properties can be designed independently through $p(t)$ and $\mathbf{w}, \mathbf{F}$, respectively. With this in mind, this work focuses on the design of the receive combiners and linear precoder, as they play important roles in spatial resolution.

This MIMO receive ambiguity function differs from previous definitions in the current literature [42, 47]. The MIMO ambiguity function in [42] compares the inner product between the signal returns from two targets with target parameters Ω_0, Ω_1. This indicates how the return from a target with parameters Ω_0 is correlated with the return from a target with parameters Ω_1, giving a sense of how well these returns can be distinguished from one another. In [47], the MIMO ambiguity function is the output of a bank of matched filters after phase shifting and summing (designed according to $\widehat{\Omega}_0$) where the return is from a target with parameters Ω_0. The MIMO receive ambiguity function extends the work in [47] by replacing the coherent phase-shifted sum by a linear receive combiner $\mathbf{w}$. For example, the MIMO ambiguity function in [47] is a specific case of the MIMO receive ambiguity function in (3.15) if $\mathbf{w} = \mathbf{1}_M \otimes \mathbf{a}_r(\widehat{\theta}_0)$, where $\mathbf{1}_M$ is a length-M vector of all ones.

3.5 Linear Precoder and Receive Combiner Design

The MIMO radar transmit signal plays an important role in multiple target detection. In general, detection of targets in MIMO radar boils down to sampling the

space in delay, Doppler, and angle. These samples are compared to a threshold for a given false alarm probability. The signal-to-interference-plus-noise ratio (SINR) of these samples proves crucial to target detection performance [48]. In addition, the lack of orthogonality in the returns from multiple targets necessitates the use of SINR as the performance metric to optimize in this work.

Consider a multiple target scenario, with M targets all at the same range and Doppler but at different angles. The receive SINR is defined as the ratio of power returned from the target of interest to the power of the returns from all other $M-1$ targets plus additive white Gaussian noise. In detecting the m^{th} target, our model expresses the returns of the other $M-1$ targets as interference. The receive SINR for the m^{th} target is calculated for a single pulse after receive combining with delay mismatch $\Delta\tau_0$ and Doppler mismatch $\Delta\gamma_0$,

$$\text{SINR}_m = \frac{E\left[|\alpha_m \mathbf{w}_m^* \text{vec}\left(\mathbf{a}_r(\theta_m)\mathbf{a}_t^*(\theta_m)\mathbf{F}\boldsymbol{\mathcal{X}}_p(\Delta\tau_m,\Delta\gamma_m)\right)|^2\right]}{E\left[\left|\sum_{l\neq m}\alpha_l \mathbf{w}_m^* \text{vec}\left(\mathbf{a}_r(\theta_l)\mathbf{a}_t^*(\theta_l)\mathbf{F}\boldsymbol{\mathcal{X}}_p(\Delta\tau_l,\Delta\gamma_l)+\bar{\mathbf{V}}\right)\right|^2\right]} \quad (3.22)$$

where $E[\cdot]$ denotes the joint expectation over the RCS values $\alpha_m \sim \mathcal{CN}(0,\sigma_m^2)$ and the receive noise. Receive SINR as a design metric was acknowledged in [6], but not utilized since the focus of that work was on transmit beamforming. The main idea in [6] of simultaneously maximizing power on target and minimizing the cross-correlation of the targets' returns is similar to the idea we use of maximizing the receive SINR. Our method serves as an alternative transmit design strategy using time-division beamforming and receive SINR as optimization criteria.

To improve the receive SINR in (3.22), $\mathbf{w}_m$ and $\mathbf{F}$ must be optimized. However, the SINR expression in (3.22) is a function of the delay and Doppler mismatch of M targets, which is likely unknown to the user. We will design the receive combiners and linear precoders to the SINR expression where it is assumed zero delay and Doppler mismatch. In this fashion, the SINR expression for the m^{th} target can be rewritten as

$$\text{SINR}_m = \frac{\mathbf{w}_m^*\left(\sigma_m^2\mathbf{R}_m\widetilde{\mathbf{f}\mathbf{f}}^*\mathbf{R}_m^*\right)\mathbf{w}_m}{\mathbf{w}_m^*\mathbf{R}_{m,\text{int}}\mathbf{w}_m}$$

where $\mathbf{R}_m = (\mathbf{I}_M \otimes \mathbf{a}_r(\theta_m)\mathbf{a}_t^*(\theta_m))$, $\widetilde{\mathbf{f}} = \text{vec}(\mathbf{F})$, and $\mathbf{R}_{m,\text{int}} = \sum_{l \neq m} \sigma_l^2 \mathbf{R}_l \widetilde{\mathbf{f}}\widetilde{\mathbf{f}}^* \mathbf{R}_l^* + \frac{\sigma_n^2}{N}\mathbf{I}$.

3.5.1 Phased Array Time-Division Beamforming

To incorporate the phased array's ability to cohere power in space, *phased array time-division beamforming* designs the individual beamforming vectors according to the array's transmit steering vectors. The m^{th} column of $\mathbf{F}$ is steered towards the estimated angle of the m^{th} target,

$$\mathbf{F} = \sqrt{\frac{\rho}{M_t M}} \left[\mathbf{a}_t(\widehat{\theta}_1) \quad \mathbf{a}_t(\widehat{\theta}_2) \quad \cdots \quad \mathbf{a}_t(\widehat{\theta}_M) \right].$$

For each subinterval, this linear precoder design maximizes power towards a specific angle. Phased array time-division beamforming possesses low complexity to design, with the added benefit of constant modulus entries for improved amplifier efficiency.

Considering a point target at θ_m, power will be placed on the target for all M subintervals. Albeit maximum power will be directed towards the target during the m^{th} subinterval, the other subintervals apply power to the target as long as it does not reside in a spatial null. Although phased array time-division beamforming maximizes power on target for a given subinterval, it cannot guarantee maximum energy on target for a given pulse. This uncovers a need to jointly optimize the complete set of beamforming vectors in $\mathbf{F}$, an optimization we denote as max-min SINR time-division beamforming.

3.5.2 Max-Min SINR Time-Division Beamforming

Transmit signal design to maximize the sum power directed at M targets was considered in [6]. In that work, it was noted that sum power may not be a suitable metric for target detection. Maximizing the sum power directed towards all M targets does not imply a sufficient amount of power is directed towards each and every target. Extending this idea to the metric of target receive SINR, maximizing the sum SINR does not guarantee a sufficient SINR for target detection. To mitigate this, we propose

a max-min optimization on the receive SINR. We denote the target with the lowest SINR as the weakest target, and form a max-min optimization to increase the receive SINR of the weakest target,

$$[\mathbf{w}_{\text{opt},1}, \ldots, \mathbf{w}_{\text{opt},M}, \widetilde{\mathbf{f}}_{\text{opt}}] = \underset{\mathbf{w}_1,\ldots,\mathbf{w}_M,\widetilde{\mathbf{f}}}{\text{argmax}} \min_m \text{SINR}_m \tag{3.23}$$

where $\widetilde{\mathbf{f}}$ obeys the total power constraint $\|\widetilde{\mathbf{f}}\|^2 \leq \rho$.

This max-min optimization focuses on maximizing the SINR of the target with the weakest (or minimum) receive SINR. This optimization solves for optimal transmit precoder and M optimal receive combiners. Since optimizing over $\mathbf{w}_m$ and $\widetilde{\mathbf{f}}$ in (3.23) is non-convex, an alternating maximization method can be used as an approach to optimize each parameter independently.

Given $\widetilde{\mathbf{f}}$, the receive combining matrix $\mathbf{W}$ is constructed by designing the individual receive combiners, $\mathbf{w}_m$. The per target receive SINR is maximized by choosing the receive combiner as the MMSE combiner,

$$\mathbf{w}_{\text{opt},m} = \mathbf{R}_{m,\text{int}}^{-1}\mathbf{R}_m\widetilde{\mathbf{f}}$$

where $\mathbf{R}_{m,\text{int}} = \sum_{l\neq m} \sigma_l^2 \mathbf{R}_l \widetilde{\mathbf{f}}\widetilde{\mathbf{f}}^* \mathbf{R}_l^* + \sigma_n^2\mathbf{I}$ and $\mathbf{R}_m = (\mathbf{I} \otimes \mathbf{a}_r(\theta_m)\mathbf{a}_t^*(\theta_m))$. The derivation of the optimal receive combiner is given in Appendix A. The optimal receive combining matrix is then $\mathbf{W}_{\text{opt}} = [\mathbf{w}_{\text{opt},1}\, \mathbf{w}_{\text{opt},2}\, \cdots \mathbf{w}_{\text{opt},M}]$.

Given $\mathbf{W}$, the optimization in (3.23) reduces to

$$\widetilde{\mathbf{f}}_{\text{opt}} = \underset{\widetilde{\mathbf{f}}\leq\rho}{\text{argmax}} \min_m \frac{\sigma_m^2 \mathbf{w}_m^* \mathbf{R}_m \widetilde{\mathbf{f}}\widetilde{\mathbf{f}}^* \mathbf{R}_m^* \mathbf{w}_m}{\mathbf{w}_m^* \left(\sum_{l\neq m} \sigma_l^2 \mathbf{R}_l \widetilde{\mathbf{f}}\widetilde{\mathbf{f}}^* \mathbf{R}_l^* + \frac{\sigma_n^2}{N}\mathbf{I} \right) \mathbf{w}_m}.$$

This optimization is equivalent to optimizing over the vectorized linear precoder's covariance matrix with a rank constraint,

$$\widetilde{\mathbf{R}}_{\text{opt}} = \underset{\substack{\widetilde{\mathbf{R}}\succeq 0 \\ \text{rank}(\widetilde{\mathbf{R}})=1 \\ \text{tr}(\widetilde{\mathbf{R}})\leq\rho}}{\text{argmax}} \min_m \frac{\sigma_m^2 \text{ tr}\left(\mathbf{w}_m^* \mathbf{R}_m \widetilde{\mathbf{R}} \mathbf{R}_m \mathbf{w}_m\right)}{\sum_{l\neq m} \sigma_l^2 \text{ tr}\left(\mathbf{w}_m^* \mathbf{R}_l \widetilde{\mathbf{R}} \mathbf{R}_l^* \mathbf{w}_m\right) + \frac{\sigma_n^2 \|\mathbf{w}_m\|^2}{N}}$$

where $\widetilde{\mathbf{R}} = \widetilde{\mathbf{f}}\widetilde{\mathbf{f}}^*$ and $\widetilde{\mathbf{R}} \succeq 0$ denotes $\mathbf{R}$ is a positive semidefinite matrix. Imposing the rank 1 constraint guarantees that $\widetilde{\mathbf{f}}$ can be found from the dominant eigenvector of $\widetilde{\mathbf{R}}$. Finally, introducing an auxiliary variable κ, referred to as the power threshold, the max-min optimization becomes

$$\begin{aligned} \max \quad & \kappa \\ \text{such that} \quad & \text{SINR}_m = \frac{\sigma_m^2 \text{tr}\left(\widetilde{\mathbf{R}}\mathbf{R}_m^*\mathbf{w}_m\mathbf{w}_m^*\mathbf{R}_m\right)}{\sum\limits_{l\neq m}\sigma_l^2 \text{tr}\left(\widetilde{\mathbf{R}}\mathbf{R}_l^*\mathbf{w}_m\mathbf{w}_m^*\mathbf{R}_l\right) + \frac{\sigma_n^2\|\mathbf{w}_m\|^2}{N}} \geq \kappa \\ & \quad \text{for } m = 1, 2, \ldots, M \\ & \widetilde{\mathbf{R}} \succeq 0 \\ & \text{rank}(\widetilde{\mathbf{R}}) = 1 \\ & \text{tr}(\widetilde{\mathbf{R}}) \leq \rho. \end{aligned}$$

This optimization can be formed as a convex optimization problem if the power threshold κ is given and the rank constraint on $\widetilde{\mathbf{R}}$ is relaxed,

$$\begin{aligned} \max \quad & \kappa \\ \text{such that} \quad & \sigma_m^2 \text{tr}\left(\widetilde{\mathbf{R}}\mathbf{R}_m^*\mathbf{w}_m\mathbf{w}_m^*\mathbf{R}_m\right) - \kappa\sum_{l\neq m}\sigma_l^2 \text{tr}\left(\widetilde{\mathbf{R}}\mathbf{R}_l^*\mathbf{w}_m\mathbf{w}_m^*\mathbf{R}_l\right) \geq \frac{\kappa\,\sigma_n^2\|\mathbf{w}_m\|^2}{N} \\ & \quad \text{for } m = 1, 2, \ldots, M \\ & \widetilde{\mathbf{R}} \succeq 0 \\ & \text{tr}(\widetilde{\mathbf{R}}) \leq \rho. \end{aligned} \tag{3.24}$$

Fortunately, relaxing the constraint on the rank of $\widetilde{\mathbf{R}}$ is an equivalent optimization to constraining $\widetilde{\mathbf{R}}$ to be rank 1 as [49] showed the optimal $\widetilde{\mathbf{R}}$ will always be rank 1. With this in mind, the optimization is convex if the power threshold κ is known. The power threshold is not known ahead of time, and is estimated using an iterative technique which chooses κ by bisecting the realizable space. In Appendix B, it is shown that κ is bounded by $0 \leq \kappa \leq \rho M N M_t M_r \|\mathbf{w}_m\|^2/\sigma_n^2$. Initially, the realizable space for κ is $\Upsilon_0 = \{\upsilon_0^{\min}, \upsilon_0^{\max}\}$ where $\upsilon_0^{\min}, \upsilon_0^{\max}$ are the upper and lower bounds on κ, respectively. At the initial stage, $\kappa_0 = \upsilon_0^{\max}$. At the m^{th} stage of the iterative process, κ_m is

plugged into the convex optimization in (3.24) and a convex optimization program, e.g. CVX [50], is used to determine if the optimization is feasible or not. If feasible, κ_m lies in the realizable space and this space is subsequently reduced to $\Upsilon_m = \{\kappa_m, \upsilon_{m-1}^{\max}\}$. If infeasible, $\Upsilon_m = \{\upsilon_{m-1}^{\min}, \kappa_m\}$. The next iteration chooses κ_{m+1} by bisecting Υ_m, i.e. $\kappa_{m+1} = \left(\upsilon_m^{\min} + \upsilon_m^{\max}\right)/2$. The iteration stops when the power threshold percent change is less than ϵ, $|\kappa_{m+1} - \kappa_m|/\kappa_m < \epsilon$.

In summary, the max-min SINR optimization alternates between (a) solving for $\mathbf{W}$ given $\widetilde{\mathbf{f}}$ and (b) solving for $\widetilde{\mathbf{f}}$ given $\mathbf{W}$. The initialization of $\widetilde{\mathbf{f}}$ heavily affects the performance of the optimization as this alternating method only produces a locally optimal solution [51]. Depending on the initial $\widetilde{\mathbf{f}}$, the local maximum can be the global maximum. In general, this is accomplished by running the optimization initializing with random $\widetilde{\mathbf{f}}$ and selecting the value that yields the greatest minimum SINR. Empirically, we found that initializing with $\widetilde{\mathbf{f}} = \sqrt{\frac{\rho}{M_t M}}[\mathbf{a}_t^T(\widehat{\theta}_1)\cdots\mathbf{a}_t^T(\widehat{\theta}_M)]^T$ provided results equivalent to those which were randomly initialized. A summary of the max-min SINR method is given in Algorithm 1.

3.6 Simulations

In this section, we compare the SINR performance of the proposed phased array and max-min SINR time-division beamforming signals to existing transmit schemes. We compare these schemes to omnidirectional MIMO (transmitting orthogonal waveforms from each antenna element), overlapping subarrays [8, 9], and disjoint subarrays [7]. The conventional phased array is not considered in these simulations due to its narrow main beam and subsequently poor receive SINR for multiple targets.

Consider a co-located transmit and receive array of $M_t = M_r = 9$ elements in a uniform linear array with $d = \lambda/2$ element spacing. The total transmit power is 0dB, with a $\sigma_n^2 = -10$dB receive noise variance giving a receive SNR of 10dB. All simulations assume $M = 3$ targets, with each target parametrized by $\{\tau_m, \gamma_m, \theta_m, \alpha_m\}$. We assume M is known with estimates $\boldsymbol{\theta} = [\theta_1 \cdots \theta_M]$ and $\boldsymbol{\alpha} = [\alpha_1 \cdots \alpha_M]$ and all M

Algorithm 1 Max-Min SINR Optimization

Initialize: $\widetilde{\mathbf{f}} = \sqrt{\frac{\rho}{M_t M}}[\mathbf{a}_t^T(\widehat{\theta}_1)\cdots\mathbf{a}_t^T(\widehat{\theta}_M)]^T$, $\kappa_0 = \frac{\rho M N M_t M_r \|\mathbf{w}_m\|^2}{\sigma_n^2}$
repeat
  $\mathbf{w}_m = \mathbf{R}_{m,\text{int}}^{-1}\mathbf{R}_m \qquad$ for $m = 1, 2, \ldots, M$
  repeat
    $\kappa_m = \left(\upsilon_{m-1}^{\min} + \upsilon_{m-1}^{\max}\right)/2$
    $\widetilde{\mathbf{R}} = \text{argmax}_{\widetilde{\mathbf{R}}} \min_m \text{SINR}_m$, see (3.24)
    if optimization feasible **then**
      $\Upsilon_m = \{\kappa_m, \upsilon_{m-1}^{\max}\}$
    else if optimization infeasible **then**
      $\Upsilon_m = \{\upsilon_{m-1}^{\min}, \kappa_m\}$
    end if
  until $|\kappa_m - \kappa_{m-1}|/\kappa_{m-1} < \epsilon$
  $\widetilde{\mathbf{f}}$ given by eigenvector decomposition of $\widetilde{\mathbf{R}}$
  $\text{SINR}_m = \frac{\sigma_m^2 \mathbf{w}_m^* \mathbf{R}_m \widetilde{\mathbf{R}} \mathbf{R}_m^* \mathbf{w}_m}{\mathbf{w}_m^* \mathbf{R}_{m,\text{int}} \mathbf{w}_m} \qquad$ for $m = 1, 2, \ldots, M$
  $\text{SINR}_m^{\min} = \min_m \text{SINR}_m$
until $|\text{SINR}_m^{\min} - \text{SINR}_{m-1}^{\min}|/\text{SINR}_{m-1}^{\min} < \delta$
return $\widetilde{\mathbf{f}}, \mathbf{w}_1, \mathbf{w}_2, \ldots, \mathbf{w}_M$

targets are located in a common range bin. The common range bin assumption stems from the orthogonal subpulse assumptions. If the set of M subpulses are designed to be approximately orthogonal, matched filtering on receive would be able to separate the returns from multiple targets except when the targets are all located at the same range. The assumption that the number of targets is known could apply to air traffic control, where this information is tracked. Estimates of the target locations $\widehat{\boldsymbol{\theta}}$ and RCS amplitudes $\widehat{\boldsymbol{\alpha}} = [|\alpha_1| \cdots |\alpha_M|]$ can be acquired through another system or through previous scans of the space using time-division beamforming. For example, designing the time-division beamforming transmit signal to beamform towards M angle bins with $\widehat{\alpha}_m = 1$ represents a target detection problem. The M angle bins per transmission could be chosen in a random or deterministic manner to cover the entire visible space, with a target present or target absent decision made for each range-angle bin.

The normalized transmit beampattern is shown in Figure 3.6, where power is concentrated towards $\widehat{\boldsymbol{\theta}} = [-30°, 15°, 20°]$. A vertical line is plotted at each target location. The beampattern is a function of the power averaged over the entire pulse duration T_0. We note that the max-min SINR transmit signal doesn't necessarily produce the maximum transmit power among all schemes. The max-min SINR transmit signal was designed to maximize the per target SINR on receive. Since the return from a target at $-30°$ would remain fairly uncorrelated from the targets at $15°$ and $20°$, less power is directed towards $-30°$. Although not shown, the time-averaged power for each element varies significantly among the schemes, a property that could affect waveform implementation. For the transmit beampatterns in Figure 3.6, the phased array time-division beamforming, omni-directional MIMO, and disjoint subarray transmit schemes all maintain constant modulus transmit signals for constant modulus subpulses. The max-min SINR time-division beamforming transmit signal has a peak-to-average power ratio of 1.1, where the overlapping subarrays signal has a peak-to-average power ratio of 1.3. Depending on the hardware, the improved

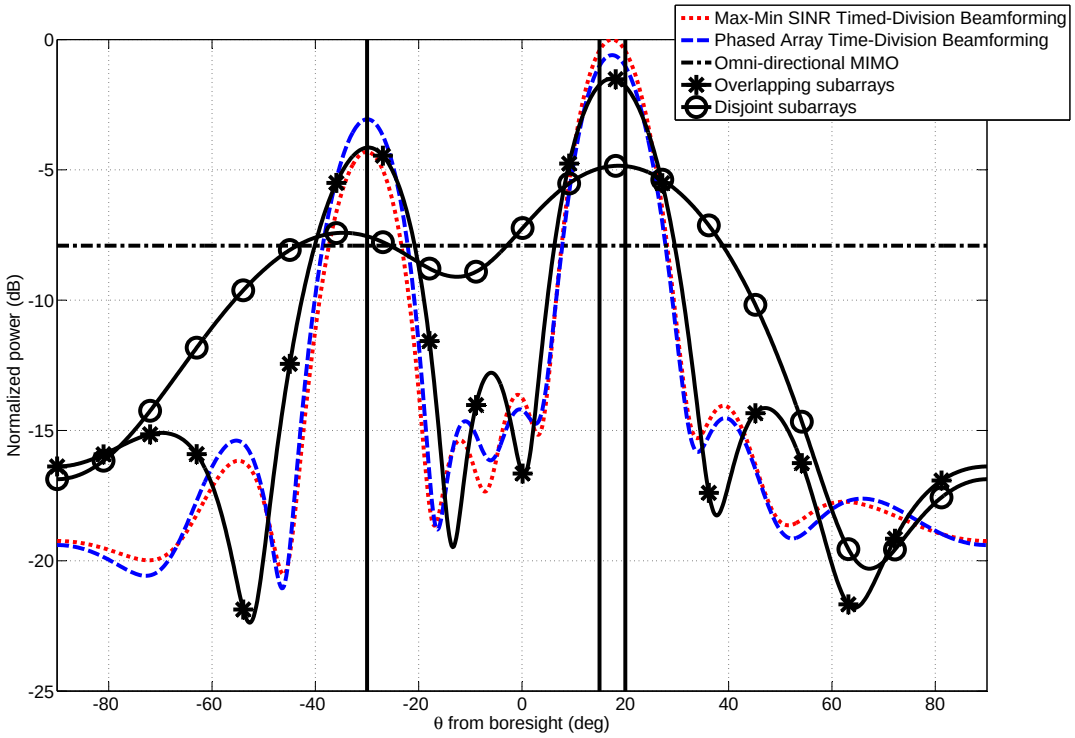

Fig. 3.6. Normalized transmit beampatterns for $M = 3$ targets and $\widehat{\boldsymbol{\alpha}} = [1\,1\,1]$. Vertical lines represent targets at $-30°, 15°, 20°$.

performance of these two schemes could be diminished due to practical amplifier constraints.

The design objective of maximizing the weakest target's SINR will serve as a benchmark to compare the various transmit schemes. To see how these transmit schemes perform for various target locations, we will define the average minimum SINR for M targets as

$$E_{\boldsymbol{\theta},\boldsymbol{\alpha}}\left[\min_{m} \mathrm{SINR}_m\right] \tag{3.25}$$

where the vector of M target locations is uniformly distributed as

$$\boldsymbol{\theta} = [\theta_1, \theta_2, \ldots, \theta_M] \sim \prod_{m=1}^{M} \mathcal{U}\left(-\frac{\pi}{2}, \frac{\pi}{2}\right) \tag{3.26}$$

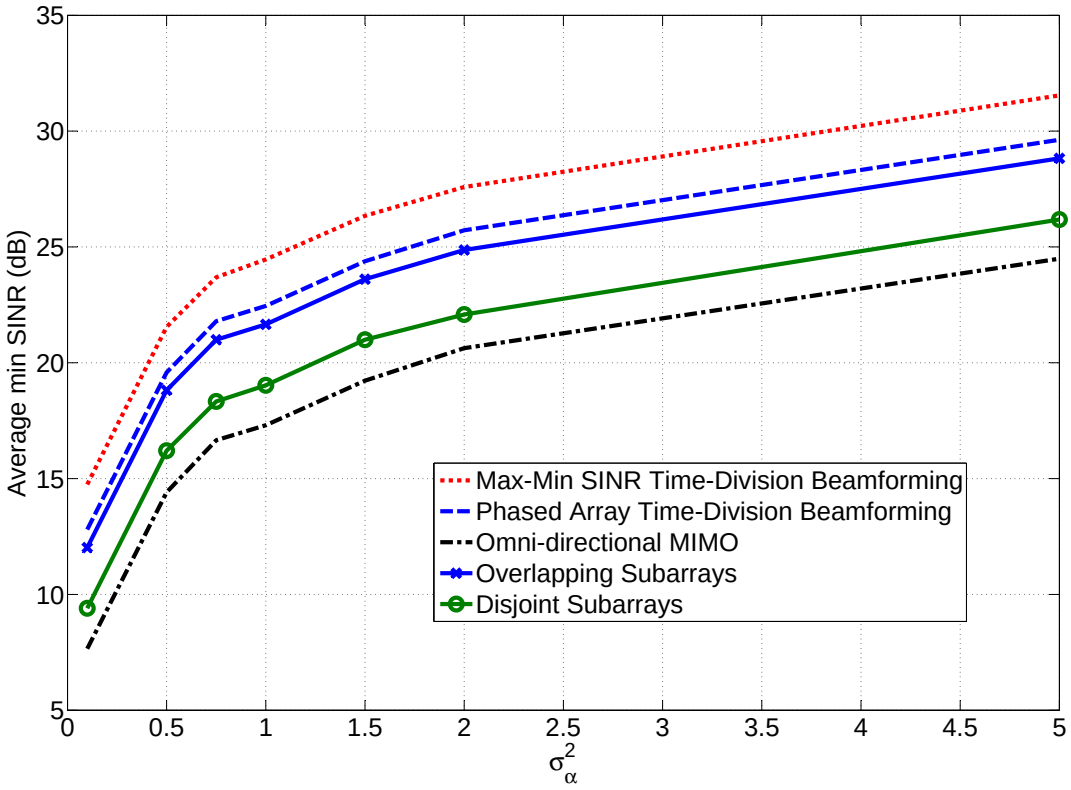

Fig. 3.7. Average minimum SINR performance for $M = 3$ targets as a function of target RCS variance, where $\alpha_m \sim \mathcal{CN}(0, \sigma_\alpha^2)$.

and the target RCS values are independently distributed as $\alpha_m \sim \mathcal{CN}(0, \sigma_\alpha^2)$.

The minimum SINR is plotted as a function of the RCS variance, σ_α^2 in Figure 3.7. For this simulation, the transmit signals are designed with perfect knowledge of target locations, $\widehat{\boldsymbol{\theta}} = \boldsymbol{\theta}$, and the minimum SINR is averaged over 700 realizations of $\boldsymbol{\theta}, \boldsymbol{\alpha}$.

The time-division beamforming schemes give an increased minimum SINR on average for random target locations and RCS values. On receive, the linear combiner for all schemes uses knowledge of $\widehat{\boldsymbol{\theta}}$ and $\widehat{\boldsymbol{\alpha}}$ to isolate the return of interest from the interference. For many of the iterations we ran, the optimal receive combiner turned out to be a zero-forcing combiner, where $\mathbf{w}_m$ was maximally correlated with the

return from the m^{th} target yet constrained to lie in the nullspace of the received interference [3]. Max-min SINR time-division beamforming gives a 2dB improvement over phased array time-division beamforming, most notably due to its use of $\widehat{\boldsymbol{\alpha}}$ in designing the transmit signal. Despite an average 2dB drop in performance, the phased array time-division beamforming transmit signal remains appealing due to its constant modulus property for improved high-power amplifier efficiency. The disjoint subarray and omnidirectional MIMO schemes perform poorly due to the weak or nonexistent directivity in their transmit beampatterns. For $M = 3$ disjoint subarrays in an $M_t = 9$ element array, each subarray contains 3 elements and poorly coheres power due to its small aperture.

For all the simulations in this section up to this point, it is assumed the linear precoder and receive combiner are designed with perfect knowledge of the target locations, $\widehat{\boldsymbol{\theta}} = \boldsymbol{\theta}$. As one might expect, the receive SINR for each target will be reduced if target location estimates are imperfect. We now introduce the alignment error for the m^{th} target (defined in radians)

$$\Delta\theta_m = \theta_m - \widehat{\theta}_m.$$

For our simulation, $\Delta\theta_m$ is independently and identically distributed as a wrapped Gaussian distribution with probability density function

$$f(\Delta\theta_m; \mu_m, \sigma_\Delta) = \frac{1}{\sigma_\Delta\sqrt{2\pi}} \sum_{m=-\infty}^{\infty} \exp\left(\frac{-\left(\Delta\theta_m - \mu_m + 2\pi m\right)^2}{2\sigma_\Delta^2}\right),$$

where μ_m and σ_Δ^2 are similar in form to the mean and variance of the normal distribution. For our simulations, $\mu_m = \theta_m$ and σ_Δ^2 is equal for all targets.

The effect of this alignment error results in beamshape loss[3]. Since the receive combiner $\mathbf{w}_m$ is also a function of $\widehat{\boldsymbol{\theta}}$, the SINR for all transmit schemes (including omnidirectional MIMO) is reduced by alignment error. The average minimum SINR as a function of alignment error variance σ_Δ^2 is shown in Figure 3.8 for $M = 3$ targets

[3]Although beamshape loss usually refers to a phased array and the loss in power on target due to beam pointing error, we use it here as the drop in SINR due to beamforming vectors designed with imperfect target location estimates.

with $M_t = M_r = 8$ and $\boldsymbol{\theta}$ chosen from the uniform distribution in (3.26) transmitted at 5dB and averaged over 900 realizations of $\Delta\theta_m$.

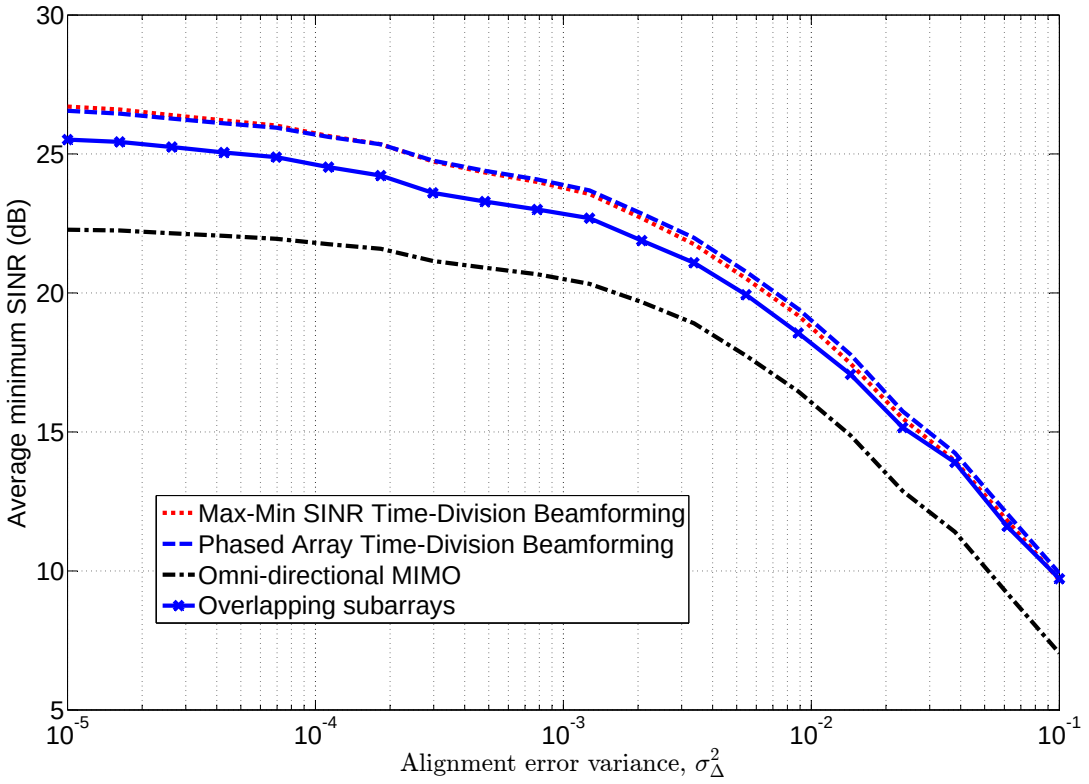

Fig. 3.8. The effect of alignment error on average minimum SINR for $M = 3$ target scenario with $\boldsymbol{\theta}$ chosen randomly.

For small alignment error variance, the results are similar to that of Figure 3.7. However, as the alignment error variance increases and the angle estimates are not as accurate, performance drops off. The time-division beamforming transmit signal appears to be more sensitive to target location estimate errors, as compared to the scanned phased array.

3.7 Conclusion for Time-Division Beamforming

Time-division beamforming separately designs the transmit signal's spatial and temporal properties through a linear precoder and pulse matrix, respectively. The pulse matrix is of similar form to the omnidirectional MIMO radar, constructed of M orthogonal waveforms. However, in this work, the orthogonality constraint is met through time-division multiplexing (i.e., a temporal orthogonality). We allow the number of pulses to be less than or equal to the number of transmit antennas, and a linear precoder maps the M orthogonal waveforms to M_t transmit antennas.

We defined a MIMO receive ambiguity function that incorporates the linear precoder, pulse matrix, and linear receiver. Time-division beamforming produces an MIMO receive ambiguity function with spatial and delay-Doppler separability. This separability allows existing signals with favorable delay and Doppler properties to be used in the pulse matrix. We then focused on designing the linear precoder for desirable spatial properties.

For M spatially separated targets located at the same range and Doppler, a max-min optimization was formed to maximize the minimum SINR, or in other words to maximize the SINR of the target with the weakest return. This optimization was carried out by the proposed max-min SINR method. The returns of the other $M - 1$ targets served as interference in the SINR model. Locally optimal linear precoders and receive combiners were found and their SINR performance compared to existing MIMO radar transmit signal schemes. Furthermore, it was shown that even with inaccurate measurements of target locations, the transmission of correlated waveforms improved the receive SINR over the transmission of orthogonal waveforms.

The performance, complexity, and power constraint of each transmit signal must be taken into account and weighted differently depending on application. No single transmit scheme works the best for all applications. For instance, the max-min SINR optimization produces a linear precoder that yields the best minimum SINR performance on average, yet is computationally intensive to construct. The phased

array linear precoder, which can be interpreted as an intrapulse steering of the beam in various directions, performed almost as well with far less complexity and met the more stringent constant modulus power constraint. The subarray techniques provide for low complexity schemes, with disjoint schemes obeying uniform element power constraints.

4. WIRELESS CHANNEL ESTIMATION

Coherent wireless communication systems require knowledge of the channel to detect the transmit signal at the receiver. For a narrowband channel, channel knowledge represents information on the complex scalar gains between the transmit and receive antennas. If channel knowledge is available (at either the transmitter or the receiver), significant capacity gains can be achieved over noncoherent signaling. For this reason, a large body of work exists on techniques to obtain channel knowledge at the transmitter and receiver.

Channel state information (CSI) is the term commonly used to describe either the instantaneous channel or the second-order statistics of the wireless channel. If the receiver has channel knowledge, the system possesses channel state information at the receiver (CSIR). Symbol estimation algorithms provide improved performance and simplicity with CSIR. If the transmitter has channel knowledge, the system possesses channel state information at the transmitter (CSIT). For single antenna systems, this is useful for power and rate control. For multiple antenna systems, this is used for transmit beamforming or linear precoding to increase SNR at the receiver.

4.1 Coherence Time for Block Fading Channels

A block-fading channel model assumes the channel remains fixed for a certain duration known as the coherence time [3]. Although wireless channels are constantly varying due to the ever changing environment, block-fading channels are appropriate for slowly varying channels. The channel remains fixed for a given coherence time, or block. An uncorrelated channel realization is then drawn for the next block. If the coherence time is less than the codeword length (i.e., the codeword spans multiple coherence intervals), a fast fading channel is assumed. Conversely, if the coherence

time is greater than the codeword length, a slow fading channel is assumed. With knowledge of the coherence time, coherent wireless communication systems divide the coherence interval into two phases, a training phase and a data transmission phase [19]. During the training phase, signals known a priori to both the transmitter and receiver are propagated through the channel. These signals are generally referred to as *pilots* or *training sequences*. With knowledge of the pilots, the receiver is able to estimate the current channel. If a feedback path exists between the receiver and transmitter, the channel estimate (or a quantized version of it) can be fed back to obtain CSIT. The channel estimate is then used during the data transmission phase to aid in symbol transmission and detection.

Given the transmit structure for block-fading channels just discussed, multiple design variables still need to be addressed to maximize channel capacity for a given coherence time. If too little resources are applied to the training phase, a poor estimate of the channel will result and suboptimal beamforming during the data transmission phase will reduce receive SNR. If too many resources are applied to the training phase, an accurate channel estimate will be had but the power and time to subsequently transmit data will be scarce. These tradeoffs are explored in [19], where the optimal training length and optimal transmit power are discussed for various SNR's.

4.2 MISO Channel

Consider a multiple-input single-output (MISO) wireless channel with M transmit antennas and a single receive antenna. In coherent communications, the wireless channel is considered known and aids in signal transmission and detection. Considering a single channel use, the input-output relationship is

$$r = \mathbf{x}^* (\alpha \mathbf{h}) + n \tag{4.1}$$

where $\mathbf{x} \in \mathbb{C}^{M \times 1}$ is the transmitted signal with $E[\|\mathbf{x}\|^2] = \rho$, ρ denotes the transmit power, $r \in \mathbb{C}$ is the received signal, $n \sim \mathcal{CN}(0, \sigma_n^2)$ the additive noise, and $\alpha \mathbf{h}$ is the

MISO wireless channel. The channel is comprised of the complex scalar channel gain α and the channel direction $\mathbf{h}$, with $\|\mathbf{h}\| = 1$. The input-output equation is defined in a slightly unconventional way, where the channel is projected onto the transmit signal. We write it in this manner to set up the problem for channel estimation, as this notation more closely resembles the linear form for vector estimation [52].

MISO wireless systems are restricted to beamforming; transmitting a single symbol from the M transmit antennas at each channel use. A beamformed transmit signal is defined as $\mathbf{x} = \mathbf{f}s$, where the beamforming vector $\mathbf{f}$ and complex symbol s are constrained to $\|\mathbf{f}\| = 1$ and $E[|s|^2] = \rho$. Fig. 4.1 shows beamforming for a MISO channel. For the MISO system described in (4.1), the receive SNR is defined as

$$\text{SNR} = \frac{\rho|\alpha|^2|\mathbf{f}^*\mathbf{h}|^2}{\sigma_n^2}. \tag{4.2}$$

Separating the channel into a scalar gain term and a vector on the complex unit-sphere clearly shows the impact the channel direction has on receive SNR. For a given power constraint ρ, the receive SNR is maximized when the beamforming gain, $|\mathbf{f}^*\mathbf{h}|^2$, is maximized. Since $\|\mathbf{f}\| = \|\mathbf{h}\| = 1$, the beamforming gain is maximized when the beamforming vector is *aligned* with the true channel direction, $\mathbf{f} = \mathbf{h}$. In general, the true channel direction is unknown for a given block, and must be estimated.

4.3 Background on MISO Channel Estimation

In wireless communications, accurate channel state information plays a central role in realizing the gains afforded by coherent communications. In light of this, much literature exists to design training sequences to estimate the channel. For a block-fading channel model, [19] addressed capacity maximizing values for various parameters, including the length of the training phase and the total power used for training.

Consider a discrete time interval T, composed of the discrete training interval K and the discrete data transmission interval D, where $T = K + D$. For the training phase, we will borrow some of the language typically used for the data transmission

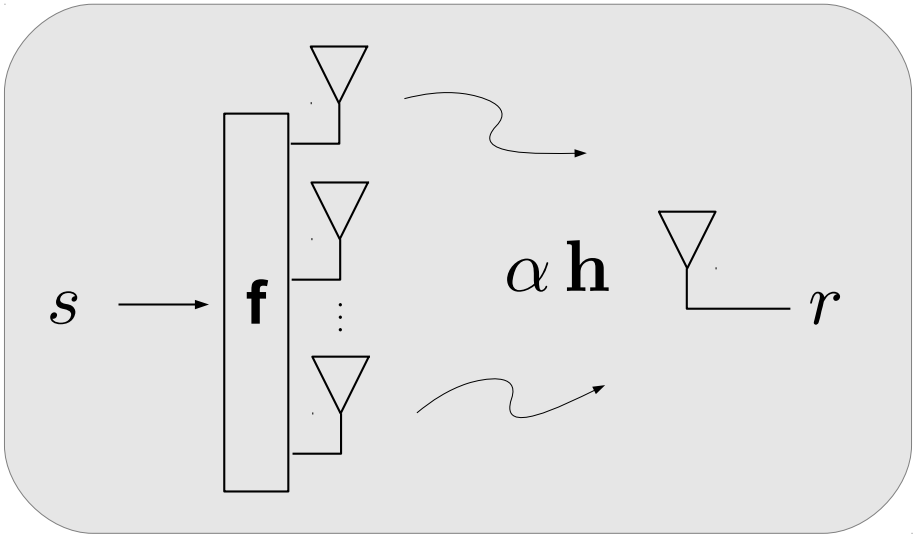

Fig. 4.1. Transmit and receive structure for beamforming across a MISO channel.

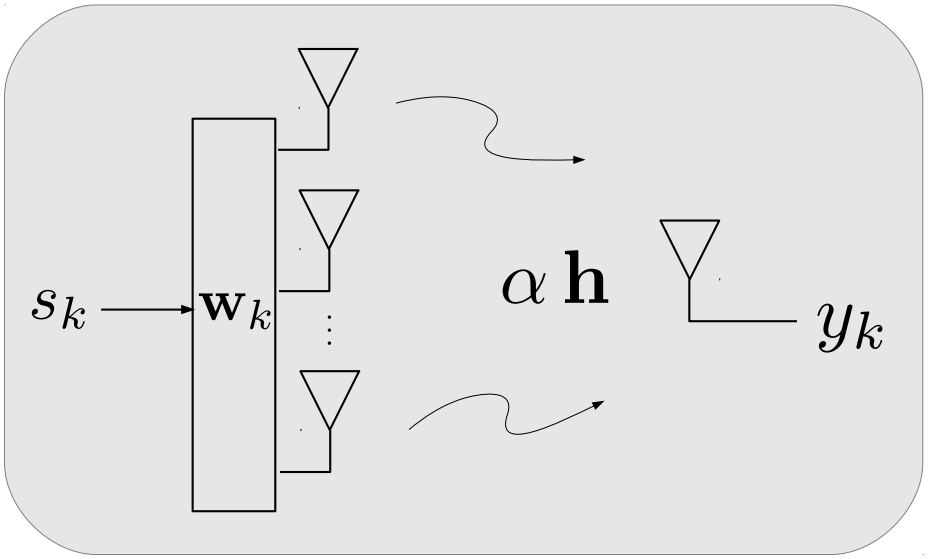

Fig. 4.2. Transmit and receive structure for training the MISO channel with sounding vector $\mathbf{w}_k$.

phase. We will refer to each discrete time use for training as a channel use. With this interpretation in mind, the beamforming vectors specifically designed for training will be termed *sounding vectors*. We will, however, use a different notation for the beamforming vectors used for training; $\mathbf{w}_k$ is the sounding vector for the k^{th} channel use. The sounding vectors and receive signal for the training phase are illustrated in Fig. 4.2.

In general, the training phase jointly estimates the channel magnitude and direction, $\mathbf{g} = \alpha\mathbf{h}$. We will use this notation to describe common channel estimation techniques. The pilots are defined by the pilot matrix $\mathbf{W} \in \mathbb{C}^{M\times K}$, and the input-output channel relationship is given by,

$$\mathbf{y} = \sqrt{\rho}\mathbf{W}^*\mathbf{g} + \mathbf{n} \tag{4.3}$$

where ρ is the total transmit power for each channel use and M is the number of transmit antennas. The sounding vector matrix $\mathbf{W}$ is composed of K sounding vectors (one for each channel use),

$$\mathbf{W} = \begin{bmatrix} \mathbf{w}_1 & \mathbf{w}_2 & \cdots & \mathbf{w}_K \end{bmatrix}.$$

Three common ways to estimate the channel are through the maximimum likelihood (ML) estimate, minimimum mean square error (MMSE) estimate, and the least squares (LS) estimate,

$$\begin{aligned} \widehat{\mathbf{g}}_{\mathrm{ML}} &= \frac{1}{\sqrt{\rho}} \left(\mathbf{W}\mathbf{W}^*\right)^{-1} \mathbf{W}\mathbf{y} \\ \widehat{\mathbf{g}}_{\mathrm{MMSE}} &= \frac{1}{\sqrt{\rho}} \left(\frac{\sigma_n^2}{\rho}\mathbf{I} + \mathbf{W}\mathbf{W}^*\right)^{-1} \mathbf{W}\mathbf{y} \\ \widehat{\mathbf{g}}_{\mathrm{LS}} &= \frac{1}{\sqrt{\rho}} \left(\mathbf{W}\mathbf{W}^*\right)^{-1} \mathbf{W}\mathbf{y} \end{aligned}$$

The maximum likelihood estimator and least squares estimator assume $\mathbf{W}$ to be of rank M, implying $K \geq M$. The mean square error of $\widehat{\mathbf{g}}_{\mathrm{MMSE}}$ is given by

$$\mathrm{MSE} = \mathrm{tr}\left[\left(\mathbf{I} + \frac{\rho}{\sigma_n^2}\mathbf{W}\mathbf{W}^*\right)^{-1}\right].$$

In [19], the pilot matrix which minimizes the mean square error of the channel estimate obeys the property

$$\mathbf{W}\mathbf{W}^* = \frac{K}{M}\mathbf{I}. \tag{4.4}$$

This result shows that $\mathbf{W}\mathbf{W}^*$ must be a scaled identity matrix; the pilot matrix must consist of orthogonal pilots, or orthogonal sequences, transmitted out of each transmit element. Of course, it is important to mention that the type of pilot matrix in (4.4) minimizes the mean square error on the channel estimate under the assumption that individual channel gains are independently drawn from a standard complex normal distribution, $[\mathbf{g}]_i \sim \mathcal{CN}(0,1)$. Optimal pilots with knowledge of the channel's second order statistics for correlated channels were designed in [20].

The problem of choosing the optimal length of the training phase was also considered in [19] for MIMO channel estimation. From that work, it was proven that

the optimal discrete training interval is equal to the number of transmit antennas, $K = M$. This holds true for all coherence times T and transmit power constraints ρ. The problem arises when the transmit array contains a large number of elements, as is assumed in much of the massive MIMO literature [21]. The length of the training phase scales with the number of transmit elements, which can have an impact on data throughput for very large arrays.

The coherence time is typically fixed or assumed fixed based on the environment. Furthermore, the coherence time is completely independent of any transmit or receive processing, and is purely a function of the electromagnetic properties of the local environment. For this reason, T is considered fixed. One can see that if the system assumes optimal pilots according to [19], with $T = K + D = M + D$, then as the number of antennas increases the number of channel uses to optimally train the channel increases as well. The problem arises when the number of channel uses to train approaches T. When this happens, there are very few channel uses left for data transmission and system throughput will suffer. Suboptimal training schemes must be used for this case, where a hit in channel estimation performance is taken when $K < M$. This provides an open area to design suboptimal training schemes for massive MIMO systems, and is exactly the scenario for which our beam alignment scheme was created.

4.4 Previous Work on Adaptive Sampling

Channel estimation with training sequences of length less than the number of transmit antennas was considered for distributed transmit beamforming systems in [53]. The set of training sequences which minimizes the mean square error of the MMSE channel estimate was shown to be approximately similar to those maximizing the expected beamforming gain, which again renders a training signal matrix with orthogonal columns. The optimal full-rank set of receive beamforming vectors for angle of arrival estimation was derived in [54]. The channel gain term was treated as

a deterministic unknown, and beamforming vectors derived to minimize the variance on the angle of arrival estimate.

Thus far, the referenced literature pertains to a class of open-loop schemes in which the training sequence is predetermined. These training sequences cannot be adapted to knowledge gathered of the instantaneous channel. Alternatively, adaptive training schemes use a feedback link from the receiver to the transmitter to guide the design of the training sequence. Closed-loop training for massive MIMO beamforming systems was considered in [55]. Improvements in average receive SNR were shown by utilizing the training sequences received in previous channel blocks. Line-of-sight channel estimation for large arrays in backhaul cellular networks is presented in [56]. Adaptive subspace sampling, where samples from previous channel uses aid in beamformer design, gave improved beamforming gain over non-adaptive techniques. Pilot beampatterns were sequentially designed for massive MIMO systems in [57] through the use of a Kalman filter for spatially and temporally correlated channels. Feedback is inherent in a radar system, where [58] adapted the transmit beamforming vector to current channel conditions. Additionally, earlier work in [59] actively designed waveforms for improved sequential hypothesis testing. Considering the compressed sensing literature, adaptive schemes estimate sparse (only a few number of nonzero elements) vectors in [60].

In this work, we consider channel estimation for beamforming systems in a single coherent channel block. A feedback channel allows adaptation of the training sequence after each channel use. The training sequence is comprised of sounding vectors, which are sequentially designed in a manner that aligns the estimated channel direction with the true instantaneous channel direction. The channel gain term is treated as a nuisance parameter, and its maximum likelihood estimate used in the channel direction estimator. With the inclusion of a feedback link, estimating the channel direction can be seen as an adaptive sampling scheme. The set of K sounding vectors behave as the projection matrix of an unknown channel direction $\mathbf{h}$. This work focuses on frequency division duplexing (FDD) systems, where channel reciprocity cannot be

used for transmit beamforming. Nonetheless, this scheme remains applicable for time division duplexing (TDD) systems without the need for a feedback channel.

5. CLOSED-LOOP BEAM ALIGNMENT FOR CHANNEL ESTIMATION

We present a feedback-enabled training algorithm targeted towards underdetermined training, where the number of channel uses for training is less than the number of transmit antennas. As we have shown in the previous chapter, the optimal training sequence requires $K \geq M$. In light of this, the algorithm presented in this chapter takes advantage of a feedback link to improve channel estimation performance when $K < M$.

To estimate the wireless channel, assume K channel uses are available for this task. Let $\mathbf{x}_k$ represent the training signal for the k^{th} channel use. If the transmit signal for data transmission is restricted to beamforming, it is natural to restrict the training signal in the same fashion. The training signal, $\mathbf{x}_k = \mathbf{w}_k s_k$, is comprised of a M-dimensional sounding vector $\mathbf{w}_k$ and a training symbol s_k. A total power constraint ρ is enforced for each channel use, so we constrain $\|\mathbf{w}_k\| = 1$ and $E[|s_k|^2] = \rho$. Both $\mathbf{w}_k$ and s_k are known ahead of time at the transmitter and receiver. Taking into account proper pulse shaping, matched filtering, and symbol detection, the receive sample for the k^{th} channel use is given by

$$y_k = \sqrt{\rho}\alpha \mathbf{w}_k^* \mathbf{h} + n_k. \tag{5.1}$$

We use this specific notation for the input-output channel equation following the convention in estimation theory, where typically the vector to be estimated is a column vector projected onto a known matrix or vector.

To aid in sub-optimal channel estimation for the case where $K < M$, we consider a limited-rate feedback channel from the receiver to the transmitter as shown in Fig. 5.1. Let $\mathcal{W}$ represent the set of possible sounding vectors, $\mathcal{W} = \{\mathbf{w}^{(\ell)} \in \mathbb{C}^{M\times 1} : \|\mathbf{w}^{(\ell)}\| = 1\}$. Due to the restricted bandwidth of the feedback channel, we design $\mathcal{W}$

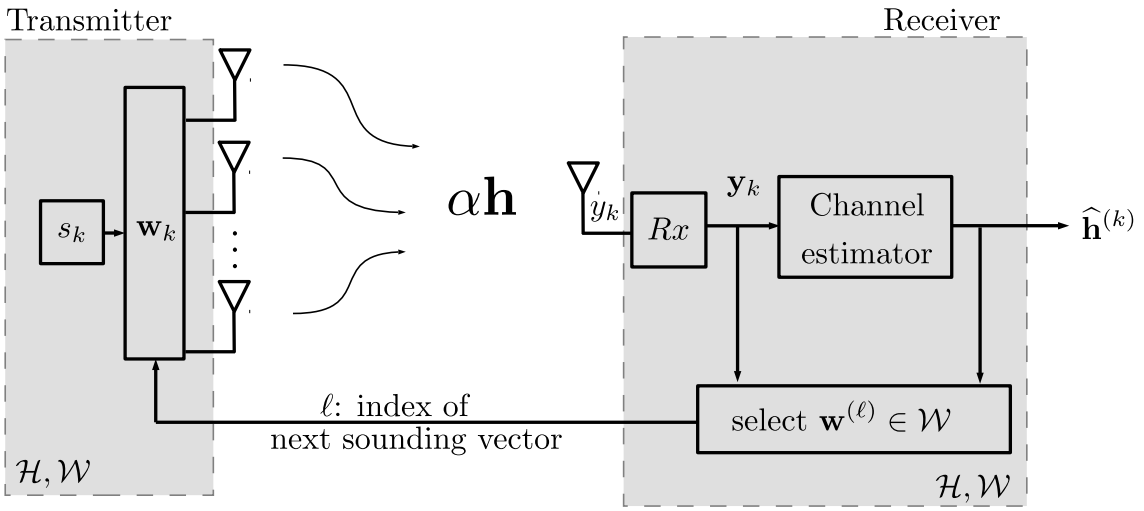

Fig. 5.1. Block diagram illustrating the proposed training scheme. The receiver selects the sounding vector from the codebook $\mathcal{W}$ for the next channel use and feeds back the codeword index to the transmitter.

to be a discrete set with $|\mathcal{W}| = L$, where $|\mathcal{W}|$ denotes the cardinality of the set $\mathcal{W}$, and make this codebook available ahead of time to both the transmitter and receiver. For the k^{th} channel use, the receiver calculates an estimate of $\mathbf{h}$ and decides on the appropriate $\mathbf{w}^{(\ell)} \in \mathcal{W}$ to sound the $(k+1)^{\text{th}}$ channel use. The index of this sounding vector is fed back to the transmitter, as described in Fig. 5.1.

Let us assume the channel direction vector belongs to the set $\mathbf{h} \in \mathcal{H}$, where $\mathcal{H}$ can be any continuous space, finite set, subspace, or manifold. We consider the vector form of the receive sample in (5.1) for k channel uses,

$$\mathbf{y}_k = \alpha\sqrt{\rho}\mathbf{W}_k^*\mathbf{h} + \mathbf{n}_k$$

where $\mathbf{W}_k = [\mathbf{w}_1, \mathbf{w}_2, \ldots, \mathbf{w}_k]$ is the set of k sounding vectors and $\mathbf{y}_k$ is the $k \times 1$ complex receive sample vector. After k channel uses, the maximum a posteriori probability (MAP) channel direction estimator is given by,

$$\widehat{\mathbf{h}}^{(k)} = \underset{\mathbf{h}\in\mathcal{H}}{\operatorname{argmax}}\, p\left(\mathbf{h}|\mathbf{y}_k, \mathbf{W}_k, \alpha\right).$$

The posterior distribution for $\mathbf{h}$ is conditioned on the received sample vector, set of sounding vectors, and channel magnitude. In general, the channel magnitude α is unknown. From (4.2), we saw that the beamforming gain is the magnitude squared of the correlation between the beamforming vector and the true channel direction; the beamforming gain is not impacted by the magnitude of the true channel α. If the beamforming vector for data transmission is $\mathbf{f} = \widehat{\mathbf{h}}^{(k)}$, then the sounding vectors should be designed to maximize beamforming gain, $|\mathbf{h}^* \widehat{\mathbf{h}}^{(k)}|^2$. Since we are only interested in accurately estimating the channel direction to maximize receive SNR, we treat α as a nuisance parameter. From a Bayesian perspective, given a prior on α the dependence on α could be removed by averaging over the prior,

$$\int p(\mathbf{h}|\mathbf{y}_k, \mathbf{W}_k, \alpha) p(\alpha) \, \mathrm{d}\alpha.$$

However if we model $\alpha\mathbf{h}$ as uncorrelated Rayleigh fading, then $\mathbf{h}$ is uniformly distributed over the M-dimensional unit-sphere and α is a real random variable with a chi distribution. Integrating over a chi prior does not give a tractable result. Hence we resort to composite estimation techniques, and take the frequentist approach and model the channel gain α as an unknown deterministic nuisance parameter.

Given $\mathbf{h}$, the maximimum likelihood of the channel magnitude is

$$\widehat{\alpha}_{\mathbf{h}} \;=\; \underset{\alpha \in \mathbb{C}}{\operatorname{argmax}} \, p\left(\mathbf{y}_k | \mathbf{h}, \mathbf{W}_k, \alpha\right) = \frac{\mathbf{h}^* \mathbf{W}_k \mathbf{y}_k}{\sqrt{\rho} \|\mathbf{W}_k^* \mathbf{h}\|^2}.$$

This result can be shown by minimizing the squared norm $\|\mathbf{y}_k - \alpha\sqrt{\rho}\mathbf{W}_k^*\mathbf{h}\|^2$ over all $\alpha \in \mathbb{C}$. The generalized channel direction estimator is given by assuming a uniform prior for $\mathbf{h}$ and substituting $\widehat{\alpha}_{\mathbf{h}}$ into the MAP estimator,

$$\begin{aligned}
\widehat{\mathbf{h}}^{(k)} &= \underset{\mathbf{h} \in \mathcal{H}}{\operatorname{argmax}} \, p\left(\mathbf{h} | \mathbf{y}_k, \mathbf{W}_k, \widehat{\alpha}_{\mathbf{h}}\right) \\
&= \underset{\mathbf{h} \in \mathcal{H}}{\operatorname{argmin}} \|\mathbf{y}_k - \widehat{\alpha}_{\mathbf{h}} \sqrt{\rho} \mathbf{W}_k^* \mathbf{h}\|^2 \\
&= \underset{\mathbf{h} \in \mathcal{H}}{\operatorname{argmax}} \, \frac{|\mathbf{y}_k^* \mathbf{W}_k^* \mathbf{h}|^2}{\|\mathbf{W}_k^* \mathbf{h}\|^2} \\
&= \underset{\mathbf{h} \in \mathcal{H}}{\operatorname{argmax}} \, d_k(\mathbf{h}) \qquad (5.2)
\end{aligned}$$

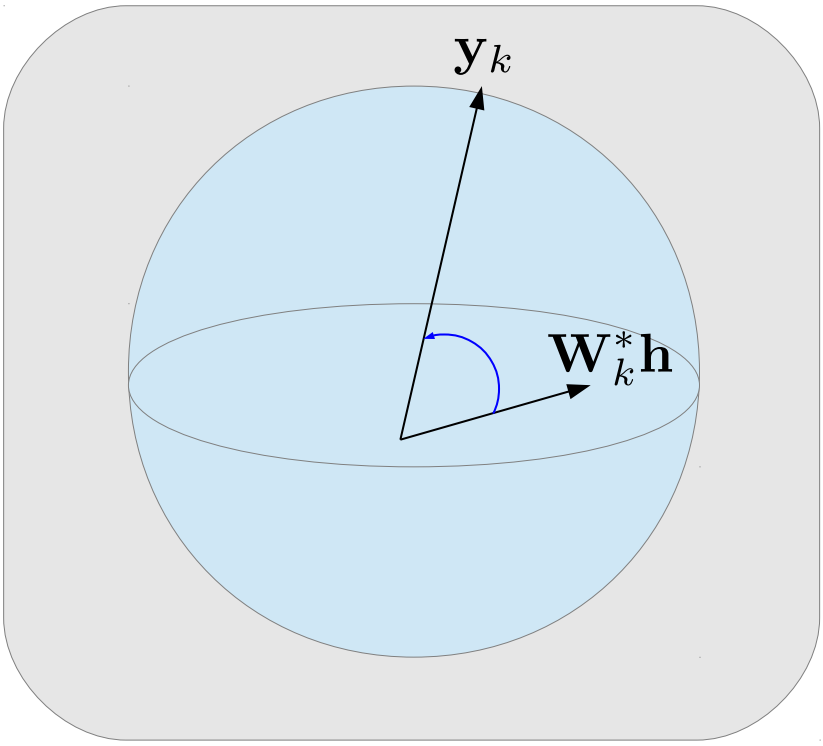

Fig. 5.2. The estimated channel direction is the $\mathbf{h}$ that best aligns the vector $\mathbf{W}_k^*\mathbf{h}$ with $\mathbf{y}_k$.

where $d_k(\mathbf{h}) = \frac{|\mathbf{y}_k^*\mathbf{W}_k^*\mathbf{h}|^2}{\|\mathbf{W}_k^*\mathbf{h}\|^2}$. In essence, this channel estimator finds the channel vector $\mathbf{h} \in \mathcal{H}$ whose projection onto $\mathbf{W}_k$ most closely aligns in the *direction* of $\mathbf{y}_k$. This is illustrated in Fig. 5.2. The normalizing term $\|\mathbf{W}_k^*\mathbf{h}\|^2$ removes any notion of vector magnitude, leaving the estimator to choose the channel estimate $\widehat{\mathbf{h}}^{(k)}$ to align $\mathbf{W}_k^*\widehat{\mathbf{h}}^{(k)}$ with $\mathbf{y}_k$. We can show that the quantity $d_k(\mathbf{h})$ is maximized when the unit vector $\mathbf{W}_k^*\mathbf{h}/\|\mathbf{W}_k^*\mathbf{h}\|$ points in the same direction as $\mathbf{y}_k$. This is equivalent to,

$$\mathbf{W}_k^*\mathbf{h} = \gamma\,\mathbf{y}_k$$

for any real scalar γ. We can then show the optimal channel direction to be,

$$\widehat{\mathbf{h}}_{\text{opt}}^{(k)} = \gamma\frac{\mathbf{W}_k\left(\mathbf{W}_k^*\mathbf{W}_k\right)^{-1}\mathbf{y}_k}{\|\mathbf{W}_k\left(\mathbf{W}_k^*\mathbf{W}_k\right)^{-1}\mathbf{y}_k\|} + \sqrt{1-|\gamma|^2}\mathbf{z}$$

where $\mathbf{z} \in \text{Null}\{\mathbf{W}_k\}$ and $0 < |\gamma| \leq 1$. In theory, there is no unique solution that maximizes (5.2). All that is required is the projection of $\mathbf{h}$ onto $\text{span}\{\mathbf{W}_k\}$ is aligned

in the same direction as $\mathbf{W}_k \left(\mathbf{W}_k^* \mathbf{W}_k\right)^{-1} \mathbf{y}_k$. Furthermore, $\mathbf{z}$ can be of any direction or magnitude as long as it lies in the subspace of the channel not yet sounded. We showed in Section 4.2 that the SNR-maximizing transmit beamformer is set to the true channel direction. If the channel direction is unknown, then the beamformer is set equal to the estimated channel direction, $\mathbf{f} = \widehat{\mathbf{h}}^{(k)}$. Physically implementing a transmit beamformer onto a real array may be limited by the hardware in practice. For example, if the phase shifters behind each element can only be set to one of 2^B phases, the transmit beamformer (considering a constant amplitude profile) can be one of M^{2^B} directions, where B is the number of bits to control each phase shifter. The set of available transmit beamformers could also be limited to the array manifold. The beamformer would then be parameterized by a single parameter, θ, which points a beam towards a particular direction θ. These two examples show restrictions on the transmit beamformer enforced by hardware constraints. It follows naturally to to restrict the channel codebook in the same fashion. Suppose the channel codebook consists of N unit-norm vectors $\mathcal{H} = \{\mathbf{h}_1, \mathbf{h}_2, \ldots, \mathbf{h}_N\}$. One can also argue that for large enough N, discretization of the channel space becomes an acceptable approximation. Consider a cap with radius ϵ on each vector $\mathbf{h}_n$, as shown in Fig. 5.3. If N is large enough, the entire channel space will be covered with N caps, and the true channel direction is guaranteed to be separated by at most a distance ϵ from one of the discretized channel codewords in $\mathcal{H}$. This applies to channel spaces that contain the entire M-dimensional space or only a portion of it, such as the array manifold.

5.1 Probability of Misalignment

As one might expect, the set of k sounding vectors in $\mathbf{W}_k$ has direct influence on the performance of the channel estimator in (5.2). We first state our assumptions before introducing the probability of misalignment, a metric optimized to select the sounding vector for the following channel use. At any given channel use, we restrict the set of sounding vectors to a codebook $\mathcal{W}$. For the $(k+1)^{\text{th}}$ channel use, $\mathbf{w}^{(l)}$ is

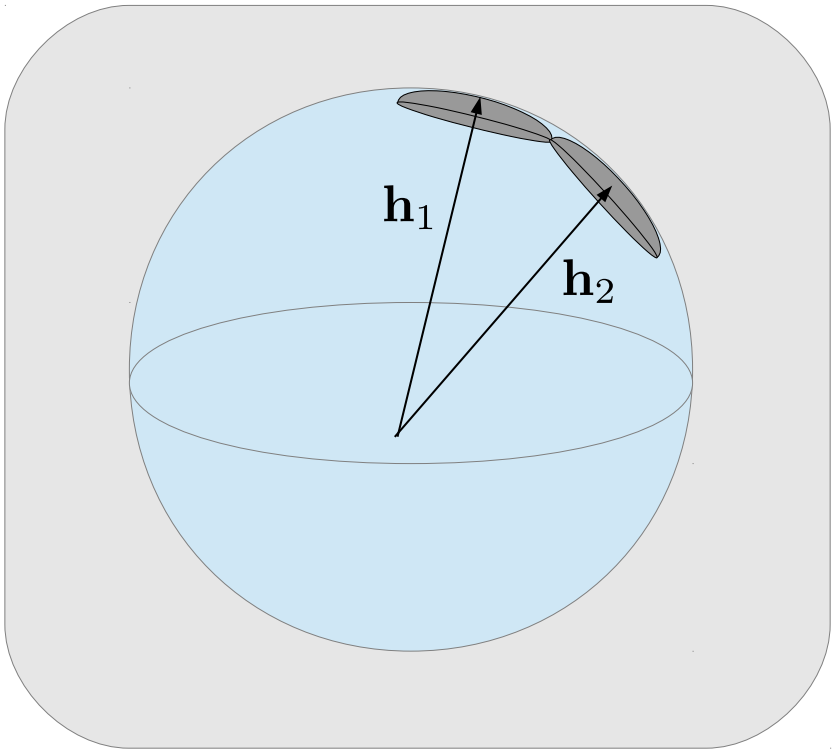

Fig. 5.3. Approximating the channel space $\mathcal{H}$ picturing each vector with a radius-ϵ cap on it. If N is large enough, the entire channel space will be covered and be well approximated by $\mathcal{H}$.

chosen from $\mathcal{W}$ to minimize the probability of misalignment. We assume the current channel direction estimate is given by (5.2) and the channel space $\mathcal{H}$ is discretized. With these assumptions, successive sounding vectors are selected by minimizing the probability of misalignment.

We adopt a similar approach to the average probability of error for symbol transmission in communications [61]. Instead of detecting signals, we are interested in detecting the true channel direction from some discrete channel codebook $\mathcal{H}$. Let us define the misalignment event as $\mathcal{M} = \left\{\widehat{\mathbf{h}}^{(k+1)} \neq \mathbf{h}\right\} \Big| \mathbf{y}_k, \mathbf{W}_{k+1}, \mathbf{h}, \widehat{\alpha}_{\mathbf{h}}$. The probability of the misalignment event is the probability the estimated channel vector is not the true channel vector given $\mathbf{h}$. Since $\mathbf{h}$ is unknown, the probability of misalignment is the expectation of $\Pr\left(\mathcal{M} = \left\{\widehat{\mathbf{h}}^{(k+1)} \neq \mathbf{h}\right\} \Big| \mathbf{y}_k, \mathbf{W}_{k+1}, \mathbf{h}, \widehat{\alpha}_{\mathbf{h}}\right)$, with the expectation taken over $\mathbf{h}$.

$$\begin{aligned} P_{\text{misalign}} &= E_{\mathbf{h}}\left[\Pr\left(\mathcal{M}\Big|\mathbf{y}_k, \mathbf{W}_{k+1}, \mathbf{h}, \widehat{\alpha}_{\mathbf{h}}\right)\right] \\ &= \sum_{i=1}^{N} \Pr\left(\mathcal{M}\Big|\mathbf{y}_k, \mathbf{W}_{k+1}, \mathbf{h}_i, \widehat{\alpha}_{\mathbf{h}_i}\right) p_i^{(k)} \\ &= \sum_{i=1}^{N} \Pr\left(d_{k+1}(\mathbf{h}_i) < \max\left[\left\{d_{k+1}(\mathbf{h}_j)\right\}_{j\neq i}\right]\right) p_i^{(k)} \end{aligned} \tag{5.3}$$

where $p_i^{(k)} = p\left(\mathbf{h}_i | \mathbf{y}_k, \mathbf{W}_{k+1}, \{\widehat{\alpha}_{\mathbf{h}_i}\}\right)$ are the updated priors after k channel uses and $\widehat{\alpha}_{\mathbf{h}}$ the maximum likelihood channel magnitude estimates given $\mathbf{h}$. Since we are conditioning on the previous k receive samples, the priors are replaced by the updated priors in the probability of misalignment expression, which are defined as,

$$\begin{aligned} p_i^{(k)} &= p\left(\mathbf{h}_i | \mathbf{y}_k, \mathbf{W}_{k+1}, \{\widehat{\alpha}_{\mathbf{h}_i}\}\right) \\ &= \frac{p\left(\mathbf{y}_k | \mathbf{h}_i, \mathbf{W}_k, \widehat{\alpha}_{\mathbf{h}_i}\right) p\left(\mathbf{h}_i | \mathbf{W}_k, \widehat{\alpha}_{\mathbf{h}_i}\right)}{\sum\limits_{\substack{n=1 \\ n\neq i}}^{N} p\left(\mathbf{y}_k | \mathbf{h}_n, \mathbf{W}_k, \widehat{\alpha}_{\mathbf{h}_n}\right) p\left(\mathbf{h}_n | \mathbf{W}_k, \widehat{\alpha}_{\mathbf{h}_n}\right)}. \end{aligned}$$

One can interpret $\Pr\left(d_{k+1}(\mathbf{h}_i) < \max\left[\{d_{k+1}(\mathbf{h}_j)\}_{j\neq i}\right]\right)$ as the probability $\mathbf{W}_k^* \mathbf{h}_i$ is not the channel codeword that most closely aligns with $\mathbf{y}_k$.

Note that $d_{k+1}(\mathbf{h}) = \frac{|\mathbf{y}_{k+1}^* \mathbf{W}_{k+1}^* \mathbf{h}|^2}{\|\mathbf{W}_{k+1}^* \mathbf{h}\|^2}$ is a random variable, with

$$\mathbf{y}_{k+1} = \begin{bmatrix} \mathbf{y}_k \\ \sqrt{\rho}\alpha \mathbf{w}_{k+1}^* \mathbf{h} + n_{k+1} \end{bmatrix}$$

where $n_{k+1} \sim \mathcal{CN}(0, \sigma_n^2)$. Given the randomness of $\mathbf{y}_{k+1}$ and the unknown channel direction and magnitude, we can choose the sounding vector for the $(k+1)^{\text{th}}$ channel use to minimize the probability of misalignment,

$$\mathbf{w}_{k+1} = \underset{\mathbf{w}^{(\ell)} \in \mathcal{W}}{\operatorname{argmin}} P_{\text{misalign}}$$

where $\mathbf{W}_{k+1} = [\mathbf{W}_k \ \mathbf{w}^{(\ell)}]$. To further see how to calculate the probability of misalignment and evaluate the expression in (5.3) for a given $\mathbf{w}_{k+1}$, $\mathbf{y}_k$ and $\mathbf{W}_k$, we first study the binary channel codebook.

5.2 Binary Channel Codebook

We approximate the channel using a binary channel codebook, $\mathcal{H} = \{\mathbf{h}_1, \mathbf{h}_2\}$. Despite being an extremely course discretization of the channel space, we show the probability of misalignment can be found in closed from for a binary channel codebook. We can write the probability of misalignment as,

$$\begin{aligned} P_{\text{misalign}} = \Pr\Big(d_{k+1}(\mathbf{h}_1) < d_{k+1}(\mathbf{h}_2)\Big) p_1^{(k)} \\ + \Pr\Big(d_{k+1}(\mathbf{h}_2) < d_{k+1}(\mathbf{h}_1)\Big) p_2^{(k)}. \end{aligned} \tag{5.4}$$

The probability of misalignment in (5.4) is the weighted sum of pairwise error probabilities (PEP), where assuming $\mathbf{h}_2$ is true the probability $\mathbf{h}_1$ is chosen is

$$\text{PEP}\left(\mathbf{h}_2 \to \mathbf{h}_1\right) = \Pr\left(\frac{|\mathbf{y}_{k+1}^* \mathbf{W}_{k+1}^* \mathbf{h}_1|^2}{\|\mathbf{W}_{k+1}^* \mathbf{h}_1\|^2} > \frac{|\mathbf{y}_{k+1}^* \mathbf{W}_{k+1}^* \mathbf{h}_2|^2}{\|\mathbf{W}_{k+1}^* \mathbf{h}_2\|^2}\right). \tag{5.5}$$

Since $\frac{\mathbf{y}_{k+1}^* \mathbf{W}_{k+1}^* \mathbf{h}_i}{\|\mathbf{W}_{k+1}^* \mathbf{h}_i\|}$ is a Gaussian random variable, the pairwise error probability is the probability the magnitude of one Gaussian random variable exceeds the magnitude of another. This is similar to the probability of error of envelope detection for correlated

binary signals in [61]. However, the results there do not hold when each variable is a linear function of the same scalar Gaussian random variable. To see this property explicitly, we can decompose the channel estimator (assuming $\mathbf{h}_2$ is true) as

$$\frac{\mathbf{y}_{k+1}^*\mathbf{W}_{k+1}^*\mathbf{h}_2}{\|\mathbf{W}_{k+1}^*\mathbf{h}_2\|} = \frac{\mathbf{y}_k^*\mathbf{W}_k^*\mathbf{h}_2 + \sqrt{\rho}\widehat{\alpha}_{\mathbf{h}_2}^*\mathbf{h}_2^*\mathbf{w}_{k+1}\mathbf{w}_{k+1}^*\mathbf{h}_2}{\|\mathbf{W}_{k+1}^*\mathbf{h}_2\|} + \frac{\mathbf{w}_{k+1}^*\mathbf{h}_2}{\|\mathbf{W}_{k+1}^*\mathbf{h}_2\|}n_{k+1}.$$

Note that each $\frac{\mathbf{y}_{k+1}^*\mathbf{W}_{k+1}^*\mathbf{h}_i}{\|\mathbf{W}_{k+1}^*\mathbf{h}_i\|}$, for all i, are functions of the same random noise component n_{k+1}. Comparing the magnitudes of variables which are functions of the same Gaussian random variable is analyzed in the following lemma.

Lemma 1 *Consider two Gaussian random variables,*

$$\begin{aligned} X &= \mu_x + q_x n \sim \mathcal{CN}(\mu_x, |q_x|^2) \\ Y &= \mu_y + q_y n \sim \mathcal{CN}(\mu_y, |q_y|^2) \end{aligned}$$

where μ_x, μ_y, q_x, q_y are all constant complex scalars and $n \sim \mathcal{CN}(0,1)$. Then,

$$Pr\left(|X|^2 > |Y|^2\right) = \tag{5.6}$$
$$\begin{cases} 1 - Q_1\left(\left|\frac{\mu_y q_y^* - \mu_x q_x^*}{|q_y|^2 - |q_x|^2}\right|, \left|\frac{\mu_x q_y - q_x \mu_y}{|q_y|^2 - |q_x|^2}\right|\right) & \text{if } |q_y|^2 > |q_x|^2 \\ Q_1\left(\left|\frac{\mu_y q_y^* - \mu_x q_x^*}{|q_y|^2 - |q_x|^2}\right|, \left|\frac{\mu_x q_y - q_x \mu_y}{|q_y|^2 - |q_x|^2}\right|\right) & \text{if } |q_y|^2 < |q_x|^2 \\ \frac{1}{2}\left[1 + \text{erf}\left(\frac{|\mu_y|^2 - |\mu_x|^2}{2\sqrt{2}|\mu_y^* q_y - \mu_x^* q_x|}\right)\right] & \text{if } |q_y|^2 = |q_x|^2 \end{cases}$$

Proof: See Appendix C. ■

Given Lemma 1, we can calculate the pairwise error probability assuming $\mathbf{h}_2$ is true,

$$\begin{aligned} &\Pr\left(d_{k+1}(\mathbf{h}_1) > d_{k+1}(\mathbf{h}_2)\middle|\mathbf{h} = \mathbf{h}_2, \mathbf{y}_k, \mathbf{W}_{k+1}, \widehat{\alpha}_{\mathbf{h}_2}\right) \\ &\qquad = Q_1\left(\left|\frac{\mu_y q_y^* - \mu_x q_x^*}{|q_y|^2 - |q_x|^2}\right|, \left|\frac{\mu_x q_y - q_x \mu_y}{|q_y|^2 - |q_x|^2}\right|\right) \end{aligned}$$

where the parameters are set (assuming $|q_y|^2 < |q_x|^2$) as

$$\begin{aligned} \mu_x &= \frac{\mathbf{y}_k^*\mathbf{W}_k^*\mathbf{h}_1 + \sqrt{\rho}\widehat{\alpha}_{\mathbf{h}_2}^*\mathbf{h}_2^*\mathbf{w}_{k+1}\mathbf{w}_{k+1}^*\mathbf{h}_1}{\|\mathbf{W}_{k+1}^*\mathbf{h}_1\|} \\ q_x &= \frac{\mathbf{w}_{k+1}^*\mathbf{h}_1}{\|\mathbf{W}_{k+1}^*\mathbf{h}_1\|} \\ \mu_y &= \frac{\mathbf{y}_k^*\mathbf{W}_k^*\mathbf{h}_2 + \sqrt{\rho}\widehat{\alpha}_{\mathbf{h}_2}^*|\mathbf{w}_{k+1}^*\mathbf{h}_2|^2}{\|\mathbf{W}_{k+1}^*\mathbf{h}_2\|} \\ q_y &= \frac{\mathbf{w}_{k+1}^*\mathbf{h}_2}{\|\mathbf{W}_{k+1}^*\mathbf{h}_2\|}. \end{aligned}$$

With the ability to calculate the pairwise error probabilities in (5.5), the probability of misalignment in (5.4) directly follows. If the probability of misalignment is calculated for each $\mathbf{w}^{(\ell)} \in \mathcal{W}$, then the sounding vector for the $(k+1)^{\text{th}}$ channel use is given by

$$\mathbf{w}_{k+1} = \underset{\mathbf{w}^{(\ell)} \in \mathcal{W}}{\operatorname{argmin}} P_{\text{misalign}}. \tag{5.7}$$

where $\mathbf{W}_{k+1} = [\mathbf{W}_k \ \mathbf{w}^{(\ell)}]$. Given $\mathbf{y}_k$ and $\mathbf{W}_k$, this optimization chooses the sounding vector which minimizes the probability of misalignment. The PEP's in the probability of misalignment expression are weighted by the updated priors. In a sense, the optimal sounding vector attempts to maximally separate the vector projections, $\mathbf{W}_{k+1}^{*}\mathbf{h}_i$, in the $(k+1)$-dimensional space. The updated priors more heavily weigh the PEP's for the likely codewords, ensuring these codewords are particularly spread out from one another.

5.2.1 Impact of Channel Codeword Correlation on Beamforming Gain

We now turn our attention to understanding how the channel direction estimator behaves as a function of channel codeword correlation. Assuming the binary channel codebook $\mathcal{H} = \{\mathbf{h}_1, \mathbf{h}_2\}$, we denote the correlation coefficient between the two channel codewords as $\rho_{\mathbf{h}} = |\mathbf{h}_1^{*}\mathbf{h}_2|$. We plot the average beamforming gain in Fig. 5.4 as a function of $\rho_{\mathbf{h}}$ for various k. The beamforming gain is averaged over 5000 iterations for $M = 4$ antennas and a receive SNR of 0dB. The sounding vector codebook $\mathcal{W}$ contains unit-norm vectors in the subspace spanning the dimensions of the two channel codewords. To isolate the performance as a function of channel codeword correlation, we restricted $|\alpha| = 1$. In the following section, we focus on the impact of $|\alpha|$ on the beam alignment performance. Each curve in Fig. 5.4 represents the average beamforming gain after the k^{th} channel use. As expected, the average beamforming gain increases as a function of channel use. Furthermore, for a given channel use, a binary channel codebook with higher correlation shows increased beamforming gain. This follows from the fact that the received samples will have high SNR if either channel codeword is true, as $\mathbf{w}_k$ projects strongly onto both channel codewords. The

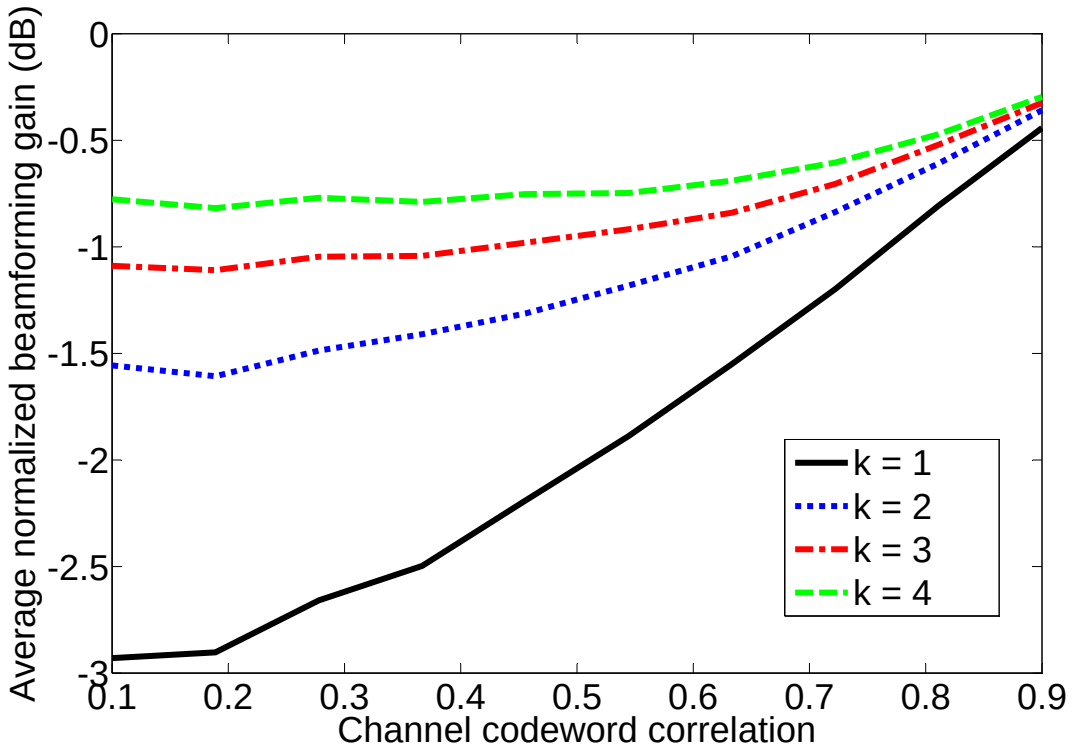

Fig. 5.4. Average beamforming gain as a function of codeword correlation, $\rho_{\mathbf{h}}$, for a binary channel codebook and $M = 4$.

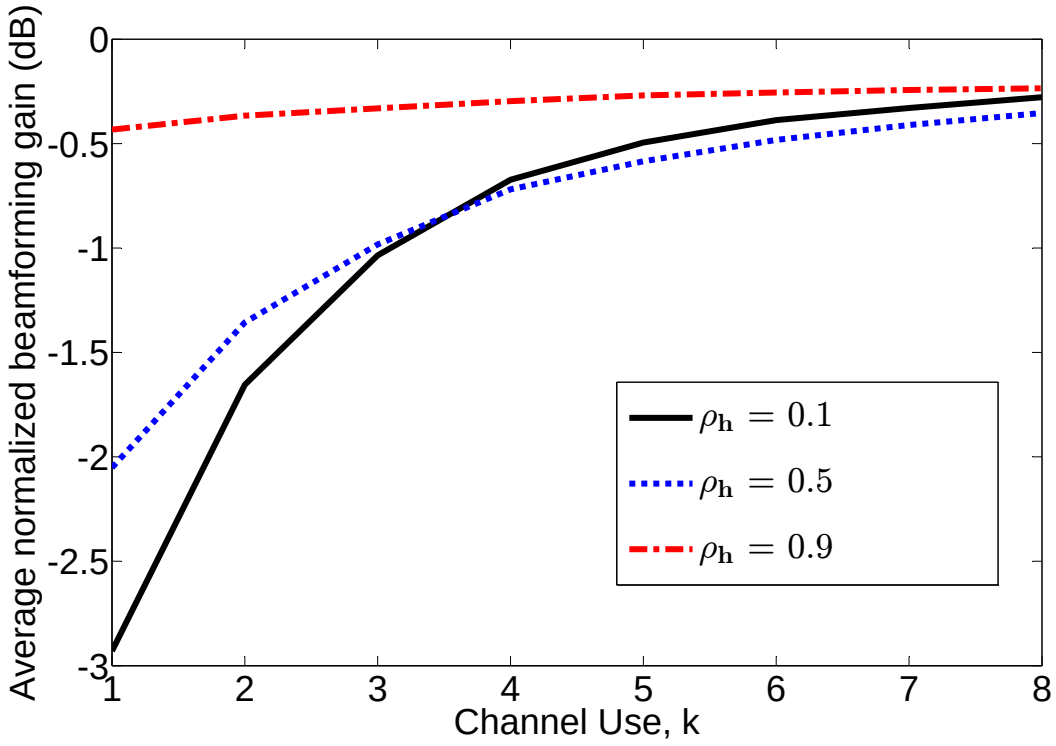

Fig. 5.5. Average beamforming gain as a function of channel use k for three different correlated binary codebooks with $M = 16$.

beamforming gain quickly saturates in the number of channel uses; for $\rho_{\mathbf{h}} = 0.9$, adding extra channel uses doesn't improve beamforming gain drastically. Even after $k = 4$ channel uses, the average beamforming gain is heavily influenced by $\rho_{\mathbf{h}}$. Low $\rho_{\mathbf{h}}$ cannot achieve the same beamforming gain on average as higher correlated channel codebooks. This stems from the fact that the energy of sounding vectors must be more spread out for slightly correlated channel codewords.

Now consider a MISO system with $M = 16$ transmit antennas and similar parameters as just described for $M = 4$. The average beamforming gain is plotted as a function of channel use k for three sets of binary channel codebooks, each with a different correlation coefficient of $\rho_{\mathbf{h}} = \{0.1, 0.5, 0.9\}$. For $\rho_{\mathbf{h}} = 0.9$, the average beamforming gain after a single channel use is high, yet additional channel uses buy very

little in terms of performance gain. Channel codebooks which are only slightly correlated receive the most benefit from additional channel uses, as shown for $\rho_{\mathbf{h}} = 0.1$. As a function of $\rho_{\mathbf{h}}$, the beamforming gain on average is larger for more highly correlated channel codewords. This is because the sounding vectors must further spread out there energy in space to detect whether $\mathbf{h}_1$ or $\mathbf{h}_2$ is true. However, we see that an interesting phenomenon at $k = 4$, where beamforming gain becomes higher for $\rho_{\mathbf{h}} = 0.1$. This can be attributed to the fact that enough power has been projected through the channel, and the increased separation of the two channel codewords now benefits channel estimation.

5.2.2 Impact of Channel Magnitude on Beamforming Gain

The receive SNR is a product of the squared channel magnitude, $|\alpha|^2$, which acts as a gain term for the transmitted signal. Using similar simulation parameters as in Section 5.2.1, we now hold the binary channel codebook correlation coefficient fixed and plot the beamforming gain as a function of $|\alpha|$. For $\rho_{\mathbf{h}} = 0.3$, the average beamforming gain is plotted in Fig. 5.6 as a function of channel use k. As one might expect, the average beamforming gain increases as $|\alpha|$ increases. However, there is a knee where the rate of increase severely drops. This knee, around $|\alpha| = 4$, shows where the effect of receive noise becomes insignificant for the channel direction detection problem. Any additional channel gain does not improve beamforming gain. When this happens, the system needs to sound additional directions instead of requiring higher SNR receive samples.

If we increase the binary channel codebook correlation to $\rho_{\mathbf{h}} = 0.7$, the average beamforming gain is plotted in Fig. 5.7. For easy comparison, we have plotted the beamforming gain in Fig. 5.7 using the same vertical scale as in Fig. 5.6. As we saw in our analysis of the effect of codebook correlation on beamforming gain, the average beamforming gain is larger for $\rho_{\mathbf{h}} = 0.7$ over $\rho_{\mathbf{h}} = 0.3$. However, for $|\alpha| \geq 2$ the additional beamforming gain for $\rho_{\mathbf{h}} = 0.7$ over $\rho_{\mathbf{h}} = 0.3$ is diminished. This effect

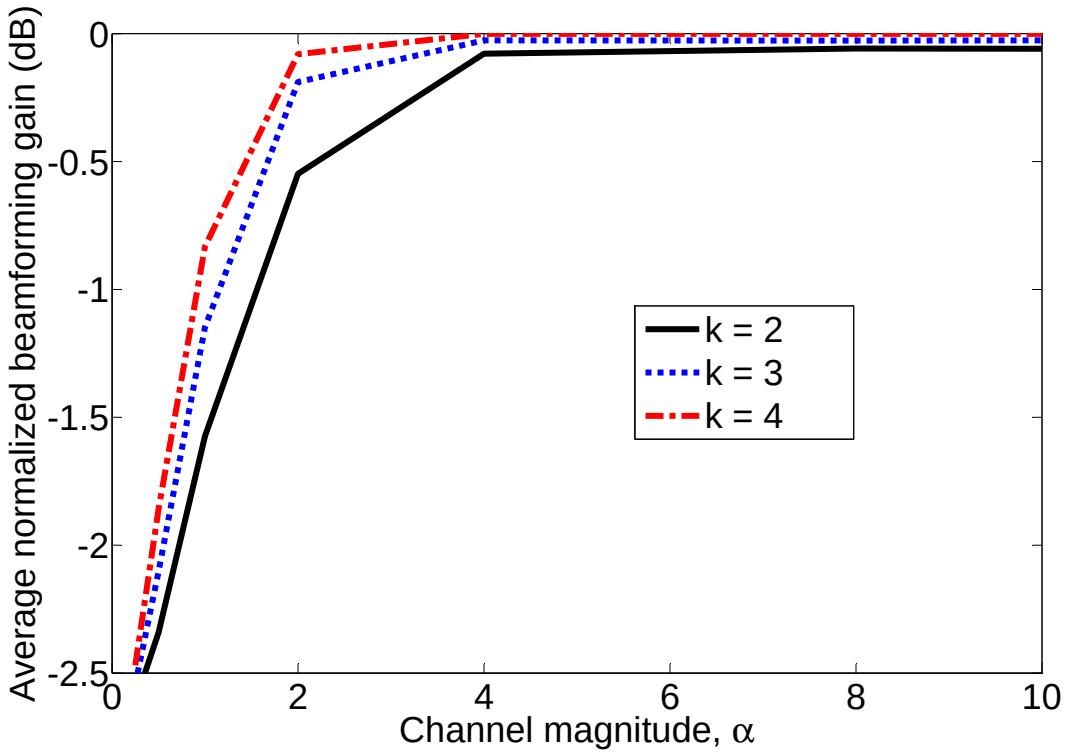

Fig. 5.6. Average beamforming gain as a function of $|\alpha|$ for $M = 4$ and a channel codebook correlation $\rho_{\mathbf{h}} = 0.3$.

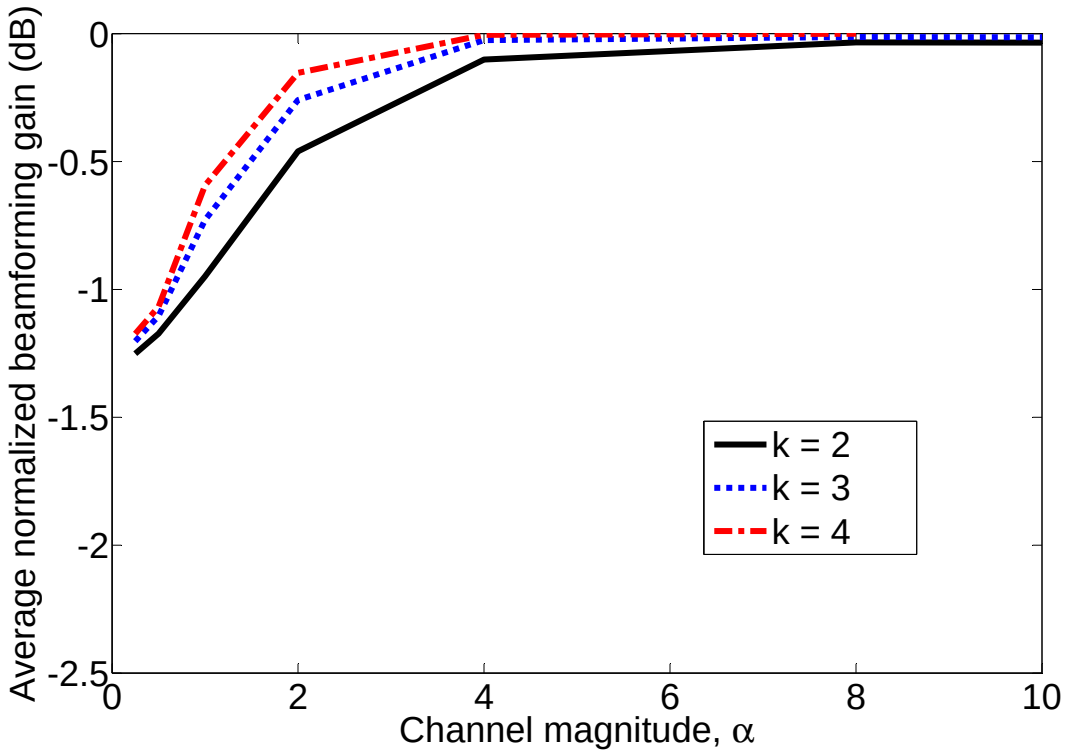

Fig. 5.7. Average beamforming gain as a function of $|\alpha|$ for $M = 4$ and a channel codebook correlation $\rho_{\mathbf{h}} = 0.7$.

can once again be attributed to the fact that the receive samples are well above the noise floor.

5.3 N-ary Channel Codebook

We now extend our scope to the N-ary channel codebook. Let,

$$\mathcal{H} = \{\mathbf{h}_1, \mathbf{h}_2, \ldots, \mathbf{h}_N\}$$

where where $\|\mathbf{h}_i\|^2 = 1$.The probability of misalignment is defined as

$$P_{\text{misalign}} = \sum_{i=1}^{N} \Pr\Big(\mathcal{M}\Big|\mathbf{y}_k, \mathbf{W}_{k+1}, \mathbf{h}_i, \widehat{\alpha}_{\mathbf{h}_i}\Big) p_i^{(k)}$$

Due to the N-ary nature of the problem, the probability of misalignment cannot be exactly defined in terms of the pairwise error probabilities, as was the case for the binary channel codebook. As with the average probability of error for multiple transmit signals, we can place an upper bound on the probability of misalignment using a union bound approximation,

$$P_{\text{misalign}} \leq \sum_{i=1}^{N} \sum_{j=1}^{N} \text{PEP}\left(\mathbf{h}_i \to \mathbf{h}_j\right) p_i^{(k)} \tag{5.8}$$

Through simulation, we have found an expression containing the pairwise error probabilities for the two most likely codewords to work well for beam alignment purposes. Let $\mathbf{h}_{(1)}$ represent the most likely channel codeword and $\mathbf{h}_{(2)}$ represent the second most likely channel codeword. A sounding vector $\mathbf{w}^{(\ell)} \in \mathcal{W}$ is chosen to minimize the expression,

$$P_{\text{misalign}} \approx \text{PEP}\left(\mathbf{h}_{(1)} \to \mathbf{h}_{(2)}\right) p_{(1)}^{(k)} + \text{PEP}\left(\mathbf{h}_{(2)} \to \mathbf{h}_{(1)}\right) p_{(2)}^{(k)}.$$

The sounding vectors are then selected from $\mathcal{W}$ in the same manner as (5.7).

5.4 Simulations

In this section, we present numerical results to validate the efficiency of the proposed closed-loop channel estimation scheme. Sampling the antennas one-by-one to

estimate the channel no longer remains practical for large arrays, as the training phase could exceed the coherence of a given channel. For this reason, these simulations target shortened training intervals, particularly the case where $K < M$.

First, we consider the channel direction to be drawn from a binary channel codebook. Although this creates a large quantization error, the exact expression for the probability of misalignment provides insight for larger codebooks. The average beamforming gain $E\left[|\mathbf{h}^*\widehat{\mathbf{h}}^{(k)}|^2\right]$ is plotted for each channel use in Fig. 5.8 for a MISO channel with $M = 16, 32$ and $|\mathcal{W}| = 32, 64$, respectively. The channel gain term α is randomly chosen as a sum of M independent zero-mean unit-variance complex Gaussian random variables. An open loop scheme is also shown, where the sounding vectors are orthonormal for all channel uses. Furthermore, the open loop scheme estimates $\alpha\mathbf{h}$ using a minimum mean square error estimator, and quantizes the estimate to the channel codebook $\mathcal{H}$.

The simulations are extended to an $N-$ary channnel codebook in Fig. 5.9. The channel direction $\mathbf{h}$ is randomly drawn from a $|\mathcal{H}| = 32$ (for $M = 16$) or $|\mathcal{H}| = 64$ (for $M = 32$) codebook. Results show up to a 2dB improvement over the open loop scheme, especially for $K = 5$.

5.5 Conclusion to Closed-Loop Beam Alignment

This work developed a closed-loop beam alignment scheme which, through the use of feedback, sequentially designs sounding vectors to probe the channel in an efficent manner. A generalized MAP detector was developed to jointly perform the channel estimation and channel quantization. Beamforming gain is maximized when the transmit beamformer aligns with the channel direction. This revealed a need to accurately estimate the channel direction, with the unknown channel magnitude replaced by its maximum likelihood estimate. The exact probability of misalignment is derived for a binary channel codebook, and an approximation is given for the N-ary channel codebook. Sounding vectors are selected from a predetermined codebook to minimize

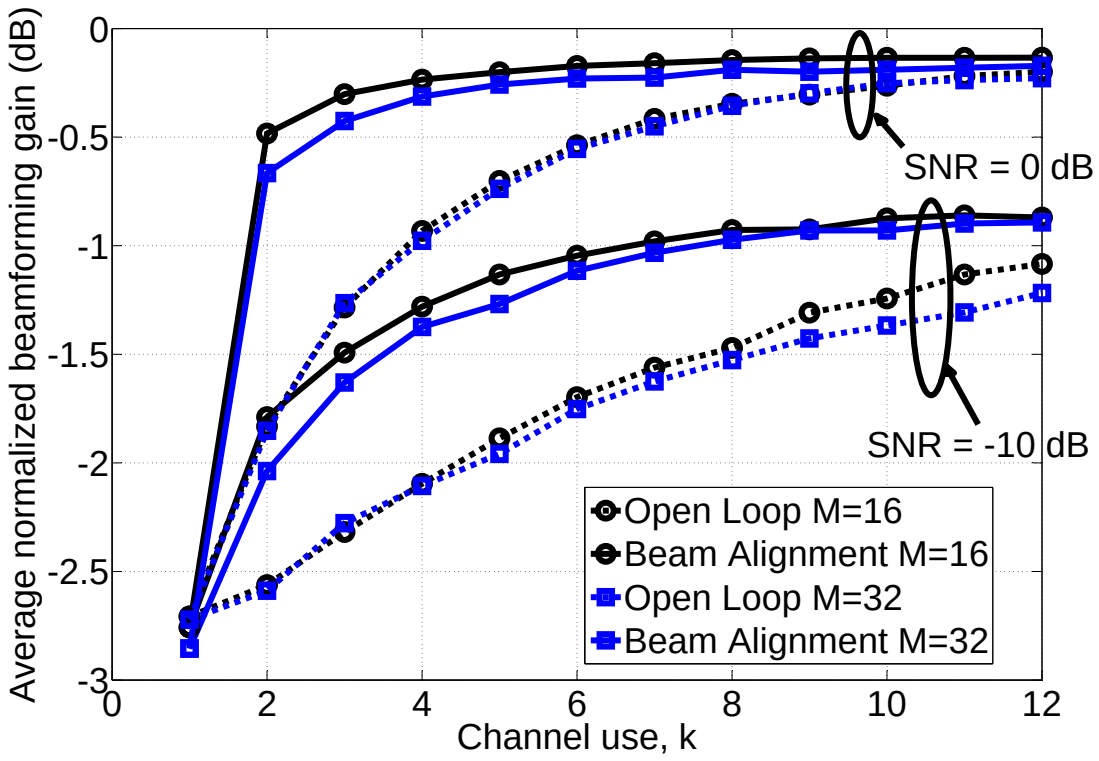

Fig. 5.8. Average normalized beamforming gain $|\mathbf{h}^* \widehat{\mathbf{h}}^{(k)}|^2$ for a binary channel codebook.

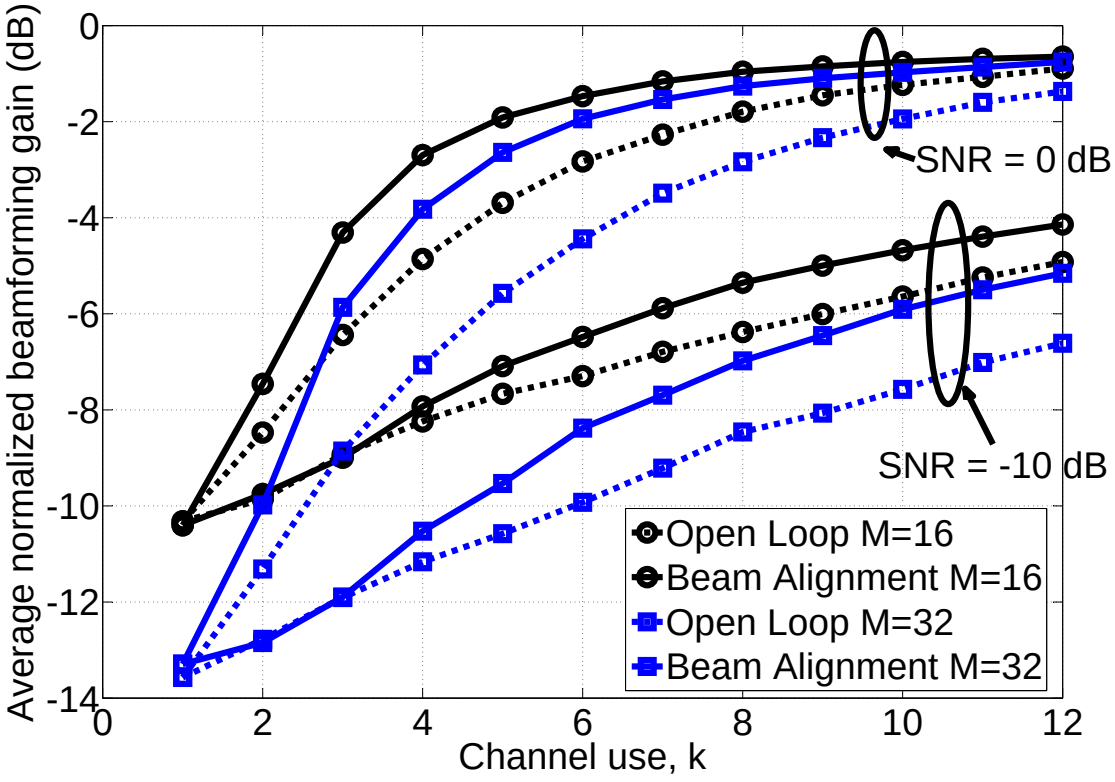

Fig. 5.9. Average normalized beamforming gain $|\mathbf{h}^*\widehat{\mathbf{h}}^{(k)}|^2$ for an N-ary channel codebook.

the probability of misalignment, a metric updated with knowledge of the previous receive samples in a Bayesian framework. The closed-loop beam alignment scheme shows improved beamforming gain over conventional orthogonal training signals. Improvement was shown especially for the $K < M$ case, which becomes increasingly important for systems with large arrays.

6. SUMMARY

The body of literature on MIMO radar signals continues to grow as the hardware technology required for implementation becomes more practical. Many issues, however, remain to be addressed to advance MIMO radar to a state usable for today's radar requirements. We review a few hybrid approaches to MIMO radar, trading off the array gain of phased array radars with waveform diversity. Our novel contribution was an additional hybrid scheme, which we termed time-division beamforming for MIMO radar. Central to time-division beamforming was the unique structure of the transmit signal matrix to include a linear precoder and a specific pulse matrix.

We defined the MIMO receive ambiguity function, which generalized the single waveform ambiguity function to multiple waveforms. Although many generalizations of the ambiguity function exist, the MIMO receive ambiguity function incorporates the receive beamformer. The receive beamformer plays a large role in the discrimination of returns from two targets closely spaced in angle. We observed a strong separability in the MIMO receive ambiguity function, where for time-division beamforming the MIMO receive ambiguity function decomposes into the product of two terms; the transmit-receive beampattern and the SISO ambiguity function. This spatial and delay-Doppler separability shows a number of interesting properties of time-division beamforming. First, the spatial properties of the transmit signal are entirely dependent on the linear precoder. The transmit beampattern is once again revealed to be the sum of the instantaneous beampatterns, which are defined as the beampatterns of the individual beamforming vectors. Accurate beampattern construction can be accomplished through design of the individual beamforming vectors in the linear precoder. Second, the delay and Doppler properties are defined by the single pulse $p(t)$, independent of the linear precoder used.

Given the time-division beamforming transmit structure, the work would not be complete without methods to design the individual beamforming vectors. We chose a multiple target scenario, with the goal to maximize detection performance of M targets located in the same range bin but separated in angle. A max-min SINR algorithm was presented to design both the transmit and receive beamformers, and performance was shown compared to simple beamformer designs and existing hybrid MIMO subarraying schemes.

Although the primary task of wireless communications is to transmit bits from the transmitter to the receiver, coherent communication requires the channel to first be estimated. The design of training sequences to estimate a wireless channel were shown to be very similar to the design of transmit signals for MIMO radar. The difference exists on the objective or criteria to evaluate. Instead of designing the transmit signal to maximize SINR on multiple targets, the problem was cast to design training sequences to estimate the MISO channel direction.

A feedback-enabled training scheme was introduced for a MISO wireless communication system. We addressed a suboptimal channel estimation solution for massive MIMO, where optimal estimation schemes become impractical for large arrays. A simple and intuitively pleasing generalized channel estimator was derived to estimate the *channel direction*. The channel magnitude was considered a nuisance parameter; designing transmit beamforming vectors to maximize receive SNR are only concerned with estimating the channel direction for MISO systems.

Given the derived channel direction estimator, it is not straightforward how to design successive sounding vectors to minimize estimation error. To overcome this, the channel space was discretized and the sounding vectors were restricted to a codebook. From there, we developed the probability of misalignment, which indicated how likely the estimator would choose a channel codeword not closest to the true channel direction. In order to derive the probability of misalignment, an important result calculated the probability the magnitude of one Gaussian random variable exceeds

the magnitude of another. This result is specific to the channel estimation problem, where each random variable is a linear function of the same noise term.

Results from the feedback-enabled training scheme showed improved beamforming gain over conventional open-loop training for a small number of channel uses. The open-loop training scheme was cited to be optimal when the number of channel uses is equal to the number of transmit antennas. We saw a significant improvement in beamforming gain for closed-loop training over open-loop for just a few channel uses. When the optimal number of channel uses to train are not available or prove too costly, the closed-loop beam alignment scheme provides improved beamforming gain over conventional open-loop schemes.

LIST OF REFERENCES

LIST OF REFERENCES

[1] A. M. Haimovich, R. S. Blum, and L. J. Cimini, "MIMO radar with widely separated antennas," *IEEE Signal Processing Magazine*, vol. 25, no. 1, pp. 116–129, 2008.

[2] Q. He, R. S. Blum, and A. M. Haimovich, "Noncoherent MIMO radar for location and velocity estimation: More antennas means better performance," *IEEE Transactions on Signal Processing*, vol. 58, no. 7, pp. 3661–3680, 2010.

[3] D. Tse and P. Viswanath, *Fundamentals of Wireless Communication*. New York, NY: Cambridge University Press, 2005.

[4] I. Bekkerman and J. Tabrikian, "Target detection and localization using MIMO radars and sonars," *IEEE Trans. Sig. Proc.*, vol. 54, pp. 3873–3883, Oct. 2006.

[5] J. Li and P. Stoica, "The phased array is the maximum snr active array [lecture notes]," *Signal Processing Magazine, IEEE*, vol. 27, pp. 143–144, Mar. 2010.

[6] P. Stoica, J. Li, and Y. Xie, "On probing signal design for MIMO radar," *IEEE Trans. Sig. Proc.*, vol. 55, pp. 4151–4161, Aug. 2007.

[7] D. R. Fuhrmann, J. P. Browning, and M. Rangaswamy, "Signaling strategies for the hybrid MIMO phased-array radar," *IEEE J. Sel. Topics Signal Process.*, vol. 4, pp. 66–78, Feb. 2010.

[8] A. Hassanien and S. Vorobyov, "Phased-MIMO radar: A tradeoff between phased-array and MIMO radars," *IEEE Trans. Sig. Proc.*, vol. 58, pp. 3137–3151, June 2010.

[9] H. Li and B. Himed, "Transmit subaperturing for MIMO radars with co-located antennas," *IEEE J. Sel. Topics Signal Process.*, vol. 4, pp. 55–65, Feb. 2010.

[10] A. Scaglione, S. Barbarossa, G. B. Giannakis, and H. Sampath, "Optimal designs for space-time linear precoders and decoders," *IEEE Trans. Sig. Proc.*, vol. 50, pp. 1051–1064, May 2002.

[11] E. Telatar, "Capacity of multi-antenna gaussian channels," *European Transactions on Telecommunications*, vol. 10, no. 6, pp. 585–595, 1999.

[12] A. J. Duly, "Transmit signal design using linear precoding for MIMO radar," 2010.

[13] V. Mecca, J. Krolik, and F. Robey, "Beamspace slow-time MIMO radar for multipath clutter mitigation," in *Proc. IEEE International Conference on Acoustics, Speech and Signal Processing*, pp. 2313–2316, Apr. 2008.

[14] S. Ahmed, J. S. Thompson, Y. R. Petillot, and B. Mulgrew, "Unconstrained synthesis of covariance matrix for MIMO radar transmit beampattern," *IEEE Transactions on Signal Processing*, vol. 59, no. 8, pp. 3837–3849, 2011.

[15] J. Li, P. Stoica, and X. Zheng, "Signal synthesis and receiver design for MIMO radar imaging," *IEEE Transactions on Signal Processing*, vol. 56, no. 8, pp. 3959–3968, 2008.

[16] T. Yoo and A. Goldsmith, "Capacity and power allocation for fading MIMO channels with channel estimation error," *IEEE Transactions on Information Theory*, vol. 52, no. 5, pp. 2203–2214, 2006.

[17] A. Paulraj, R. Nabar, and D. Gore, *Introduction to Space-Time Wireless Communications*. New York, NY: Cambridge University Press, 2003.

[18] M. Biguesh and A. B. Gershman, "Training-based MIMO channel estimation: a study of estimator tradeoffs and optimal training signals," *IEEE Transactions on Signal Processing*, vol. 54, no. 3, pp. 884–893, 2006.

[19] B. Hassibi and B. M. Hochwald, "How much training is needed in multiple-antenna wireless links?," *IEEE Trans. Inf. Theory*, vol. 49, pp. 951–963, Apr. 2003.

[20] J. H. Kotecha and A. Sayeed, "Transmit signal design for optimal estimation of correlated MIMO channels," *IEEE Transactions on Signal Processing*, vol. 52, no. 2, pp. 546–557, 2004.

[21] J. Hoydis, S. Ten Brink, and M. Debbah, "Massive MIMO: How many antennas do we need?," in *Allerton Conference on Communication, Control, and Computing*, pp. 545–550, IEEE, 2011.

[22] T. L. Marzetta, "Noncooperative cellular wireless with unlimited numbers of base station antennas," *IEEE Transactions on Wireless Communications*, vol. 9, no. 11, pp. 3590–3600, 2010.

[23] E. G. Larsson, F. Tufvesson, O. Edfors, and T. L. Marzetta, "Massive MIMO for next generation wireless systems," *arXiv preprint arXiv:1304.6690*, 2013.

[24] M. A. Richards, *Fundamentals of radar signal processing*. Tata McGraw-Hill Education, 2005.

[25] M. I. Skolnik, *Introduction to Radar Systems*. McGraw-Hill, New York, 1962.

[26] P. Swerling, "Probability of detection for fluctuating targets," *IRE Transactions on Information Theory*, vol. 6, no. 2, pp. 269–308, 1960.

[27] N. Levanon, *Radar Principles*. John Wiley and Sons, 1988.

[28] J. W. Wallace and M. A. Jensen, "Mutual coupling in MIMO wireless systems: A rigorous network theory analysis," *IEEE Transactions on Wireless Communications*, vol. 3, no. 4, pp. 1317–1325, 2004.

[29] M. C. Wicks, E. L. Mokole, and S. D. Blunt, *Principles of waveform diversity and design*. SciTech, 2010.

[30] J. Li and P. Stoica, "MIMO radar with colocated antennas," *IEEE Signal Processing Magazine*, vol. 24, no. 5, pp. 106–114, 2007.

[31] L. Xu, J. Li, and P. Stoica, "Target detection and parameter estimation for MIMO radar systems," *IEEE Transactions on Aerospace and Electronic Systems*, vol. 44, no. 3, pp. 927–939, 2008.

[32] D. R. Fuhrmann and G. S. Antonio, "Transmit beamforming for MIMO radar systems using signal cross-correlation," *IEEE Trans. Aerosp. Electron. Syst.*, vol. 44, pp. 171–186, Jan. 2008.

[33] J. Li and P. Stoica, "MIMO radar with colocated antennas," *IEEE Signal Process. Mag.*, vol. 24, pp. 106–114, Sept. 2007.

[34] D. Rabideau, "Adaptive MIMO radar waveforms," in *Proc. IEEE Radar Conference*, pp. 1–6, May 2008.

[35] P. Stoica, J. Li, and X. Zhu, "Waveform synthesis for diversity-based transmit beampattern design," *IEEE Trans. Sig. Proc.*, vol. 56, pp. 2593–2598, June 2008.

[36] T. Aittomaki and V. Koivunen, "Signal covariance matrix optimization for transmit beamforming in MIMO radars," in *Proc. Asilomar Conference on Signals, Systems, and Computers*, pp. 182–186, Nov. 2007.

[37] T. Aittomaki and V. Koivunen, "Beampattern optimization by minimization of quartic polynomial," in *Proc. IEEE/SP Statist. Signal Process. Workshop*, pp. 437–440, Sept. 2009.

[38] J. Stiles, V. Sinha, and A. P. Nanda, "Space-time transmit signal construction for multi-mode radar," in *Proc. IEEE Radar Conference*, pp. 573–579, Apr. 2006.

[39] D. Bliss, K. Forsythe, S. Davis, G. Fawcett, D. Rabideau, L. Horowitz, and S. Kraut, "GMTI MIMO radar," in *Proc. Waveform Diversity and Design Conference*, pp. 118–122, Feb. 2009.

[40] B. Friedlander, "On the relationship between MIMO and SIMO radars," *IEEE Trans. Sig. Proc.*, vol. 57, pp. 394–398, Jan. 2009.

[41] G. Frazer, Y. Abramovich, and B. Johnson, "Spatially waveform diverse radar: Perspectives for high frequency OTHR," in *Proc. IEEE Radar Conference*, pp. 385–390, Apr. 2007.

[42] G. S. Antonio, D. Fuhrmann, and F. Robey, "MIMO radar ambiguity functions," *IEEE J. Sel. Topics Signal Process.*, vol. 1, pp. 167–177, June 2007.

[43] T. Higgins, S. Blunt, and A. Shackelford, "Space-range adaptive processing for waveform-diverse radar imaging," in *Proc. IEEE Radar Conference*, pp. 321–326, May 2010.

[44] D. R. Fuhrmann, J. P. Browning, and M. Rangaswamy, "Advanced signaling strategies for the hybrid MIMO phased-array radar," in *Proc. IEEE Radar Conference*, pp. 1128–1133, May 2010.

[45] H. Urkowitz, C. Hauer, and J. Koval, "Generalized resolution in radar systems," *Proceedings of the IRE*, vol. 50, no. 10, pp. 2093–2105, 1962.

[46] N. Levanon and E. Mozeson, *Radar Signals*. John Wiley and Sons, Inc., 2004.

[47] C. Chen and P. Vaidyanathan, "MIMO radar ambiguity properties and optimization using frequency-hopping waveforms," *IEEE Trans. Sig. Proc.*, vol. 56, pp. 5926–5936, Dec. 2008.

[48] L. Brennan and L. Reed, "Theory of adaptive radar," *IEEE Trans. Aerosp. Electron. Syst.*, vol. 9, pp. 237–252, Mar. 1973.

[49] A. Gershman, N. Sidiropoulos, S. Shahbazpanahi, M. Bengtsson, and B. Ottersten, "Convex optimization-based beamforming," *IEEE Signal Process. Mag.*, vol. 27, pp. 62–75, May 2010.

[50] M. Grant and S. Boyd, "CVX: Matlab software for disciplined convex programming, version 1.21." http://cvxr.com/cvx, Oct. 2010.

[51] I. Ziskind and M. Wax, "Maximum likelihood localization of multiple sources by alternating projection," *IEEE Trans. Acoust., Speech, Signal Process.*, vol. 36, pp. 1553–1560, Oct. 1988.

[52] S. M. Kay, *Fundamentals of statistical signal processing: estimation theory*. Prentice Hall, 1993.

[53] J. Zhang, T. Yang, and Z. Chen, "Under-determined training and estimation for distributed transmit beamforming systems," *IEEE Trans. Wireless Commun.*, vol. 12, pp. 1936–1946, Mar. 2013.

[54] D. Fuhrmann, "Adaptive sensing of target signature with unknown amplitude," in *42nd Asilomar Conference*, pp. 218–222, Oct. 2008.

[55] D. J. Love, J. Choi, and P. Bidigare, "A closed-loop training approach for massive MIMO beamforming systems," in *Conference on Information Sciences and Systems*, pp. 1–5, Mar. 2013.

[56] S. Hur, T. Kim, D. J. Love, J. V. Krogmeier, T. A. Thomas, and A. Ghosh, "Millimeter wave beamforming for wireless backhaul and access in small cell networks," *to appear in IEEE Trans. on Commun.*, 2013.

[57] Y. S. S. Noh, M. D. Zoltowski and D. J. Love, "Optimal pilot beam pattern design for massive MIMO systems," in *Proc. IEEE Asilomar (to appear)*, 2013.

[58] P. Nielsen and N. Goodman, "Integrated detection and tracking via closed-loop radar with spatial-domain matched illumination," in *International Conference on Radar*, pp. 546–551, Sep. 2008.

[59] N. Goodman, P. Venkata, and M. Neifeld, "Adaptive waveform design and sequential hypothesis testing for target recognition with active sensors," *IEEE J. Sel. Topics Signal Process.*, vol. 1, pp. 105–113, Jun. 2007.

[60] J. Haupt, R. Nowak, and R. Castro, "Adaptive sensing for sparse signal recovery," in *Digital Signal Processing Workshop and 5th IEEE Signal Processing Education Workshop, 2009. DSP/SPE 2009. IEEE 13th*, pp. 702–707, 2009.

[61] J. G. Proakis, *Digital Communications*. McGraw-Hill, 4 ed., 2001.

APPENDICES

A. SINR-MAXIMIZING RECEIVE COMBINER

The SINR of the m^{th} target can be written in Rayleigh quotient form as

$$\text{SINR}_m \;=\; \frac{\sigma_m^2 \left| \mathbf{w}_m^* \left(\mathbf{I} \otimes \mathbf{a}_r(\theta_m)\mathbf{a}_t^*(\theta_m) \right) \widetilde{\mathbf{f}} \right|^2}{\mathbf{w}_m^* \mathbf{R}_{m,\text{int}} \mathbf{w}_m}$$

where $\widetilde{\mathbf{f}} = \text{vec}(\mathbf{F})$ and $\mathbf{R}_{m,\text{int}} = \sum_{l \neq m} \sigma_l^2 \left(\mathbf{I} \otimes \mathbf{a}_r(\theta_l)\mathbf{a}_t^*(\theta_l) \right) \widetilde{\mathbf{f}}\widetilde{\mathbf{f}}^* \left(\mathbf{I} \otimes \mathbf{a}_r(\theta_l)\mathbf{a}_t^*(\theta_l) \right)^* + \sigma_n^2 \mathbf{I}$. Furthermore, since $\mathbf{R}_{m,\text{int}}$ is positive semi-definite, we can use any standard decomposition method and let $\mathbf{R}_{m,\text{int}} = \mathbf{D}^*\mathbf{D}$. Making a change of variables gives $\mathbf{z}_m = \mathbf{D}\mathbf{w}_m$,

$$\text{SINR}_m \;=\; \frac{\sigma_m^2 \left| \mathbf{z}_m^* (\mathbf{D}^*)^{-1} \left(\mathbf{I} \otimes \mathbf{a}_r(\theta_m)\mathbf{a}_t^*(\theta_m) \right) \widetilde{\mathbf{f}} \right|^2}{\mathbf{z}_m^* \mathbf{z}_m}.$$

Designing $\mathbf{z}_m$ to maximize SINR_m is achieved by maximizing the numerator (as this fraction is scale invariant to $\mathbf{z}_m$). Note that the numerator is quadratic in $\mathbf{z}_m$ and can be written as,

$$\begin{aligned} &\sigma_m^2 |\mathbf{z}_m^* (\mathbf{D}^*)^{-1} \left(\mathbf{I} \otimes \mathbf{a}_r(\theta_m)\mathbf{a}_t^*(\theta_m) \right) \widetilde{\mathbf{f}}|^2 \\ \leq\; &\sigma_m^2 \|\mathbf{z}_m\|^2 \, \|(\mathbf{D}^*)^{-1} \left(\mathbf{I} \otimes \mathbf{a}_r(\theta_m)\mathbf{a}_t^*(\theta_m) \right) \widetilde{\mathbf{f}}\|^2. \end{aligned}$$

The above Schwartz inequality reaches equality when $\mathbf{z}_m = (\mathbf{D}^*)^{-1} \left(\mathbf{I} \otimes \mathbf{a}_r(\theta_m)\mathbf{a}_t^*(\theta_m) \right) \widetilde{\mathbf{f}}$. Substituting this into $\mathbf{z}_m = \mathbf{D}\mathbf{w}_m$ gives the value of $\mathbf{w}_m$ that maximizes SINR_m,

$$\mathbf{w}_m \;=\; \mathbf{R}_{m,\text{int}}^{-1} \left(\mathbf{I} \otimes \mathbf{a}_r(\theta_m)\mathbf{a}_t^*(\theta_m) \right) \widetilde{\mathbf{f}}.$$

B. POWER THRESHOLD UPPER BOUND

Since κ is a power threshold, it must be nonnegative and hence is lower bounded by $\kappa \geq 0$. The upper bound can be calculated by taking the SINR for a single target scenario, where there is no interference from other targets

$$\begin{aligned}
\kappa_{\max} &= \frac{\mathrm{tr}\left(\widetilde{\mathbf{R}}\mathbf{R}_m^*\mathbf{w}_m\mathbf{w}_m^*\mathbf{R}_m\right)}{\sigma_n^2} \\
&\leq \frac{\rho N \mathrm{tr}\left(\mathbf{R}_m\mathbf{R}_m^*\mathbf{w}_m\mathbf{w}_m^*\right)}{\sigma_n^2} \\
&= \frac{\rho MN\|\mathbf{w}_m\|^2 \mathrm{tr}\left(\mathbf{a}_r(\theta_m)\mathbf{a}_t^*(\theta_m)\mathbf{a}_t(\theta_m)\mathbf{a}_r^*(\theta_m)\right)}{\sigma_n^2} \\
&= \frac{\rho MN\|\mathbf{w}_m\|^2 M_t \mathrm{tr}\left(\mathbf{a}_r(\theta_m)\mathbf{a}_r^*(\theta_m)\right)}{\sigma_n^2} \\
&= \frac{\rho MNM_tM_r\|\mathbf{w}_m\|^2}{\sigma_n^2}
\end{aligned}$$

where $\mathrm{tr}(\mathbf{A}\otimes\mathbf{B}) = \mathrm{tr}(\mathbf{A})\mathrm{tr}(\mathbf{B})$, $\mathrm{tr}(\mathbf{AB}) \leq \mathrm{tr}(\mathbf{A})\mathrm{tr}(\mathbf{B})$, and $\mathbf{R}_m = \mathbf{I}_M \otimes \mathbf{a}_r(\theta_m)\mathbf{a}_t^*(\theta_m)$.

C. PROBABILITY THE MAGNITUDE OF ONE RANDOM VARIABLE EXCEEDS ANOTHER CORRELATED RANDOM VARIABLE

Consider two Gaussian random variables

$$\begin{aligned} X &= \mu_x + q_x n \\ Y &= \mu_y + q_y n \end{aligned}$$

where both X and Y are functions of the same *scalar* noise term $n \sim \mathcal{CN}(0,1)$. In this format, $\Pr(|X|^2 > |Y|^2)$ distinguishes itself from the expression in Appendix B of [61], where for a *scalar* noise term n, $E[|X-\mu_x|^2]E[|Y-\mu_y|^2] - |E\left[(X-\mu_x)(Y-\mu_y)^*\right]|^2 = 0$. Thus, we must find another method to solve for $\Pr(|X|^2 > |Y|^2)$.

First, let's analyze the inequality,

$$\begin{aligned} |X|^2 &> |Y|^2 \\ |\mu_x + q_x n|^2 &> |\mu_y + q_y n|^2 \\ 0 &> |\mu_y|^2 + |q_y|^2|n|^2 + 2\mathrm{Re}\{\mu_y^* q_y n\} - \left(|\mu_x|^2 + |q_x|^2|n|^2 + 2\mathrm{Re}\{\mu_x^* q_x n\}\right) \\ 0 &> \left(|q_y|^2 - |q_x|^2\right)|n|^2 + 2\mathrm{Re}\{(\mu_y^* q_y - \mu_x^* q_x)n\} + \left(|\mu_y|^2 - |\mu_x|^2\right) \\ 0 &> |n|^2 + 2\mathrm{Re}\left\{\frac{\mu_y^* q_y - \mu_x^* q_x}{|q_y|^2 - |q_x|^2} n\right\} + \frac{|\mu_y|^2 - |\mu_x|^2}{|q_y|^2 - |q_x|^2} \end{aligned}$$

assuming $|q_y|^2 > |q_x|^2$. Completing the square results in,

$$\begin{aligned} \left| n + \frac{\mu_y q_y^* - \mu_x q_x^*}{|q_y|^2 - |q_x|^2} \right|^2 &< \frac{|\mu_y q_y^* - \mu_x q_x^*|^2}{(|q_y|^2 - |q_x|^2)^2} - \frac{|\mu_y|^2 - |\mu_x|^2}{|q_y|^2 - |q_x|^2} \\ \left| n + \frac{\mu_y q_y^* - \mu_x q_x^*}{|q_y|^2 - |q_x|^2} \right|^2 &< \left| \frac{\mu_x q_y - q_x \mu_y}{|q_y|^2 - |q_x|^2} \right|^2 \end{aligned}$$

Since $n \sim \mathcal{CN}(0,1)$, the left side of the inequality is a noncentral chi-squared random variable with $k = 2$ degrees of freedom and a mean,

$$\lambda = \left| \frac{\mu_y q_y^* - \mu_x q_x^*}{|q_y|^2 - |q_x|^2} \right|^2$$

The cumulative distribution function of a noncentral chi-squared random variable is $P(x;k,\lambda) = 1 - Q_{\frac{k}{2}}(\sqrt{\lambda},\sqrt{x})$, where $Q_M(\cdot,\cdot)$ is the generalized Marcum Q-function. It follows that,

$$\Pr\left(\left|n + \frac{\mu_y q_y^* - \mu_x q_x^*}{|q_y|^2 - |q_x|^2}\right|^2 < \left|\frac{\mu_x q_y - q_x \mu_y}{|q_y|^2 - |q_x|^2}\right|^2\right) = 1 - Q_1\left(\left|\frac{\mu_y q_y^* - \mu_x q_x^*}{|q_y|^2 - |q_x|^2}\right|, \left|\frac{\mu_x q_y - q_x \mu_y}{|q_y|^2 - |q_x|^2}\right|\right).$$

The above derivations holds for the case when $|q_y|^2 > |q_x|^2$. We can completely determine the probability for three separate cases (which depend on the magnitudes of q_x and q_y) as,

$$\Pr\left(|\mu_x + q_x n|^2 > |\mu_y + q_y n|^2\right) = \begin{cases} \Pr\left(|Z|^2 < \left|\frac{\mu_x q_y - q_x \mu_y}{|q_y|^2 - |q_x|^2}\right|^2\right) & \text{if } |q_y|^2 > |q_x|^2 \\ \Pr\left(|Z|^2 > \left|\frac{\mu_x q_y - q_x \mu_y}{|q_y|^2 - |q_x|^2}\right|^2\right) & \text{if } |q_y|^2 < |q_x|^2 \\ \Pr\left(V < \frac{|\mu_y|^2 - |\mu_x|^2}{2}\right) & \text{if } |q_y|^2 = |q_x|^2 \end{cases}$$

where $Z = n + \frac{\mu_y q_y^* - \mu_x q_x^*}{|q_y|^2 - |q_x|^2}$ is a complex Gaussian random variable and $V = \mathrm{Re}\{\mu_y^* q_y - \mu_x^* q_x\}\mathrm{Re}\{n\} - \mathrm{Im}\{\mu_y^* q_y - \mu_x^* q_x\}\mathrm{Im}\{n\}$ is a real Gaussian random variable. $|Z|^2$ is a noncentral chi-squared random variable with $\Pr(|Z|^2 < z) = 1 - Q_1(\sqrt{\lambda},\sqrt{z})$ and V is the sum of two independent real Gaussian random variables, with $\Pr(V < v) = \frac{1}{2}\left(1 + \mathrm{erf}\left(v/\sqrt{2|\mu_y^* q_y - \mu_x^* q_x|^2}\right)\right)$. We then conclude the result in (5.6).

VITA

VITA

Andrew J. Duly received the B.S. degree from The Ohio State University in 2008 and the M.S. degree from Purdue University in 2010.

During the fall and summer of 2011 and 2012, respectively, Andrew was with the Sensors Directorate of the Air Force Research Laboratory at Wright-Patterson Air Force Base in Ohio. In 2010, he was awarded the ASEE SMART Scholarship in cooperation with the Air Force Research Laboratory.